



UNIVERSITÀ DEGLI STUDI DI MILANO

FACOLTÀ DI SCIENZE MATEMATICHE FISICHE E NATURALI

DEPARTMENT OF CHEMISTRY

DOCTORATE SCHOOL IN CHEMICAL SCIENCE AND TECHNOLOGIES

Curriculum

Chemical Science XXVII cycle

“A versatile polymeric coating for microarrays using copper-mediated click chemistry”

PhD Thesis of
CATERINA ZILIO
R09676

Tutor: Prof. Anna Bernardi
Co-Tutor: Dr. Marcella Chiari

Academic year 2013-2014

1. INTRODUCTION	5
1.1. AIM OF THE WORK.....	6
2. SURFACE MODIFICATION	8
2.1. SURFACE COATING IN BIOSENSOR APPLICATIONS	9
2.1.1. POLYMERIC MODIFICATION OF SURFACES	10
2.2. SURFACE CHARACTERIZATION: INSTRUMENTATION	12
2.2.1. CONTACT ANGLE	12
2.2.2. DUAL POLARIZATION INTERFEROMETRY (DPI)	14
3. MICROARRAY TECHNOLOGY	17
3.1. MICROARRAY SUPPORTS	19
3.1.1. CHARACTERISTICS OF THE SUPPORTS	20
3.1.2. PLANAR CHIP SURFACES	21
3.1.3. CHIPS WITH 3D MATRIXES.....	23
3.1.4. DESIGN PRINCIPLES FOR MINIMIZING NONSPECIFIC ADSORPTION.....	24
3.1.5. POLYMER COATING.....	25
3.1.6. LIGANDS IMMOBILIZATION CHEMISTRY.....	28
3.1.6.1. Click-chemistry.....	29
3.2. PROTEIN MICROARRAYS	33
3.2.1. THE CRITICAL ROLE OF PROTEIN ORIENTATION	34
3.2.1.1. Antibody immobilization: carbohydrate moieties.....	37
3.3. GLYCAN MICROARRAYS	41
3.3.1. MULTIVALENCY AND CARBOHYDRATES PRESENTATION	44
3.3.2. GLYCAN MICROARRAYS: TOOLS FOR RESEARCH AND DIAGNOSTICS	46
4. LECTINS: GLYCAN BINDING PROTEINS	49
4.1. LEGUME LECTINS	50
4.1.1. STRUCTURAL FEATURES	50
4.1.2. CARBOHYDRATE-BINDING SITE	51
4.1.3. PHYSIOLOGICAL FUNCTIONS.....	52
4.2. CONCAVALIN A.....	53

5. HIGH-PERFORMING MICROARRAY PLATFORM: SOLID SUPPORT AND POLYMERIC MATRIX...	56
5.1. CLICK-CHEMISTRY FOR SURFACE MODIFICATION: INTRODUCTION OF AN ALKYNE FUNCTIONALITY	56
5.1.1. DESIGN OF POLY(DMA-PMA-MAPS): STRUCTURE AND CHARACTERIZATION.....	58
5.1.1.1. Synthesis of poly(DMA-PMA-MAPS).....	58
5.1.1.2. Characterization of poly(DMA-PMA-MAPS)	59
5.1.2. POLY(DMA-PMA-MAPS) COATING: CHARACTERISTICS AND ADVANTAGES.....	62
5.2. HIGH-PERFORMING SUPPORT SELECTION	68
6. GLYCAN MICROARRAYS	70
6.1. FLUORESCENCE BIOASSAY: A QUALITATIVE ANALYSIS OF CARBOHYDRATES-LECTIN INTERACTION	70
6.1.1. DETERMINATION OF THE SURFACE EQUILIBRIUM CONSTANT ($K_{D,SURF}$): QUANTITATIVE ESTIMATION OF CARBOHYDRATES-LECTIN AFFINITY	75
6.1.1.1. Microarray experiment: $K_{D,SURF}$ and glycans multivalent presentation	75
6.1.1.2. Microarray experiment: $K_{D,SURF}$ at lower glycans' surface density.....	77
6.2. CONCLUSION: POLY(DMA-PMA-MAPS)-Si/SiO₂ PLATFORM IN GLYCAN ARRAYS	80
7. ANTIBODY MICROARRAYS	81
7.1. ORIENTED ANTIBODY MICROARRAYS: HIGH-PERFORMING BIOSENSOR.....	81
7.1.1. SYNTHESIS OF UDP-GALNAZ.....	83
7.1.2. ANTIBODY SITE-SPECIFIC MODIFICATION.....	89
7.1.3. ANTIBODY IMMOBILIZATION	90
7.1.3.1. Copper-mediated click-chemistry and its biocompatibility.....	90
7.1.3.2. Optimization study using IgG from porcine serum(p-IgG).....	91
7.2. INTERLEUKIN-6 BIOASSAY: THE ADVANTAGE OF ORIENTATION	97
7.3. CONCLUSION. POLY(DMA-PMA-MAPS)-Si/SiO₂ PLATFORM IN ANTIBODY MICROARRAYS: THE ROLE OF PROBES ORIENTATION	101
8. CONCLUSIONS	102
9. MATERIALS AND METHODS	104
9.1. MATERIALS	105
9.2. EXPERIMENTAL SECTION.....	107
9.2.1. POLY(DMA-PMA-MAPS) SYNTHESIS AND CHARACTERIZATIONS.....	107

9.2.2. TOTAL SYNTHESIS OF URIDINE 5'-(6-AZIDO-6-DEOXY-A-D-GALACTOPYRANOSYL) DIPHOSPHATE BIS-TRIETHYLAMMONIUM SALT (UDP-6-AZIDOGALACTOSE).	111
9.2.3. MICROARRAY SURFACE COATING AND CHARACTERIZATION.....	122
9.2.4. MICROARRAY EXPERIMENTS	123
9.2.4.1. Qualitative fluorescence analysis	123
9.2.4.2. Determination of the surface dissociation constant ($K_{D,surf}$)	124
9.2.5. ANTIBODY MODIFICATION	125
9.2.5.1. Site-specific enzymatic modification	125
9.2.5.2. Random modification.....	126
9.2.6. INTERLEUKIN-6 SANDWICH TEST	126

1. Introduction

This body of work introduces a clickable copolymer, which was used as a tri-dimensional coating for microarray technology and employed for the study of glycan-protein and antibodies interactions. To give the reader a good background to understand the results presented here, a broad introduction to each theme is presented.

First, the introduction focuses on solid surface modifications, in particular on a polymeric coating that allows high performance microarray analysis, both for glycan and antibody assays.

Once the chemical modification is discussed, a deeper illustration of the microarrays analysis procedure is provided. Antibody and glycan microarrays are then examined separately, because of their wide areas of interest.

Thanks to their involvement in many biological systems, antibody microarray analysis is gaining increasing acceptance in the proteomic field. The need for high-sensitivity biosensors leads the scientific community to investigate in depth the chemical approaches that could be adopted for antibodies immobilization, considering the importance of orienting the antibodies immobilization¹. Various state of the art immobilization strategies are depicted and the advantages of the strategy proposed are illustrated.

Finally, a presentation of glycan microarrays, as a novel tool for glycomics, is reported. In particular, attention is focused on the interaction of glycans with legume lectins. This interaction was used to set up a protocol for efficient glycan immobilization onto a clickable 3D matrix.

1.1. Aim of the work

In this thesis we introduce a method to functionalize the surface of glassy materials with alkynes using a polymer that produces a coating by a facile 'dip and rinse' method. The alkyne groups on the tri-dimensional surface can be subsequently linked to azide-containing carbohydrates using Cu-catalyzed azide/alkyne cycloaddition (CuAAC, click chemistry). The research is aimed at developing a new strategy to generate a polymer coating enabling the attachment of complex sugars via click chemistry by a method that does not require skilled personnel and chemistry laboratories. The proposed approach combines the advantages of high sensitivity and superior signal-to-noise ratio of a Si-SiO₂ substrate with the quality of a 3D coating. The Si/SiO₂ surface was used as the substrate to take advantage from the superior optical properties of this material (see 3.1.2). A novel polymer named poly (DMA-PMA-MAPS), obtained from the polymerization of N,N-dimethylacrylamide (DMA), 3-trimethylsilyl-prop-2-yn methacrylate (PMA) and 3(trimethoxysilyl)-propylmethacrylate (MAPS) (**Figure 11b**, paragraph 2.1.1.) was synthesized and characterized. It consists of: 1) a segment of polydimethylacrylamide that interacts with the surface by weak, non covalent interactions such as hydrogen bonding, Van der Waals or hydrophobic forces, 2) a pending silane hydrolysable monomers that promote condensation of the polymer with surface silanols or between contiguous chains and 3) chemically active monomers whose reactivity is selected on the basis of the reactivity of the molecules that have to be immobilized. (see paragraph 2.1.1.).

The polymer reported herein is similar to another polymer developed in 2004 by Pirri et al.¹⁰ to form a coating on glass slides by a combination of physi- and chemi-sorption. The proposed approach has found widespread application in protein and DNA microarray analysis. The novelty of this work consists in the presence of an alkyne functional monomer that replaces the succinimide active ester (see **Figure 11**, paragraph 2.1.1.). The 3D matrix adsorbed onto the surface, was characterized by contact angle measurements and by dual polar interferometric analysis (DPI). This latter technique highlights the solution-like environment created by the polymer onto the solid surface and will be discussed in **Chapter 5**.

Furthermore, by exploiting the presence of a stable coating that allows regio-specific and bio-orthogonal immobilization, a glycan microarray was built and its performance was deeply investigated. First, a qualitative assay (fluorescence analysis) was carried out to obtain a fast screening of the affinity of the interaction of nine glycomimetics with Concanavlin A. Second, thanks to the high-sensitivity of the Si/SiO₂ platform used, a study of the influence of the multivalency presentation of glycans during lectin interaction was made. The high-performing substrate used allows a dramatic decrease of glycan surface densities (from $1,96 \cdot 10^{14}$ down to $5,07 \cdot 10^{12}$ molecules/cm²), offering the possibility to calculate and compare the avidity in different conditions by providing density dependent surface dissociation constants ($K_{D,surf}$) (**Chapter 6**).

In a different application, the new poly(DMA-PMA-MAPS) copolymer coating was used to functionalize microarray slides with orientated antibodies taking advantage from the regio-specific reaction between alkyne on the surface and azido groups on the biomolecule.

Inspired by the work of Zeglis et al.¹³², described in paragraph 3.2.1.1., an enzymatic procedure was devised to obtain site-specific modified antibodies using an unnatural UDP-6-azidogalactose and two commercially available enzymes: β -(1,4)-galactosidase and β -(1,4)-galactosyltransferase (**Chapter 7**). As the 6-azidogalactose is sterically less hindered, it is expected to display a higher reactivity in the surface immobilization process. The strategy adopted was, in part, mutated from the procedure reported by Bosco et al.².

To validate the methodology and highlight its advantages, a sandwich microray test for the detection of interleukin-6 (IL-6) was developed (section 7.2.).

Cytokines, a set of proteins implicated in the onset and development of almost every major life-threatening disease are amongst the most intensively studied biomarkers. They play a prominent role in cancer, neurodegenerative diseases, cardiovascular diseases, sepsis and many other pathologies³. Although enzyme-linked immunosorbent assay (ELISA) is the gold standard for the measurement of a single cytokine concentration, the key to successful identification of biomarkers is the simultaneous detection of multiple cytokines with high sensitivity. IL-6 was chosen as a model of a typical inflammatory biomarker, to demonstrate the sensitivity provided by an oriented immobilization of the capturing antibody in a microarray based immunoassay.

Our site-specifically modified antibody was compared to both a randomly azido-pegylated antibody and a site-specifically modified antibody derivatized by a commercial Kit (Site-Click Antibody Labelling purchase from Life Technology), which makes use of an unnatural UDP-2-azidogalactose instead of UDP-6-azidogalactose, and of a mutant GalT (Y289L) instead of a commercially available GalT. Furthermore, through the use of the label-free sensing platform IRIS, we have correlated the efficiency of the Ab-antigen interaction given by the fluorescence signal with the mass of antibody immobilized per surface unit (ng/mm^2). The fluorescence per mass unit allows to assess the importance the antibody orientation on its capturing ability. In particular it was demonstrated that a higher amount of immobilized probe does not necessary lead to a higher antibody-antigen interaction.

2. Surface modification

Recent progresses in micro fabrication techniques and microarray technology have led to the development of miniaturized and fully integrated solid phase analytical devices that allow to perform complex analysis such as the study of cellular processes, the high throughput screening and the parallel diagnosis of multiple analytes on a chip. They imply a scaling down of the entire analytical process (time, sample and reagent volumes, costs.) while maintaining very high sensitivity. Considering the tiny dimensions of the aforementioned devices, their surface to volume ratio is extremely high and the surface must be perfectly designed and controlled in order to maximize probe immobilization and target binding efficiency, to reduce background noise and to prevent non specific molecular interaction.

When the modification of a suitable substrate must be performed to promote covalent attachment of oligonucleotides and proteins at specific locations, the control of surface chemical-physical characteristics is of remarkable importance in order to maximize probe density immobilization and to maintain their native and functional conformation. Besides, in order to obtain accurate analysis and a high of *signal-to-noise* ratio, the surface chemistry should minimize hydrophobic interactions, which are the main source of biomolecules non specific binding.

Therefore, there are several requirements that must be taken into account when chemically modify a surface:

- The chemically modified surface must be inert and resistant to non-specific adsorption;
- The surface must contain functional groups for the facile immobilization of molecules of interest;
- Bonding between a biomolecule and a solid surface must be strong enough to retain the molecule on the surface, but also sufficiently non intrusive to have minimal effect on the delicate 3D structure;
- The linking chemistry must allow the control of biomolecule orientation;

What follows is a short, non exhaustive review on the state-of-art regarding surface derivatization methods.

2.1. Surface coating in biosensor applications

Thin coatings applied to the surface of materials can improve the properties of objects dramatically as they allow control of the interaction of a material with its environment. This has been known more or less empirically to humankind for several thousand years. Lacquer generated from tree sap was used as a protective coating for wooden objects. Varnishes, enamels and coatings from pitch and balsam were used by Egyptians to render ships waterproof. Lacquers and varnishes coatings were applied to homes and ships for decoration and as protective measures against adverse environmental conditions. In modern times, the coatings industry is a multi-billion dollar business and, especially if the value of the protected objects is considered, a very important contribution to the world economy. Today, however, the application range of coatings extends much beyond the simple decoration and protection aspects, and functional coatings have become an enabling technology in a vast variety of different high-tech areas. Fields in which such high-tech coatings are applied range from computer chips⁴ and hard disk manufacturing⁵ to the use of special coatings in biomedical and aviation applications⁶.

When considering such applications, thin organic coatings are applied to control the interactions between the material and its environment. Examples of interface properties which can be controlled by deposition of a thin organic film onto a surface include friction^{7,8}, adhesion, adsorption of molecules from the surrounding environment, or wetting with water or other liquids. In medical applications, coatings allow to control of the interaction of biological cells and biomolecules with artificial materials in order to enhance the biocompatibility of an implant, or to avoid the nonspecific adsorption of proteins onto the active surfaces of an analytical device⁹. In addition, the application of functional coatings allows the coverage of a surface with groups that interact with other molecules in their environment through specific molecular recognition processes^{10,11}.

Depending on the type of interaction between the molecules which are constituents of the coating and the substrate which is to be modified, two strategies for the deposition of thin organic coatings can be distinguished. In the first one, the molecules interact with the substrate by physical forces¹², whereas in the second case the molecules are attached to the surfaces through chemical bonds. In the latter case, a monomolecular layer or a surface-attached network is strongly (“irreversibly”) attached to the surface.

A number of technologically relevant coating techniques rely on physical interactions between the deposited molecules and the substrate, including: a) painting/droplet evaporation b) spray coating c) spin coating d) dip coating e) doctor blading.

In addition to such processes, more sophisticated coating techniques have been developed, including the Langmuir-Blodgett technique¹³, the adsorption of monomolecular layers of homo- and block copolymers¹⁴ from solution, and the Layer-by-Layer (LbL)¹⁵ technique in which multilayer stacks of oppositely charged polyelectrolytes are deposited onto a (charged) substrate.

The films obtained by physical interactions are not very stable and can be subjected to destruction by: 1) desorption during solvent exposure, 2) displacement by molecules which have stronger interaction with the surface, 3) dewetting (for films above the glass transition temperature, T_g) and 4) delamination (for films below T_g).

An alternative to improve stability of coatings even in very adverse environments is to attach the molecules of the coating to the surface through covalent bonds. The price that must be paid for an enhanced stability of the system is a more complicated coating procedure and/or the requirement to choose the coating conditions more carefully, so that the surface reaction proceeds in high yield and with limited side reactions. A current, very frequently employed strategy for the preparation of well-controlled surface layers is the use of small molecules with a reactive head group that is amenable to form a covalent bond with a corresponding chemical moiety on the surface, which is to be modified. Such layers are commonly called self-assembled monolayer (SAM)¹⁶. Examples are silanes anchored on silanol groups of glass surfaces, phosphates or phosphonate on metal(oxide)s, and thiols or disulfides on noble metal surfaces (gold surfaces). In this way, very stable surface coatings can be obtained and may even have a strong degree of positional and orientational order. If such molecules expose a specific chemical moiety or a biochemically active group, it is possible to obtain a more or less strict 2D arrangement of these functionalities¹⁷. Examples are molecules which contain "ligands" as recognition sites in bio-affinity assays. In this way, surfaces can be generated (for example, on top of the transducer of a biosensor) that bind proteins very specifically from solution^{18,19}. The intrinsic limitations of this strictly 2D arrangement of the functional groups are evident: the maximal surface density of the functional moieties is limited by the surface area cross-section causing a limited accessibility of functionalities. One obvious solution to the above problem is the extension into the third dimension, that is, the use of polymers carrying the functional groups along the chain, thus generating higher cross-sectional densities of these groups and simultaneously guaranteeing good accessibility.

2.1.1. Polymeric modification of surfaces

Polymeric coatings, usually referred as tri-dimensional chemistries, provide a homogenous surface derivatization presenting a high reactive group concentration and resulting, depending on the circumstances, in an increased binding capacity of targets or to its suppression. Furthermore, they act as linkers distributing the bound probe also in the axial position (away from the surface), thus

causing a faster reaction with the target involved in biomolecular recognition. Additionally, 3D scaffolds can be engineered to customize their properties for specific applications.

Most approaches that aim at attaching polymers to a surface use a system where the polymer carries an “anchor” group, either as an end group or in a side chain. This anchor group can react with appropriate sites at the support surface, thus yielding surface-bound monolayers of polymer molecules (termed “grafting to”) (Figure 1)^{20,21}.

Another straightforward technique is to carry out a polymerization reaction in the presence of a surface onto which monomers have been attached^{22, 23}. During the polymerization reaction, the surface-anchored monomers are incorporated into growing polymer chains (Figure 1).

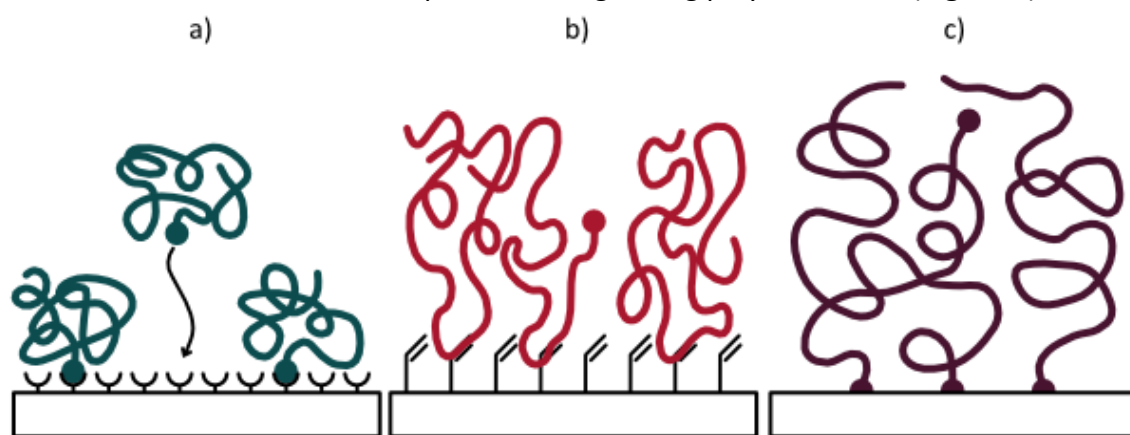


Figure 1: Schematic illustration of different processes used for the attachment of polymers to surfaces: (a) “grafting to”; (b) grafting *via* incorporation of surface-bound monomeric units; (c) “grafting from/surface-initiated polymerization”.

Although this technique, called “grafting from” coating, enables the synthesis of polymer brushes with a high surface density and thickness, the synthesis requires several steps including an initial step of organosilanization to graft a silane initiator.

In 2004 Pirri et al. presented a third technique that combines physisorption and chemisorption to simplify the coating process. The polymer used in this technique is grafted to the surface using pending silanols and is physisorbed to the surface (glass or Si/SiO₂) thanks to H-bond interactions from a mostly dimethylacrylamide (DMA) backbone¹⁰. In this way, coating can be easily achieved by dip and rinse procedure. Despite the simplicity of the process, the 3D matrix formed is covalently linked to the surface and therefore stable. Furthermore, the presence of a third functionality on the polymer (an active ester of succinimide, NHS) allows covalent immobilization of probes (from small molecules to proteins).

In this thesis, the synthesis of a similar copolymer carrying a different functionality for probe binding, is reported. All the advantages of the previous polymeric coating are maintained in the

new structure, and the main difference lies in the chemistry used for the immobilization of small molecules or protein that have to be studied.

2.2. Surface characterization: Instrumentation

2.2.1. Contact angle

Measure of Contact Angle is the easiest and cheapest analytic technique to characterize a surface. The contact angle is the angle at which a liquid/vapor interface meets a solid surface. The equilibrium contact angle is specific for any given system and is determined by the interactions across the three interfaces. Most often the concept is illustrated with a small liquid droplet resting on a flat horizontal solid surface. The shape of the droplet is determined by the Young-Laplace equation, with the contact angle playing the role of a boundary condition.

The theoretical description of contact arises from the consideration of a thermodynamic equilibrium between the three phases: the liquid phase of the droplet (L), the solid phase of the substrate (S), and the gas/vapour phase of the ambient (G). At equilibrium, the chemical potential in the three phases should be equal. The relationship between contact angle and solid surfaces is expressed by Young equation (**Equation 1**):

$$\cos \theta = \frac{\gamma_{SL} - \gamma_{SG}}{\gamma_{LG}}$$

Equation 1

where γ_{LG} is the liquid/vapor interfacial energy, γ_{SG} is the solid–vapor interfacial energy, γ_{SL} is the solid–liquid interfacial energy, and θ is the equilibrium contact angle, as shown in Figure 2.

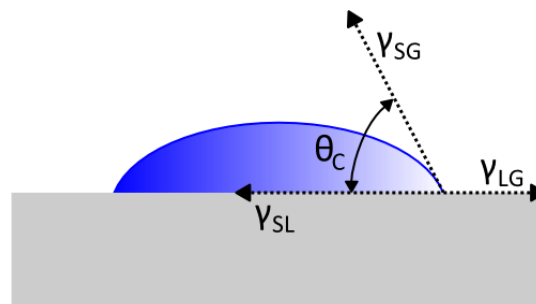


Figure 2: Schematic representation of a drop on a surface and formation of the contact angle.

The Young equation assumes a perfectly flat surface, and in many cases surface roughness and impurities cause a deviation in the equilibrium contact angle from the contact angle predicted by Young's equation.

If the molecules of a liquid are strongly attracted to the molecules of a solid (for example water on a strongly hydrophilic solid) then a drop of the liquid will completely spread out on the solid surface, corresponding to a contact angle of 0° . Less strongly hydrophilic solids will have a contact angle up to 90° . On many highly hydrophilic surfaces, water droplets will exhibit contact angles of 0° to 30° (**Figure 3b**); if the solid surface is hydrophobic, the contact angle will be larger than 90° , while on highly hydrophobic surfaces the surfaces have water contact angles as high as $\sim 120^\circ$ (e.g. fluorinated surfaces), see **Figure 3a**.

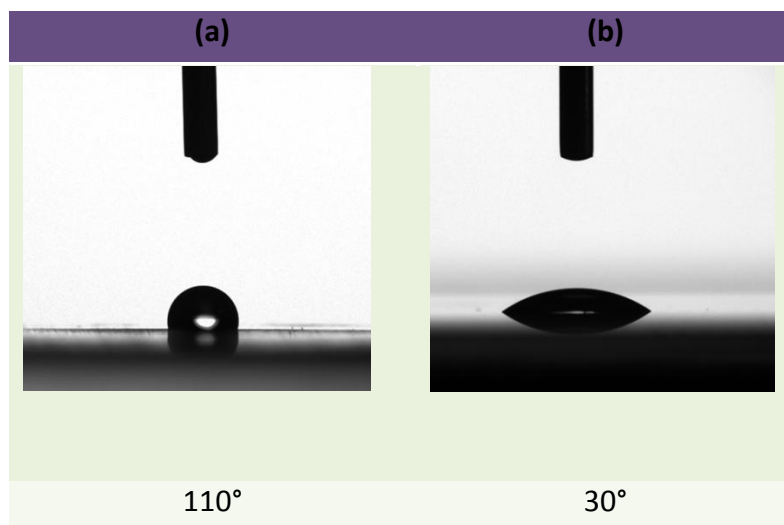


Figure 3: Images of contact angle on two different surfaces. Behavior of a water-droplet on a (a) hydrophobic and (b) hydrophilic surface.

2.2.2. Dual Polarization Interferometry (DPI)

Dual Polarization Interferometry is an optical surface analytical technique that provides multiparametric measurements of surface coatings providing information on their molecular dimension (layer thickness), packing (layer refractive index, density) and surface loading (mass)²⁴. The instrument used in this work was the Analight Bio200 (Farfield Sensors Ltd., Salford, UK), that is the principal product of the Farfield Company. It uses a silicon chip which contains two channels, and each channel is made up of a reference waveguide and a sensing waveguide. Focused coherent laser light enters the two waveguides and undergoes a total internal reflection passing along the guide. The reference waveguide is sandwiched between two surfaces providing a constant refractive index and therefore the passage of light is highly consistent and the upper surface of the sensing waveguide is exposed. The light leaving each waveguide passes through a pin hole and combines, forming a 2D interference pattern in the far field (on the detector), see **Figure 4**.

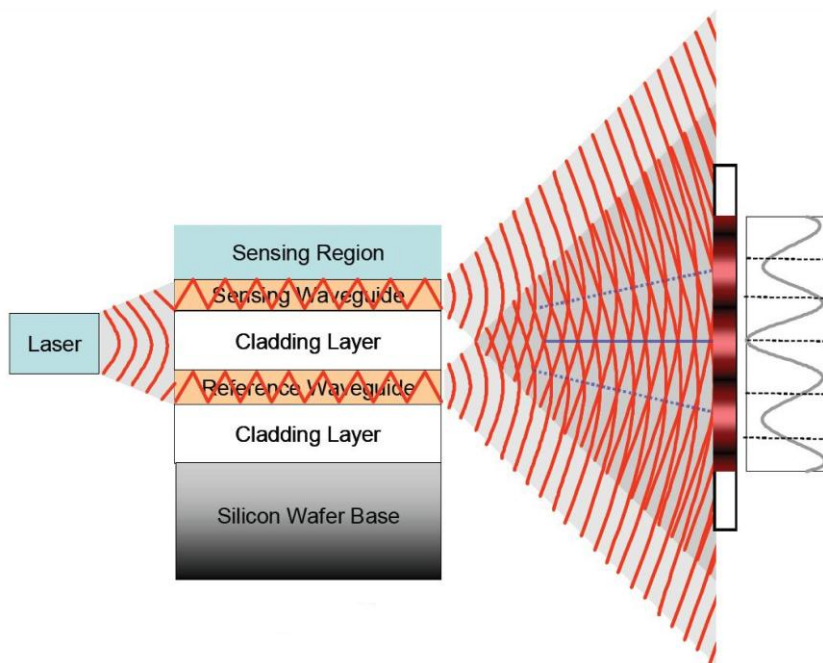


Figure 4: Dual waveguide sensor chip (viewed from the side).

As molecules, or thin films, are absorbed onto the surface of the sensing waveguide, changes in the evanescent field of the light occur due to a change in the refractive index. Therefore the light exiting the top waveguide will be out of sync compared to the reference lower guide. This is seen as a shift in the interference pattern of the upper guide with respect to the reference (**Figure 5**).

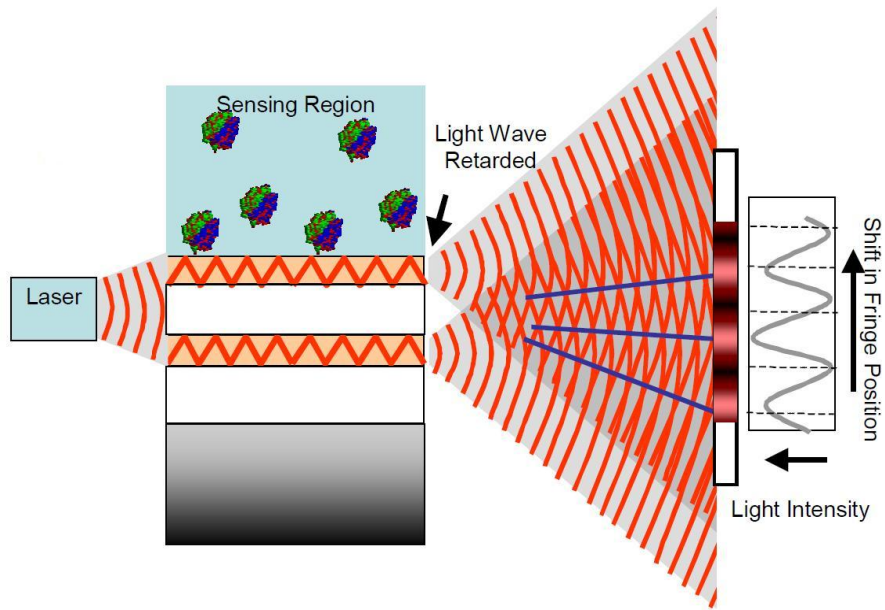


Figure 5: sensor chip with changes occurring at the sensor surface causing a shift in the fringe position.

The DPI technique rotates the polarization of the laser to alternately excite two polarization modes of the waveguides: the transverse electric (TE) and the transverse magnetic (TM) modes. Each polarization has a different depth of evanescent field and the TE (transverse electric) mode is more sensitive than the TM (transverse magnetic) mode to changes occurring in close proximity to the waveguide surface(**Figure 6**). The relative responses can be used to obtain an estimate of the layer structure.

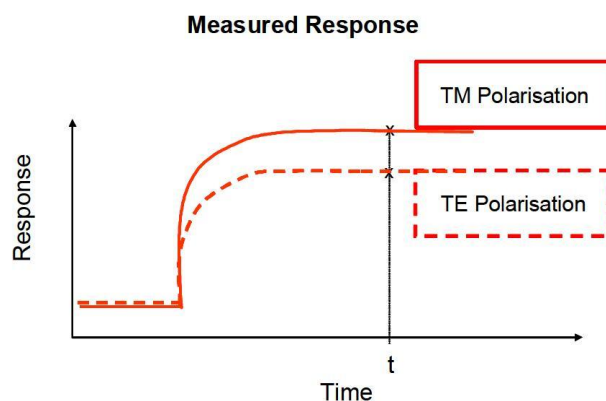


Figure 6: response observed to the TE and TM modes of polarization.

A single TM mode measurement cannot be used to differentiate between a very thick but low refractive index layer (a diffuse layer) or a very thin but high refractive index layer (a dense layer),

as all the combinations of thickness and refractive index in the range plotted are allowable for the given TM polarization mode response.

By solving Maxwell's equations for both the TM mode and TE mode, a single point of intersection can be found that will give the exact layer condition (**Figure 7**).

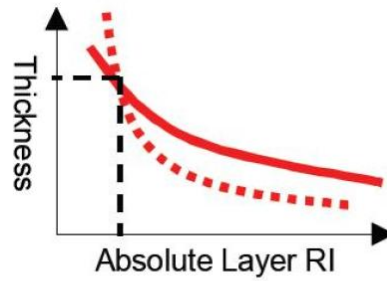


Figure 7: Overlaying the two calculated thickness and RI (refractive index) ranges, obtained by resolving the Maxwell's equation for the TM (bold red line) and TE (dotted red line) mode, the exact layer condition was obtained.

3. Microarray Technology

From the beginning of the nineties the demand of new tools to handle the enormous quantity of genomic information²⁵ has considerably grown. Such a necessity led to the development of microarray technology, which was found to be a powerful technique for analysing thousands of genes of several biological systems since its very first application. This technology consists in an orderly arrangement of probes with known identity used to determine complementary targets in solutions.

Briefly, considering DNA microarrays, microscopic drops of DNA oligonucleotides, each containing picomoles of a specific DNA sequence (e.g. short section of a gene, DNA segments) are deposited onto a surface to hybridize DNA or RNA samples²⁶.

The construction of microarrays involves the immobilization or *in situ* synthesis of DNA probes onto the specific test sites of the solid support or substrate material. High-density DNA microarrays contain hundreds of thousands of oligonucleotides immobilized onto a surface. DNA microarrays have attracted scientist interest because of their potential in clinical diagnostics, genotyping, determination of disease-relevant genes, detection of Single Nucleotide Polymorphisms (SNPs) and of post-translational modifications^{27,28,29}.

However, some difficulties occurred when analyzing, for example, mRNA transcript levels expressed under various conditions. In fact, mRNA expression level and the corresponding protein abundances (or activities) do not always correlate because of changes in translation rates and protein lifetimes³⁰. Therefore analysis of mRNA is not fully representing the real conditions of a cell protein expression and distribution. Furthermore, analysis of mRNA transcripts does not take into account post-translational modifications, such as proteolysis, phosphorylation, glycosylation, or acetylation, although many signaling pathways are mediated by such structural alterations. As a consequence, the motivation to overcome such difficulties has led to the development of promising technology that allows large-scale analysis of proteins in a parallel and miniaturized fashion.

Over the past decade, the combination of two-dimensional gel electrophoresis/mass spectrometry (MS) has been the major tool in comprehensive proteomic studies. Even though this process offers good resolution in the separation of protein isoforms that are modified by post-translational processes (for example, phosphorylation³¹, glycosylation³², and deamination³³ it presents some drawbacks including: 1) lack of a good automation of the processes involved, 2) low detection limit, that is fundamental in the field of proteins analysis (always present in low amount), 3) low reproducibility, 4) time-consuming protocols, and v) difficulties in the separation of hydrophobic membrane proteins and basic or high-molecular-mass proteins^{34,35,36}. Another approach widely used in proteomics is the combined use of liquid chromatography (LC) and mass spectrometry (MS) methods. In this approach it is possible to combine ion-exchange, reversed-phase, and affinity-

based separations to improve the resolution of each protein species. However, despite the theoretical proposal of these two technologies, to cover the complete proteome, parallelization and miniaturization, required for high-throughput screening of proteins, is still absent/lacking.

Recently, the so-called protein microarray technique has emerged as an alternative technology^{37,38} to overcome some of the limitations of the above mentioned approach. Protein microarrays comprise a large number of capture agents that selectively bind to the proteins of interest on solid surfaces.

As in the case of nucleic acid microarrays, both multiplexing and miniaturization are achieved relative to traditional methods, thus dramatically increasing the amount of data that can be obtained per volume of biological sample. For example, when 100 μ L of sample are applied to a flat surface with 10000 spatially and biochemically distinct features (for example, each one being derivatized with a different antibody), 10 000 data points can be obtain in just one experiment. By comparison, a conventional 96-well ELISA type assay would only produce a single data point from the same amount of sample³⁹.

A general scheme of a typical array experiment is shown in **Figure 8**: a large set of capture ligands (DNA, protein or peptide probes) is arrayed on a solid functionalized support using a robot (spotter) able to spot few nano-litres of a probe solution. After washing and blocking the surface unreacted sites, the array is probed with a sample containing (among a variety of unrelated molecules) the counterparts (target) of the molecular recognition event under study. If an interaction occurs, a signal is revealed on the surface by a variety of detection techniques. The most used one is the scanning of fluorescent labelled target molecules which allows detecting a large number of binding events in parallel.

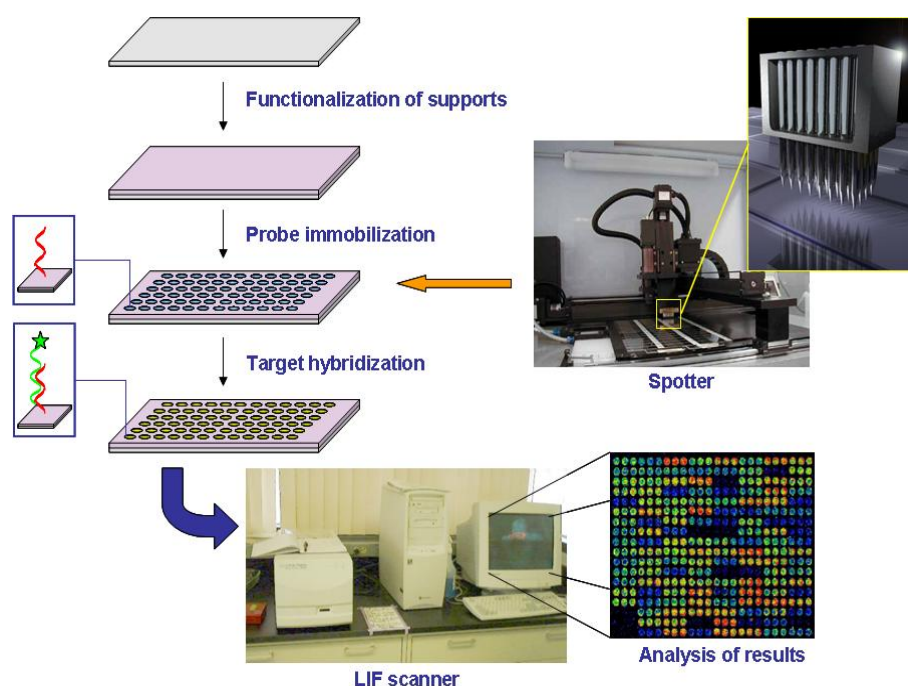


Figure 8: General scheme of a typical microarray experiment.

As a natural extension of the successful development of printed arrays of the above described biomolecules, and thanks to the wide range of carbohydrates interactions with biological targets, at the beginning of this century glycan microarrays were first introduced by several research groups^{40,41,42}. The principle of this technique, as for DNA and proteins microarrays, consists in the immobilization of glycans onto a properly modified solid surface. The advantages introduced using glycan microarrays in carbohydrates research is that, starting from small quantities of carbohydrates (picoliters), analysis of several carbohydrate molecules could be obtained, avoiding the waste of a material so difficult to obtain (both from synthetic and natural sources).

3.1. Microarray supports

The aim of microarray technology is the study of molecular interactions occurring between two partners: one contained in a liquid sample and one immobilized on a solid support. The chemistry used for the immobilization of probe molecules on the substrate plays a significant role in the success of any microarray experiment. This is particularly true with protein arrays. Unlike DNA, proteins tend to bind to surfaces in a non-specific manner and, sometimes this causes a loss of biological activity⁴³. The surfaces typically used for the immobilization of DNA are rarely suitable for proteins due to the biophysical differences between the two classes of analytes.

Therefore, the attributes for a substrate used to immobilize proteins are different from those for a DNA microarray. The key requirements of the surface hosting a protein microarray assay are:

- (1) Provision of an optimal binding capacity of capture ligands (probes).
- (2) Retaining of biological activity of capture ligand (proteins tend to unfold when immobilized onto a support, in order to allow internal hydrophobic side chains to form hydrophobic bonds with the solid surface).
- (3) Accessibility of the ligand by the interaction partner (protein–surface interactions reduce the accessibility of the target, possibly leading to false negative results). This issue is particularly important for peptide and carbohydrates microarrays due to the small molecular mass of capture ligands.
- (4) Low degree of non-specific interactions (the achievement of a low degree of a-specific binding is extremely difficult when the sample is a complex mixture of thousands of molecules such as serum), resulting in a high S/N ratio.

This is of outstanding importance because, for example, the abundance of some proteins in animal plasma is very low (also lower than 1 pg/ml) and their detection is very problematic. Therefore one of the main goals in manufacturing optimal chips is the correct choice of a solid surface and the development of a surface chemistry that is compatible with a diverse set of biomolecules while maintaining their integrity, native conformation, and biological function.

3.1.1. Characteristics of the supports

The final performance of a microarray biochip strongly depends on parameters related to the immobilization process itself. These include:

- (a) the chemical and physical properties of the surface, as they influence both specific and nonspecific binding of target and non-target biomolecules;
- (b) the distance between the immobilized probes and the chip surface;
- (c) the orientation of the immobilized probes, which might impair binding, especially of large analytes such as proteins;
- (d) the probe density on the surface, which determines chip's sensitivity and limit of detection.

The selection of the solid surface employed for generating microarray chip depends on the intended application. For example, gold surfaces are often used for the development of biosensors with electrochemical and SPR read-out⁴⁴ because of their outstanding electrical conductivity and convenient functionalization by means of thiol chemisorption. In contrast, glass or silicon⁴⁵ is typically preferred for optical sensors because of their transparency (in the case of glass) and low intrinsic fluorescence. In general, these surfaces are characterized by their chemical homogeneity and stability, their controllable surface properties (such as polarity and wettability), their reactivity towards a wide range of chemical functionalities, and the reproducibility of surface modification.

3.1.2. Planar Chip Surfaces

Glass slides are the favoured surfaces for microarrays for a number of reasons such as availability, cost, flatness, rigidity, transparency, amenability to chemical modification and non-porosity⁴⁶. Methodologies for functionalizing glass slides with chemical groups have been reported for the development of small-molecule⁴⁷ and DNA microarrays^{48, 49}. The main method for the functionalization of glass slides uses reactive silanol groups (Si-OH) on the glass surface that can be activated by a pre-treatment of the surface with, for example, piranha solution (H₂O₂/ H₂SO₄) or NaOH solution or oxygen plasma. Organofunctional silanes of the general structure (RO)₃Si(CH₂)_nX or trichlorosilanes are then used to introduce new functional groups on the surface⁵⁰. A large variety of silane reagents are commercially available, bearing amine, thiol, carboxy, epoxide, and other functional groups for subsequent modification steps. Various protocols for silanization can be found in the literature, employing deposition of silanes from organic solutions, aqueous solutions, gas phase, or by chemical vapour deposition⁵¹. Dendrimers are compounds with branched chemical structures that carry a range of chemically reactive groups at their periphery; they have been applied for surface derivatization to create a larger functional surface area. The dendritic structure can either be synthesized *in situ* by derivatization of the surface with multifunctional linkers⁵² or be generated by direct surface modification with a pre-synthesized branched structure, such as polyamidoamine⁵³, phosphine⁵⁴, or poly(propylene imine) dendrimers⁵⁵.

The majority of researches in the microarray community utilize glass slides as the “gold standard” support. To enhance fluorescence intensity, that is fundamental for microarray sensitivity, silicon/silicon oxide (Si/SiO₂) substrates of variable thickness were recently investigated⁵⁶. These layered substrates are widely available, inexpensive, and compatible with established glass surface chemistries, have a low roughness and provide a tuneable wavelength enhancement. A paper published by Cretich et al. in 2009⁴⁵ demonstrates using AFM analysis that the thermally grown silicon/silicon oxide surface has a better physical configuration (more regular, less rough) (**Figure 9a**), compared to the classical glass surface (**Figure 9b**), validating the more ordered and reproducible covering of the substrate with biomolecules observed⁴⁵.

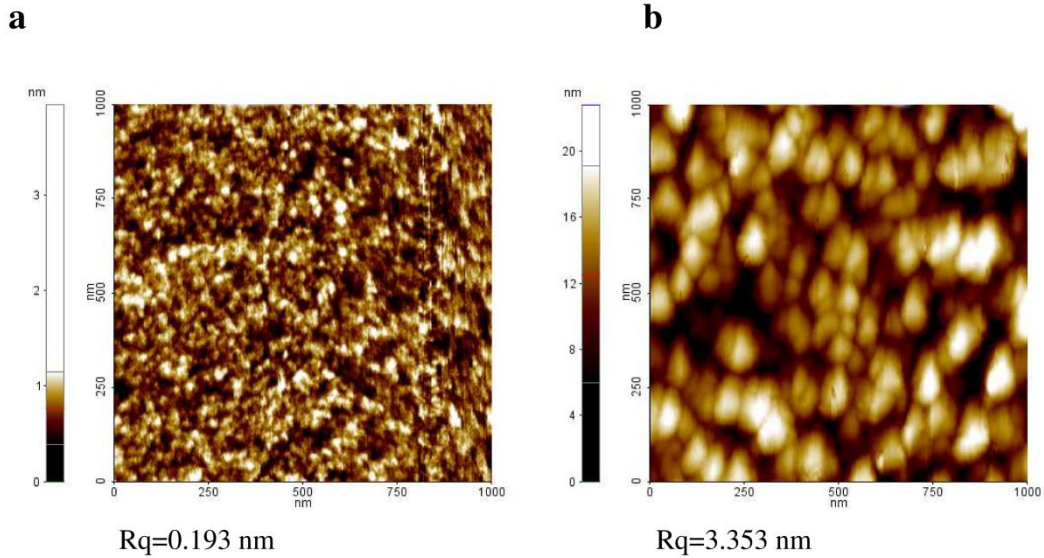


Figure 9: Atomic Force micro-graphs and Rq values of thermal SiO₂ slide (a) and of conventional glass slide surface (b). AFM measurements were carried out in the tapping mode with either a PSIA XE-150 apparatus or an NT-MTD instrument.

Furthermore, the optically transparent SiO₂ acts as a spacer to bring the fluorophore into the plane of constructive interference. By varying the thickness of the SiO₂ layer, the emission wavelength of any fluorophore of choice can be enhanced by constructive interference. Using the dipole emission model^{57,58} to simulate fluorophore emitters near a dielectric interface on layered substrate, the structure can be designed and optimized for a range of wavelengths as depicted in **Figure 10**⁵⁹. This concept has been proven with the development of a 100-nm SiO₂ layer for broadband enhancement (**Figure 10a** and **10b**) and a 320-nm SiO₂ layer for the selective enhancement of Cy3 and Cy5 fluorophore (**Figure 10a**)⁵⁹.

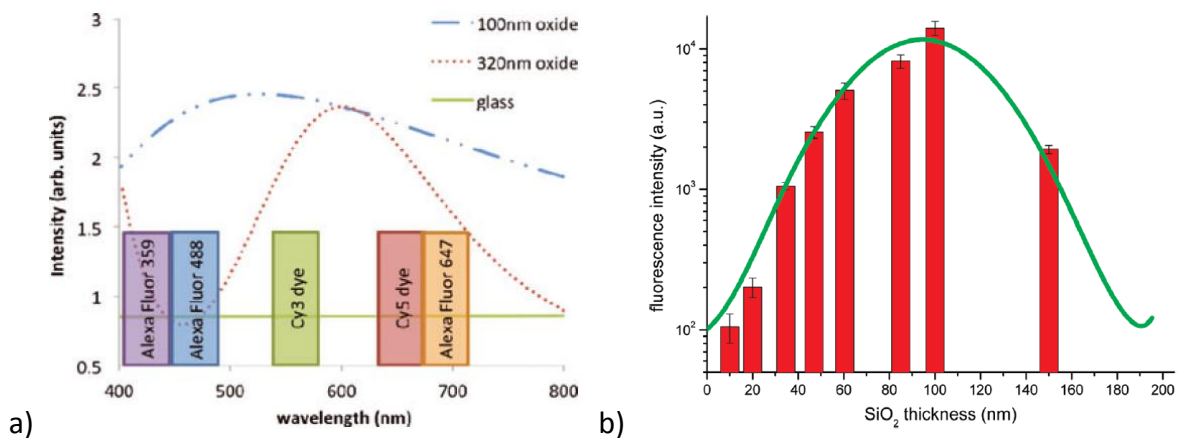


Figure 10: a) simulated fluorescence enhancement of 100-nm and 320-nm of SiO₂ and glass for commonly used fluorophores; b) simulation of fluorescence emission of Cy3 labelled

oligonucleotides placed over silicon crystals coated with silicon oxide layers of different thickness. The simulation curve is scaled to fit experimental data (histogram) obtained by fluorescence scanning of silicon slides spotted with 2.5 μM Cy3 labelled oligonucleotides.

Notably, the use of Si/SiO₂ substrates with an optimized oxide layer of 100 nm provides a fluorescent enhancement up to 7 times in comparison with conventional glass thus leading to improved limits of detection in microarray assay⁴⁵.

A silicon/silicon oxide substrate, with a 500-nm of SiO₂ layer, was also used in a label-free detection methodology called the interferometric reflectance imaging sensor (IRIS). This platform is a microarray sensing technique that utilizes a Si/SiO₂ biochip for high-throughput and multiplexed detection. This technique utilizes optical interferometry with a buried reference plane to detect binding of biomolecular interaction on the surface. Binding interactions are recorded through sampling the reflectivity signatures of the surface with multiple wavelength sources and a camera. After a stack of images is acquired, the reflectivity curves for each area are mapped and fitted through the Fresnel reflectivity equation of the silicon chip structure⁶⁰. IRIS allows a precise quantification of the amount of immobilized biomaterial on the silicon chips.

In this thesis, Si/SiO₂ biochips with a 100-nm layer of SiO₂ were used for the fluorescence glycan microarrays experiments to get fluorescence enhancement, whereas for the antibodies microarrays, IRIS biochips were used to enable a correlation between the amounts of immobilized antibodies on the solid surface with the recorded fluorescence signal.

3.1.3. Chips with 3D Matrixes

Instead of spotting probes onto a two-dimensional solid surface, molecules can diffuse into a porous matrix formed by polymer membranes or hydrogels. These matrices show a high capacity for probe immobilization and can provide a more homogeneous “natural” aqueous environment than flat surfaces, thus preventing denaturation of biomolecules. However, they suffer from problems related to mass transport effects and sometimes high background signals. Traditional membrane materials that have been used are nitrocellulose and nylon, the latter providing greater physical strength and binding capacity. Probe attachment to nylon is also generally more stable than to nitrocellulose: nylon allows positive or negative electrostatic interactions or photocross-linking, while nitrocellulose is believed to bind biomolecules by means of hydrophobic interactions⁶¹. Further improvement of mechanical stability is offered by anodically oxidized porous alumina. This material offers readily available surface chemistries, in particular silanization

methods, which can lead to higher densities of biomolecular probes, and thus to higher sensitivity in array applications⁶².

Polymeric hydrogels represent hydrophilic matrices into which probes can diffuse, leading to an immobilization capacity 100 times higher than the one found for planar surfaces⁶³. Covalent attachment of the gels to solid surfaces generates stable microarray chips. For example, agarose and acrylamide can be photopolymerized onto a surface functionalized with acrylic groups⁶⁴. Subsequently, the polymer can be activated with hydrazine or ethylenediamine to generate amine groups on the surface⁶⁵. Other examples of polymeric gel surfaces that can be used for the immobilization of biomolecules involve polysaccharides, such as chitosan or dextran. Chitosan is an amine-modified, natural, nontoxic polysaccharide, and it is biodegradable. Because of its pH-responsive properties, it can simultaneously be immobilized onto glass supports and bind proteins through electrostatic interactions. Dextran is a complex branched polysaccharide consisting of glucose molecules joined into chains of varying lengths. Dextran hydroxy groups can be oxidized to aldehyde functionalities that can then be covalently immobilized onto amine-functionalized supports and unreacted aldehyde groups can be further used for probe immobilization. Supramolecular hydrogels composed of glycosylated amino acids have been introduced as a surface material for protein arrays⁶⁶. Biodegradable polyesters, such as poly(L-lactic acid) and its various copolymers with D-lactic acid and glycolic acid, have also been studied as surfaces for biological applications⁶⁷.

3.1.4. Design Principles for Minimizing Nonspecific Adsorption

In contrast to DNA microarray applications, nonspecific binding represents a major obstacle in the development of microarray assays for proteins and glycans. As nucleic acids are uniformly negatively charged, spontaneous adsorption to a given surface is much easier for proteins, which can adsorb through electrostatic, van der Waals, and Lewis acid–base forces as well as through hydrophobic interactions and conformational changes⁶⁸. However, the quality of a microarray assay is determined not only by the desired binding events between biomolecules but also by the suppression of undesired binding of analytes and other components within the biological sample. Such nonspecific binding can give rise to background signals and thus to low *signal-to-noise* ratios. Effective reduction of non-specific adsorption has been achieved by careful selection of the surface material, for instance by using naturally occurring surfaces such as elastin⁶⁹, sarcosine⁷⁰, agarose⁷¹, cellulose⁷² and polysaccharides⁷³, or by using synthetic polymeric surfaces such as fluorocarbon polymers and molecules⁷⁴, polyethylene glycol⁷⁵, poly(vinyl alcohol)⁷⁶, or polyelectrolytes⁷⁷. One particularly versatile approach to suppressing non-specific adsorption is based on surfaces that present oligo (ethylene glycol) derivative^{78,79}. A meticulous study by Whitesides and Prime showed

that crystalline helical and amorphous forms of SAMs of oligo(ethyleneglycol)-functionalized alkanethiolates on gold are resistant to protein adsorption⁸⁰. It is hypothesized that binding of interfacial water by the ethylene glycol layer is important for the ability of the SAM to resist protein adsorption⁸¹. However, the susceptibility of ethylene glycol chains to autoxidation limits their long-term application. Surface phospholipids also minimize nonspecific binding. Their strong hydration capacity, achieved by electrostatic interaction, is postulated to be responsible for this effect⁸¹. The zwitterionic properties of monolayers of, for example, oligophosphorylcholine SAMs result in suppression of kinetically irreversible nonspecific adsorption of proteins, but unfortunately, phosphorylcholine monolayers are not very stable. In an attempt to further rationalize the design of surfaces resistant to protein adsorption, Whitesides and coworkers formulated a hypothesis correlating the preferential exclusion of a “solute” to its ability to render surfaces resistant to the adsorption of proteins. When elements of known osmolytes (organic compounds affecting osmosis) or kosmotropes (organic compounds contributing to the stability and structure of water–water interactions) were incorporated into alkanethiolates such as betaine, taurine, or hexamethylphosphoramide, SAMs of these compounds displayed improved protein repellency⁸². Although these elaborate approaches have proven to be effective for minimizing nonspecific adsorption, it must be clearly stated that the old fashioned blocking of reactive surface sites by the addition of blocking agents such as the protein bovine serum albumin (BSA), skim milk powder, or other reagents and the presence of surfactants such as Tween-20 and sodium dodecyl sulfate (SDS) are usually indispensable to the suppression of nonspecific protein adsorption⁸³.

The need of minimizing the non-specific adsorption on the surface in carbohydrates microarray is the same as for protein assays above described. The BSA is usually employed to minimize the analyte non-specific interactions, whereas for probes binding, in the case of synthetic small molecules (like the ones studied in this thesis), it would be easier to obtain a specific interaction by introducing specific functional groups that will selectively react with properly functionalized surface (i.e. azide or alkyne).

The same idea was translated also on biomolecules analysis, such as antibodies, and a chemical modification was adopted to introduce unnatural functional groups to avoid non-specific interaction during antibodies immobilization step.

3.1.5. Polymer coating

The reactivity of a chip surface is determined by the functional groups it displays. The density of the reactive groups is one important factor controlling the amount of protein that can be immobilized on a specific surface area and thus consequently influences the limit of detection attainable with the particular chip. For example, the direct attachment of a protein to a surface without a spacer

can cause steric constraint of protein's reactivity or interaction capability, compared to the protein in solution. Moreover, multiple direct contacts with the surface can induce complete or partial denaturation and thus a decreasing in its biological activity. By introducing a spacer between the protein and the reactive group on the surface, these effects can be minimized.

In general, proteins offer many functional groups, mainly in the amino acid side chains, that are suitable for immobilization purposes. Such functional groups can be used to covalently couple proteins to surfaces by a range of different reactions.

In case of DNA, sequences can be synthetically modified at one end, so a functional group, which easily reacts with the derivatized surface, is exposed.

Therefore, the development of more complex three-dimensional structure, that moves away from the surface and exposes the functional groups, it is one of the most important field of research in our laboratory.

In an attempt to obtain a suitable polymer coating with high capacity for probes immobilization offering a homogeneous "natural" aqueous environment, a hydrophilic copolymer made by *N,N*-dimethylacrylamide (DMA), *N*-acryloyloxysuccinimide (NAS), and 3-(trimethoxysilyl)propyl methacrylate (MAPS) (poly(DMA-NAS-MAPS)), firstly reported for the preparation of low-density DNA microarrays, was developed (**Figure 11 a**)¹⁰.

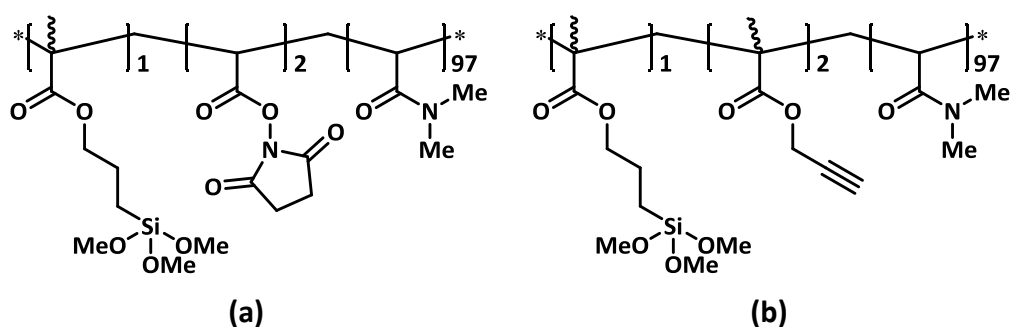


Figure 11: structure of the two ter-polymer (a) poly(DMA-NAS-MAPS) from Pirri et al. 2004¹⁰ and (b) poly(DMA-PMA-MAPS) copolymer synthesized in this thesis.

The innovative aspect of this approach relies on the fact that the polymer self-adsorbs onto the glass surface very quickly, simply by immersing glass slides in a diluted aqueous solution of the polymer and without time consuming glass pre-treatments. Therefore, the coating procedure provides a fast and inexpensive method for producing hydrophilic functional surfaces bearing active esters, able to react with amino groups of modified DNA, proteins and peptides. The poly(DMA-NAS-MAPS) slide performance was investigated in the assessment of rheumatoid factor (RF) in human serum samples⁸⁴ and in pathogen detection upon functionalization of poly(dimethylsiloxane) (PDMS) by chemisorption in DNA microarrays⁸⁵. The results have demonstrated that immobilized probes maintain an active conformation and are easily accessible;

moreover, after the assay, the slides exhibited a very low background. The polymeric surface was also tested as a peptide microarray support in an epitope mapping study^{43,86}. This study suggested that although the poly(DMA-NAS-MAPS) coated slides bind the capture molecule in a random conformation, the aqueous micro-environment created by the polymeric coating provided a good accessibility of the ligand.

Moreover, Cretich et al. demonstrated by AFM analysis that the presence of a poly(DMA-NAS-MAPS) ultrathin film coating did not influence the roughness of a Si/SiO₂ surface (**Figure 12**), maintaining all the advantages previously described for this surface (paragraph 3.1.2.).

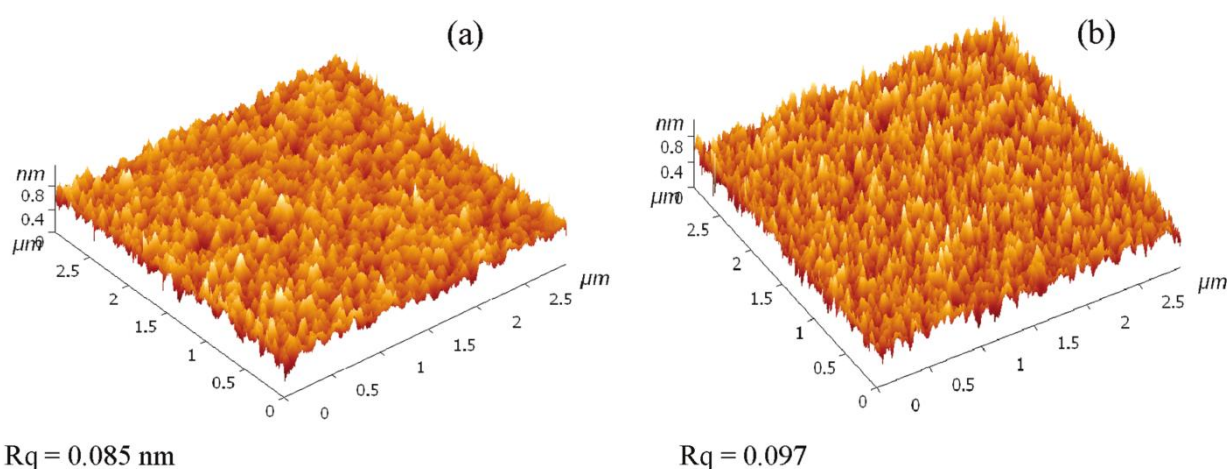


Figure 12: atomic force micrographs of thermal SiO₂ (a) and polymer coated SiO₂ (b) surfaces.

Thanks to the success of this copolymer (in terms of sensitivity, dose-response interactions, probes accessibility, etc.) and because of the growing interest in the use of click chemistry, due to the possibility of obtaining fast, simple, versatile and regiospecific reactions with high products yields⁸⁷, one of the main goals of my thesis consisted in the synthesis of a new copolymer similar to poly(DMA-NAS-MAPS), in which the NAS functionality is replaced with an alkyne functionality (**Figure 11 b**).

This new copolymer would allow the immobilization of small molecules, and/or any kind of probes carrying azide functionality, and give us the chance of study copper-mediated click reaction directly on the surface.

3.1.6. Ligands immobilization chemistry

As previously described, a microarray consists of an orderly arrangement of the probes immobilized onto a properly functionalized solid surface. The immobilization occurs in a non-covalent or covalent fashion, depending on the substrate that has to be attached and on the availability of functional groups present both on the substrate and surface (**Figure 13**).

Furthermore, the two immobilization strategies can be divided into two subclasses, which are the non-oriented and oriented immobilization. This topic will be discussed in depth later (paragraph 3.2.1.), because it correlates better with proteins microarray analysis.

Some of the interactions exploited for non-covalent immobilizations techniques include: the naturally strong biotin-avidin binding point (in particular streptavidin); lectin-carbohydrates pair, that belong to the receptor-ligand mechanism, hydrophobic binding (synthetically fluorinated-tagged probes to fluorinated slides) and simple physisorption^{88,74}. For antibodies it is possible also to employ the specific interaction of protein A, G or L with their Fc region¹.

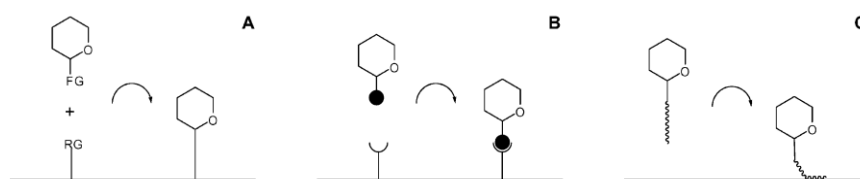


Figure 13: (a) covalent coupling, (b) receptor-ligand non-covalent coupling, (c) adsorption, non-covalent coupling.

The use of non-covalent immobilization, during the years, was substituted with the more stable covalent binding that, in particular for biomolecules, takes advantage mostly from the natural abundance of amine groups that are very reactive toward a wide range of functional groups (i.e. active esters, aldehyde, etc).

Nowadays the dominating microarray format relies on the covalent binding of probes to microarray slides, thanks to their higher stability during the whole analysis^{89,90}.

The choice of the reactive group mainly depends on the synthesis strategy of the probes that has to be immobilized. The coupling reaction should be fast, specific and high yielding. The group should not interfere during the synthesis and should not react with other groups present on the substrate. Fast reactions are preferable, since reactions with surfaces are significantly slower than that of the corresponding reactions in solution. Fast covalent immobilizations that have been exploited are depicted in **Figure 14**. Initial examples include the classical and efficient reaction between amine and N-hydroxysuccinimide active ester (**Figure 14a**)⁹⁰ or epoxides (**Figure 14b**)⁹¹, that could be

applied to biomolecules without modification. However the immobilization of a compound could be a disadvantage: if the compound, usually present in small amount, is not completely available to the binding interaction it might not be recognized by the analyte in solution, which would lead to false negative results. To overcome this problem, special attention has been given to chemoselective and biorthogonal reactions for the immobilization mechanism (i.e. Staudinger ligation, photoactivatable immobilization and copper-mediated cycloaddition). So, later, the so-called “click reactions” were used. They include thiol and maleimides reaction (**Figure 14c**)⁹², as well as cyclizations of azides and alkynes (**Figure 14d**) or properly substituted phosphines or photoreactive groups (**Figure 14e**)⁹³, that are suitable for synthetically modified probes, such as glycans and engineered or chemically modified biomolecules (proteins, antibodies, peptides, etc).

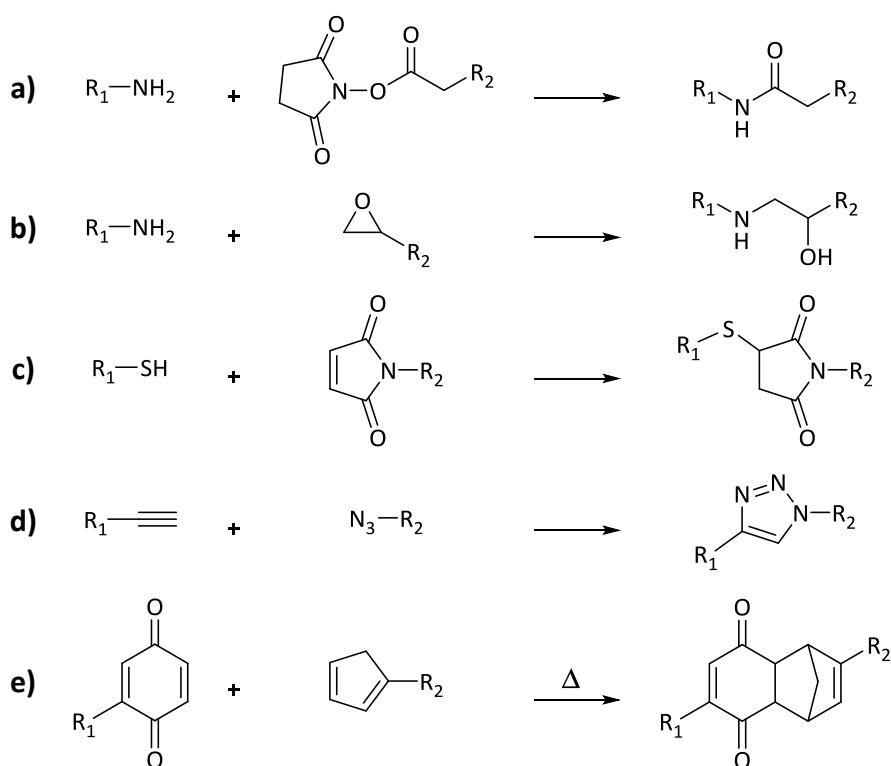


Figure 14: Surface covalent coupling chemistries

In this thesis we investigated the possibility to immobilize small molecules and biomolecules through the well known copper-mediated 1,3-dipolar Huisgen cycloaddition.

3.1.6.1. Click-chemistry

The Huisgen 1,3-dipolar cycloaddition reaction of organic azides and alkynes⁹⁴ has become more popular from 2001, when Cu(I) catalysis was introduced at the same time by Sharpless, Meldal and

Tornøe. Sharpless and co-worker revised the Huisgen 1,3-dipolar cycloaddition in aqueous condition, finding out that in water medium the reaction proceeds better than in an organic solvent⁹⁵. Simultaneously Tornøe and Meldal⁹⁶ reported copper catalysis in a work on solid-phase peptidotriazoles, that led to an improvement in both rate and regioselectivity of the reaction. This condition allows a quantitative, very robust, insensitive and orthogonal coupling reaction, suitable for both biomolecular ligation⁹⁷ and in vivo targeting⁹⁸. The triazole formed is essentially chemical inert to reactive conditions, such as oxidation, reduction and hydrolysis⁹⁹.

In the set of “clickable” reaction (that include reaction such as Diels-Alder cycloaddition) the Huisgen 1,3-dipolar cycloaddition copper-catalyzed, thanks to the dramatically acceleration rate obtained with the catalyst and the beneficial effects of water used as solvent, gained all the attentions.

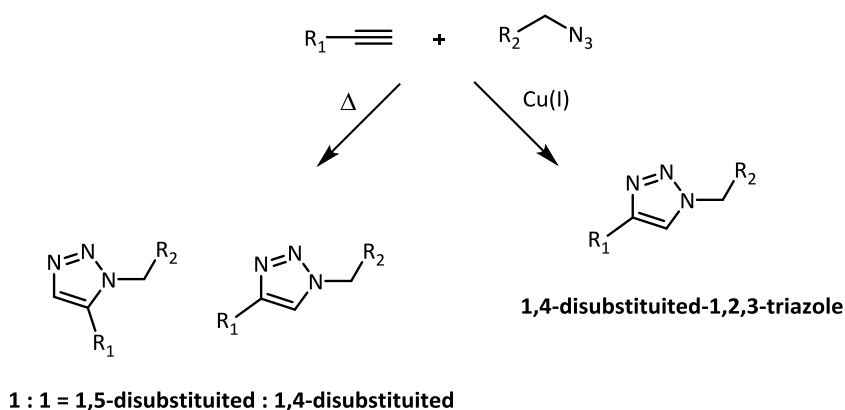


Figure 15: Huisgen cycloaddition non catalyzed and catalyzed by Cu(I).

This reaction process do not requires protecting groups on the most common functionalities of biomolecules, and proceeds with almost complete conversion and selectivity for the 1,4-disubstituted 1,2,3-triazole, see **Figure 15**, with a surprising indifference to solvent and pH.

Therefore it is widely applied also in the derivatisation of biomolecules and pseudo-biomolecules providing more challenging tasks in the field of bioconjugation. Chaikof et al. used copper-mediated click chemistry to immobilized both carbohydrates and proteins on a SAM modified solid surface. Thanks to the regioselectivity of this cycloaddition, the reduction of biomolecular activity through denaturation, caused by random orientation on solid surface, could be avoided incorporating a triazole linker obtained via click chemistry between proteins and surface carrying alkyne functionality. The same concept was translated to carbohydrates immobilization on solid surfaces derivatised with alkyne functionality (**Figure 16**)¹⁰⁰.

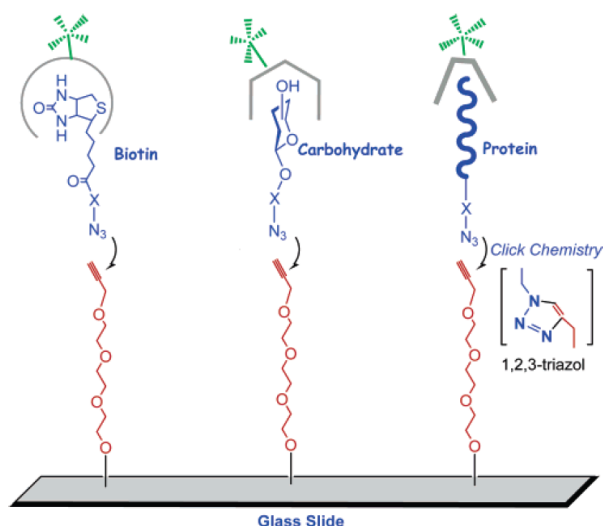


Figure 16: Schematic illustration of azide-alkyne cycloadditions of azide derivatized biomolecules (from carbohydrates to protein).

The results obtained demonstrated that Cu(I) catalyzed click reaction is suitable for both carbohydrates and proteins immobilization, without the production of unwanted side products, and the easy procedure could be extended to the immobilization of a wide range of substances onto properly modified solid surfaces.

However, the presence of a copper catalyst may be a problem. Some examples of in vitro copper-induced degradation of viruses¹⁰¹ or oligonucleotide strands¹⁰² have been reported. In this case, maybe the use of thermal initiated Huisgen cycloaddition could help, but such approach is rather specific and cannot be extended to all the standard ligation situations. An interesting copper-free azide-alkyne cycloaddition strategy has been reported by Bertozzi and co-workers¹⁰³ in 2007, and it is based on the use of strained cycloalkynes differently substituted for dynamic in vivo imaging. However, this strained-promoted alkyne-azide cycloaddition (SPAAC), that is gaining increasing acceptance in particular in the modifications of biomolecules and living system, would give a slower cycloaddition kinetics if compared with copper-mediated click reaction (CuAAC). Even the fastest of the strained cycloalkynes react with azides >10 times more slowly than terminal alkynes in the presence of Cu(I)¹⁰⁴.

For these reasons, in accordance with the literature, in this thesis the CuAAC cycloaddition was used coupled with a protector/accelerating ligand (THPTA) for antibodies immobilization, to maintain all the advantages related to copper-mediated cycloaddition without damaging the investigated biomolecules^{104,105,106}.

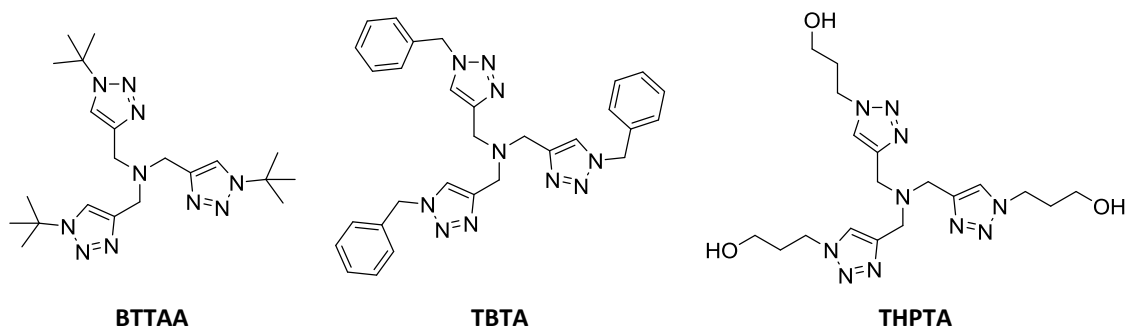


Figure 17: Structures of three ligands reported in literature for the acceleration of click-chemistry reaction rate.

Many studies were made on the function and utility of these ligands (**Figure 17**), and many structures were presented.

3.2. Protein microarrays

Protein-detecting microarrays have gained increasing interest in the last few years; they mainly allow performing two different types of analyses. One is to determine the abundance of proteins of interest in complex protein mixtures using highly specific capture agents for each target protein, for example, by antigen-antibody interactions. The other is to find out the function of proteins of interest, providing information on protein–protein interaction, receptor-ligand interaction, enzymatic activity. Protein arrays generally fall in the following two categories¹⁰⁷:

- (1) functional arrays (comprising reverse-phase arrays)
- (2) detection arrays (or analytical arrays).

In functional arrays (which are generally aimed at discovering protein function in fundamental research) a large set of purified proteins or peptides or even an entire proteome is spotted and immobilized. The array is then used for parallel screening of a range of biochemical interactions. Protein functional arrays¹⁰⁸ can be used to study the effect of substrates or inhibitors on enzyme activities¹⁰⁹ protein-drug or hormone effector interactions¹¹⁰ or in epitope mapping studies⁴³. In *reverse phase microarrays*¹¹¹, tissues, cell lysates or serum samples are spotted on a surface and probed with one antibody per analyte for a multiplex readout. The reverse-phase microarrays fall, generally, in the category of functional microarray.

In protein detection microarrays, an array of well-characterized affinity reagents (antigens or antibodies) rather than the native proteins themselves, is immobilized on a support and used to determine protein abundances in a complex matrix such as serum. Analytical arrays can be used to assay antibodies (for diagnosis of allergy¹¹²) or autoimmunity diseases or to monitor protein expression on a large scale).

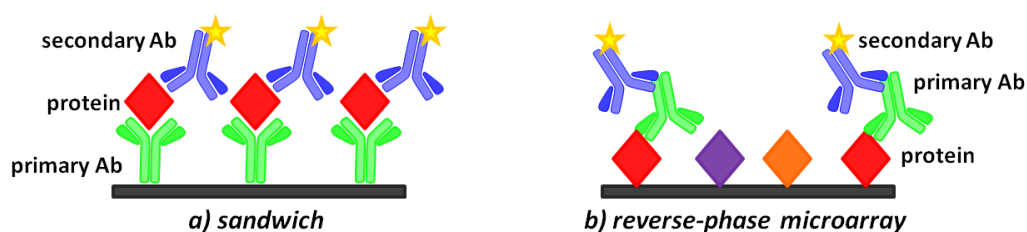


Figure 18: Examples of analytical (or detection) proteins microarrays: (a) is the useful sandwich microarray test, while (b) is a representation of the so-called reverse phase microarrays.

The microarray assay format is ideally suited to the panel of tests that are emerging from the proteomic and genomic initiatives because this method of highly parallel testing is more rapid than serial assays. Examples of clinical assays that are suited to a protein microarray format are tests for autoimmune diseases, detection of cytokines and assessing of allergic responses. A commercially available protein microarray for allergy diagnosis is, for instance, one of the first examples of a protein microarray that really entered into routine clinical analysis¹¹³.

Antibody microarrays belong to the family of protein microarrays. Thanks to the specificity of antibody-antigen binding, they have great potential in many fields, such as clinical diagnostics, assessment of environmental pollution and quality control in the food industry, or simply as comprehensive research tools¹¹⁴. Proteome profiling is the most exciting application of antibody microarrays for systems biology, very similar to the gene expression microarray. Many studies using antibodies microarrays have recently been reported, and also the list of commercial antibody microarrays is expanding rapidly. In theory, with antibodies microarrays, using one specific antibody for each human protein, one would be able to profile, in a few hours, all the human proteome¹¹⁵.

3.2.1. The critical role of protein orientation

The study of protein structure and function is certainly of significant importance for fundamental scientific research, but also critical for the development of biomedical and biotechnological applications because of their implication in many biological systems.

Thanks to its high-throughput character, protein microarray analysis is gaining increasing acceptance in proteomics. Compared to its counterpart in genomics, i.e. DNA microarrays, there are two principal difficulties associated with protein immobilization: surface background and the conformation and orientation of proteins once immobilized¹¹⁶.

The background has to be minimized as much as possible by suppressing the non-specific adsorption of proteins onto the chip solid surface in order to keep a high signal-to-noise ratio during fluorescence analysis and avoiding false negative results.

On the other hand, the conformation and orientation of immobilized proteins has to be taking into account. Proteins have complex structures and activities, and their printed quantities are very low, so the immobilization chemistry has to preserve proteins native state providing an optimal orientation to increase the exposure of the protein functional domain to better interact with the target in solution^{1,116}.

The most common methods of protein immobilization in microarrays are based on non-specific random adsorption and covalent bond formation between natural available functional groups on protein molecules (e.g. -NH₂) and complementary coupling groups (e.g., aldehyde or epoxide) on

the surface . However, non covalent binding by hydrophobic interaction may causes protein denaturation, leading to a loss of functional activity; while the use of covalent binding enhances the stability of immobilized proteins, sometimes proteins denaturation cannot be prevented. In fact, if the most abundant functional groups on protein (-NH₂) is used to covalently attach molecules onto the surface, a loss of activity could be observed because no control is achievable on protein orientation.

Various substrates, as well as various functional groups on the same substrate, were tested and compared^{1,117}. Since the most crucial disadvantages of non-oriented immobilization are insufficient exposure of functional domains, spacer arms (e.g. N-hydroxysuccinimide)¹¹⁸ and polymeric matrix¹⁰ have been used to separate proteins from substrate to enhance ligands accessibility. In spite of these precautions, protein orientation after immobilization on surface cannot be predicted; this would results in binding of fraction of proteins with improper orientation that cannot bind to their ligands¹.

Given this background, the importance of oriented immobilization of protein molecules has been extensively investigated¹. Strategies were demonstrated including the use of fusion proteins¹¹⁹, immobilized protein A or G (which binds selectively the Fc portion of antibodies)¹, m-RNA protein hybrids¹ and chemical modifications based on biotin-streptavidin interaction or Staudinger ligation reaction¹²⁰. Although proteins or antibodies with uniform controlled orientation have shown higher activity than those of random orientation¹²⁰, chemical modifications and recombinant methodology still have limited applicability due to their laborious achievement.

In the field of proteins, antibodies (Abs) represent a class of glycoproteins with a well-defined structure (as it will be briefly described in Section 3.2.1.1.). Since Abs posses only two binding sites on the top of the Y-shape, it can be highly advantageous to orient these molecules to improve biosensor performance, with improvement factors as high as 200 being reported upon orientation^{121,122}.

Immobilized IgG can adopt four exemplary molecular orientations: side-on (one Fc and one Fab attached to the surface), tail-on (Fc attached to the surface), head-on (both Fabs attached to the surface) or flat-on (all three fragments attached to the surface) (**Figure 19**).

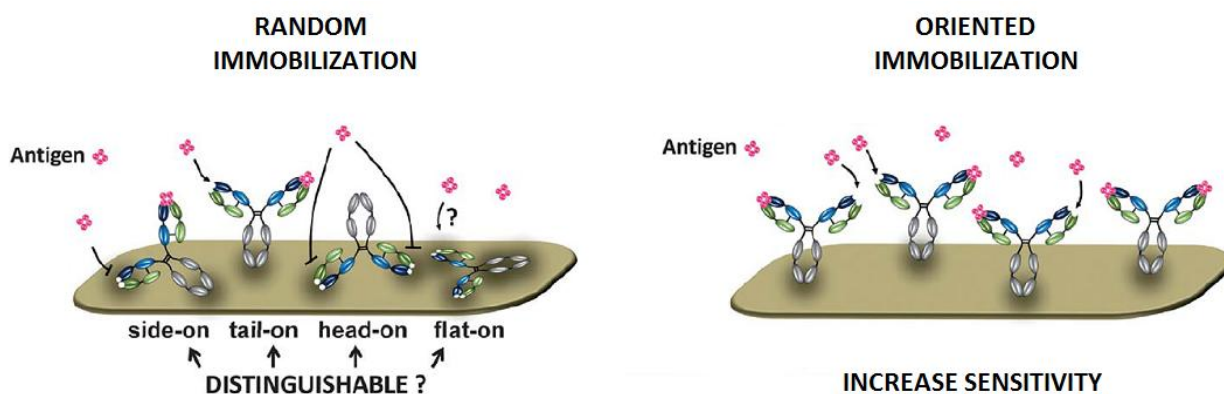


Figure 19: Schematic representation of a random and oriented Abs immobilization onto a solid surface. The oriented immobilization improves the availability of Abs toward the antibody-antigen interaction, increasing the sensitivity of the biosensor.

For the highest analyte binding, Abs should assume tail-on orientation, displaying free antigen-binding regions after immobilization. As a consequence, controlling Abs orientation will lead to better analyte binding, resulting in improved biosensor sensitivity.

To reveal the presence and study the binding function of immobilized Abs, many techniques have been used, such as: Fourier transform infrared reflection (FTIR) spectroscopy, used to characterize the presence of specific chemical groups; various fluorescence microscopies to visualize efficient binding of analyte to Ab-functionalized surfaces¹²³ and Surface Plasmon Resonance (SPR), used to calculate Ab coverage and affinity. In particular with SPR the obtained data on the relationship between the adsorbed amount and molecular orientation on the surface has been used to distinguish between tail/head-on and side/flat-on orientation¹²⁴. Nonetheless, using these techniques only minimal direct information about Abs orientation could be deduced.

To better understand their immobilization mode, more sophisticated techniques have been reported, such as: Atomic Force Microscopy (AFM), used to deduce Abs orientation by determining the dimensions of the Abs; High-resolution Time-of-Flight Secondary Ion Mass Spectrometry (ToF-SIMS), that determined surface structure providing biophysical information about the molecular structure; Dual Polarization Interferometry (DPI), used to determine Abs orientation combining the known dimensions of the molecules with the information obtained from the instrument (layer thickness, density, or layer refractive index, and mass). These and other techniques are examined in depth in a minireview published last year on Analyst by Trilling et al.¹²².

3.2.1.1. Antibody immobilization: carbohydrate moieties

Antibody Structure: brief overview

Antibodies play key roles in humoral adaptive immune response. Thanks to their unique structure they are able to control immunity by binding specific antigens and linking them to the innate immune system. Their structure has been successfully exploited in development of therapeutic treatments for many disease types, such as cancers, autoimmune diseases, and inflammatory disorders^{125,126}.

Human immunoglobulins can be categorized into five classes (IgG, IgA, IgD, IgE and IgM) referencing the heavy chain. IgG and IgA are further separated into four (IgG1-4) and two subclasses (IgA1-2). Our attention will be focused on IgG, which are the most abundant class in serum, with the longest half-life (75% of antibodies in circulation).

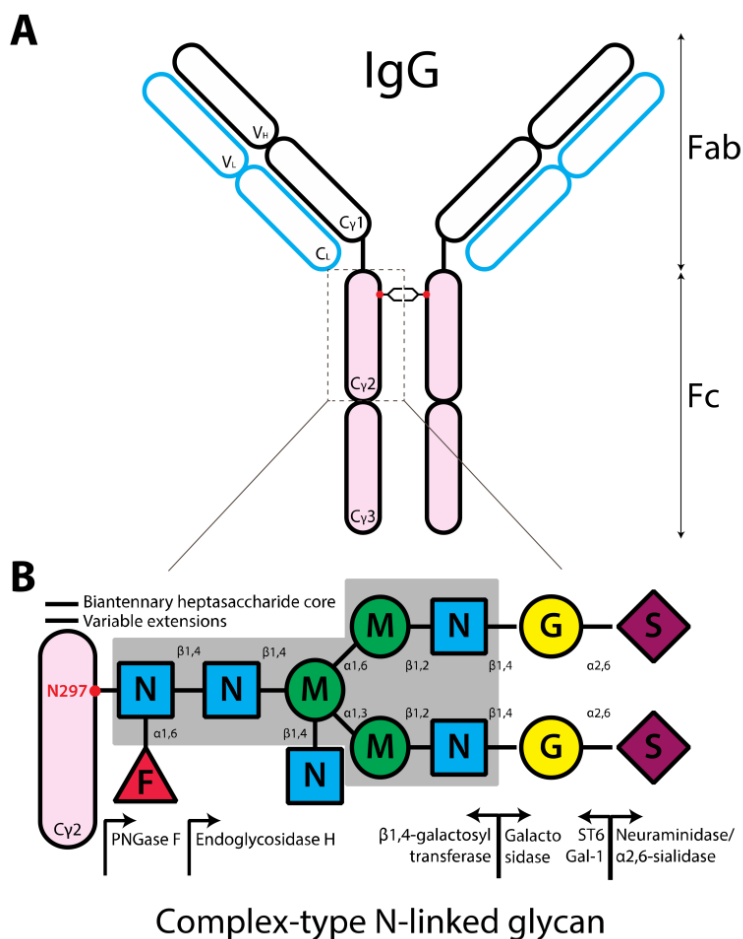


Figure 20: (a) IgG structure. (b) Composition of complex-type N-linked glycans. The enzymes, glycosyltransferases (left arrow) and glycosidases (right arrow), responsible for the addition or removal of the specific sugar, are placed directly underneath of the sugar linkage.

IgG proteins (~150 kDa, 143 x 77 x 40 Å³) are constituted by two heavy chains (**Figure 20 A**, black outline) and two light chains (**Figure 20 A**, blue outline), linked by disulfide bonds to form the characteristic Y-shape structure. Each IgG heavy chain includes a variable region (VH) and a constant region containing three domains (C γ 1-3). On the second heavy chain constant region (C γ 2), IgGs contains carbohydrate moieties (**Figure 20 B**). The line between C γ 1 and C γ 2 represents the hinge region, while the red dot represents N-linked glycans of complex-type. As for the heavy chains also the light chains has a variable (VL) and constant region (CL). The IgGs structure could be divided into antigen-binding fragment, Fab (**Figure 20 A**, empty ovals), and fragment crystallizable region, Fc (**Figure 20 A**, pink ovals). The variable domain bears three hypervariable regions, known as complementary-determining regions (CDRs), which are responsible for the specific antibody-antigen interaction. The diversity in this area justifies the presence of an almost infinite number of types of Abs with different specificity and binding strength (affinity)¹²². The complex-type N-linked glycans is composed by a biantennary heptasaccharide core (**Figure 20 B**, gray block) and a variable extension (**Figure 20 B**, dash line out of the gray block).

The majorities of human IgG Fc glycans are highly fucosylated (<92%) and can be separated into three subsets as determined by the number of terminal galactose, IgG; G0F (~35%), G1F (~35%), and G2F (~16%) for the fucosylated glycans terminating in zero, one or two galactose, respectively. A small portion of these IgG Fc glycans contains a bisecting GlcNAc (>11%). Only 5-10% of IgG Fc glycoforms are mono-sialylated. Furthermore, <1% of IgG Fc glycoforms have two sialic acids^{125,127}.

Keeping in mind the above described Abs structure, it is quite clear that, to preserve the biological recognition activity of the immobilized Ab, an ideal immobilization method should enable the binding at solely single point with a proper orientation, to promote antigen binding under mild conditions (aqueous buffer solutions). To improve antibodies orientation, many immobilization strategies were adopted exploiting the presence of carbohydrate moieties on a unique position on the stem region (Fc, **Figure 20 B**).

Most of the reaction investigated to chemically modify the glycoside chain of the Abs, consist in the oxidation of the sugar chain presents on the Fc region, by different chemical or enzymatic approaches.

Starting from the high-specific non-covalent biotin-streptavidin interaction (**Figure 21a**), Peluso et al. used periodate to selectively oxidize the conserved N-linked glycosylation site on the Fc portion of the Ab. The obtained aldehyde were subsequently biotinylated using the biotin-aminooxy compound ARP, and the biotinilated Abs were immobilized on a streptavidin coated surface¹²⁸. Turkova et al. exploited enzymatic oxidation pathway using galactose oxidase. Once obtained, the

aldehyde functionality was used to selective react with hydrazide groups present on the solid surface (**Figure 21b**)¹²⁹.

As for non-covalent immobilization mechanism, in addition to the previously cited streptavidin-biotin interaction, in the field of carbohydrates lectin interaction has to be taking into account. As it would be later examined in depth (paragraph 3.3.), carbohydrates-lectin is a high-specific and strong interaction, that could be used to selective immobilize the Fc portion of antibodies. Pyrohova et al. used this strong affinity to increase the density of immobilized Abs in an oriented manner¹³⁰.

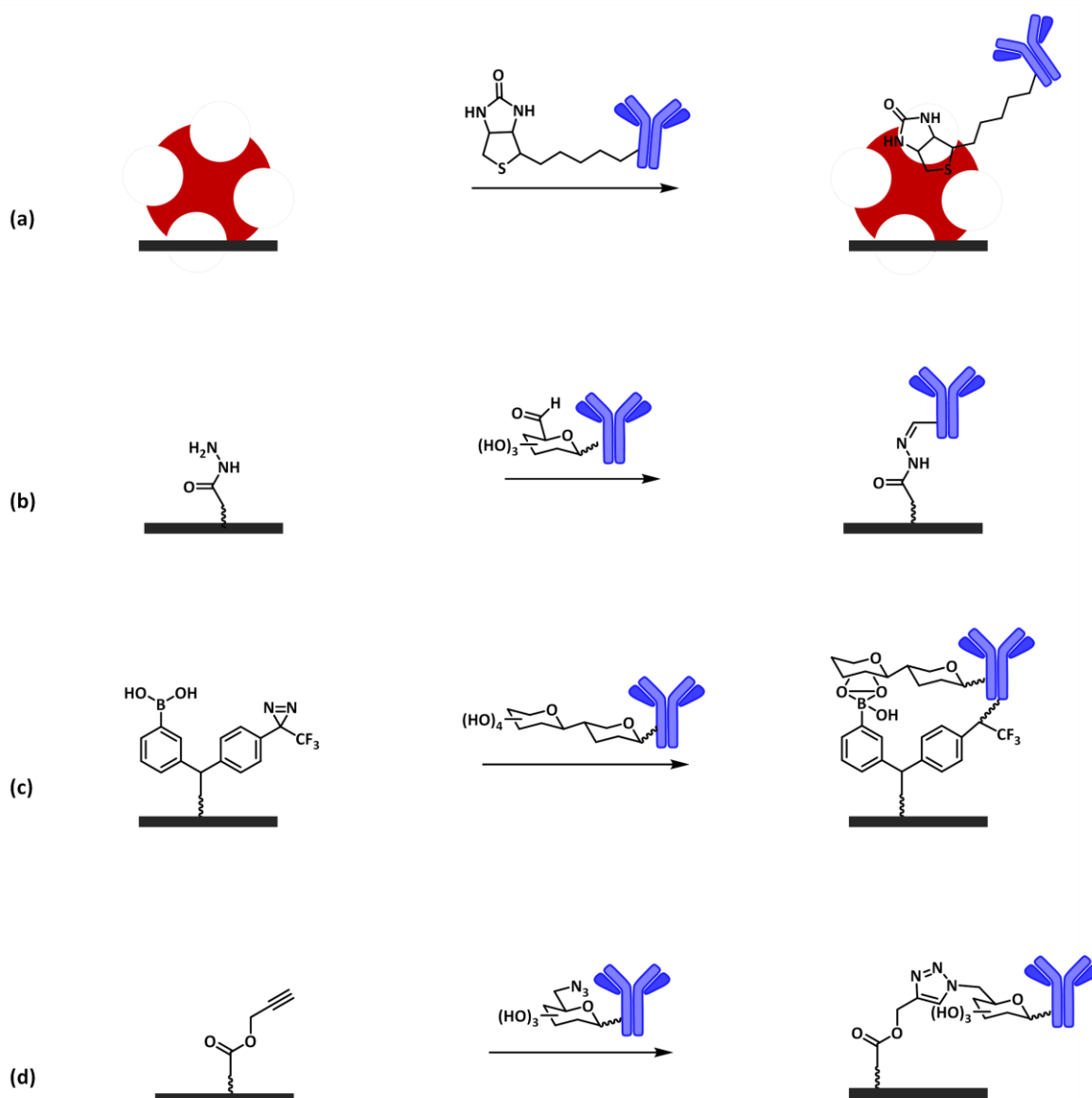


Figure 21: scheme of some of the immobilization chemistry cited above: (a) biotinylated Ab sugar portion to obtain an oriented immobilization through the strongest non-covalent interaction (biotin-avidin) toward a streptavidin coated surface, (b) oxidation of galactose lead to the formation

of an aldehyde functionality, that selective reacts with coated hydrazide solid surface, (c) a photoactive boronic acid surface that is reactive toward glycans Ab portion using a UV photo-cross-linking approach¹³¹ and (d) copper-mediated 1,3-dipolar Huisgen cycloaddition.

Furthermore Adak et al.¹³¹ recently presented a UV photo-cross-linking approach, that utilizes a photoactive boronic acid probe in which boronic acid provided good affinity and specificity for the recognition of glycan chains on the Fc region of the antibody (**Figure 21c**), enabling covalent binding to the antibody upon exposure to UV light. In this way they achieved an oriented immobilization of different antibodies on a surface, retaining their antigen-binding activity.

Moreover, considering the growing application of click chemistry from the beginning of this century, Zeglis et al.¹³² exploited the possibility to enzymatically modify the galactose moieties present on the Fc antibody portion using a system based on an unnatural UDP-galactose substrate azido-modified and a substrate permissive mutant of β -1,4-galactosyltransferase, GalT(Y289L), first designed, engineered, and expressed by Ramakrishnan and Qasba¹³³. Differently from the previously discussed methodology, this system has been used in a number of different settings, and in particular Zeglis et al. proposed this approach for the site-specific radio-labeling of antibodies, combining both enzyme-mediated GalNAz incorporation and bio-orthogonal, strain-promoted, copper-free azide/alkyne cycloaddition click chemistry¹³².

Given the themes discussed above and motivated by the great potential of antibody microarrays as a rapid and effective diagnostic tool, we focused our attention on antibody site-specific enzymatic modifications to optimize antibody microarrays, using a covalent, regio-specific and oriented, copper-mediated, click chemistry immobilization (**Figure 21d**) coupled to the previously introduced polymeric matrix (paragraph 3.1.5.).

3.3. Glycan Microarrays

In recent years, carbohydrate research has gained increase interest as the function of cells and organisms cannot be explained by proteins and nucleic acids alone¹³⁴.

Most oligo and polysaccharides are cell surface carbohydrates or part of the extracellular matrix, while only few polysaccharides are found inside cells¹³⁵. Cell surface sugars are either part of the protective layer that shields cells from harmful physical forces or regulate interactions of cells with the environment. Thus, carbohydrates are involved in most cell–cell interactions, cell motility and cell adhesion processes and in general all the processes that involved cell interactions with their environment, including differentiation, inflammation, fertilization, apoptosis and cell growth^{134,136}. Carbohydrates act in a variety of ways to transmit signals. Some sugars are classical ligands or co-receptors that facilitate cell attachment or mediate signaling.

Unnatural expression of carbohydrates is associated with many diseases including cancer and thus, they are also important drugs and drug targets^{137,138}.

Many studies are dedicated to exploiting the cell specific expression of carbohydrates for cell targeting. Carbohydrates or carbohydrate binding proteins are also present on the cell surface of pathogens and can mediate their cellular absorption. Unique carbohydrate structures on pathogens are exploited to generate carbohydrate-based vaccines¹³⁹. Some viruses and bacteria use cell surface sugars to gain entry into host cells¹⁴⁰. For example, blocking carbohydrate-processing enzymes with inhibitors, such as Tamiflu¹⁴¹, at an early stage can terminate influenza virus infections.

Carbohydrate complexity is a major challenge for studies focusing on interactions with other biomolecules¹⁴².

The assessment of the biological function of a particular carbohydrate remains challenging. Knock-out techniques yield insights into sugar function and interactions¹⁴³, but they are time-consuming. Biochemical studies of carbohydrates are complicated by the fact that the interactions are often weak. Efficient binding relies on multivalent interactions¹⁴⁴ that are experimentally difficult to measure. Carbohydrate heterogeneity and the cross-reactivity of sugar binding proteins require large numbers of carbohydrate ligands to be screened. To overcome or circumvent these challenges, novel tools for glycomics have been developed¹⁴⁵, including carbohydrate microarrays that specifically are focused on the needs of studying carbohydrate interactions.

Glycan microarrays were first introduced in 2002 with publications by several independent groups aiming to systematically array this class of biological molecules. Two reports demonstrated

robotically printed arrays of diverse glycan libraries⁴⁰, and many other laboratories demonstrated various approaches for immobilization of glycans in printed slide or multi-well plate formats^{41,42}. These achievements were a natural extension of the successful development of printed arrays of other classes of biomolecules, including DNA arrays in 1995¹⁴⁶, and recombinant protein arrays a few years later¹⁴⁷.

In the years following the first reports of large-scale glycan microarrays, there has been an explosion of interest for developing glycan libraries, efficient methods of immobilization of glycans on array surfaces, and applications for analysis of glycan binding protein specificity.

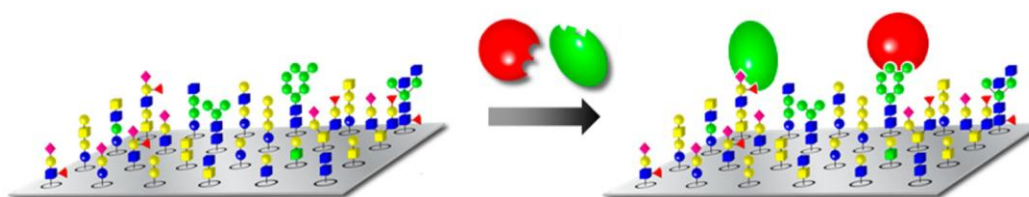


Figure 22: Figurative glycan microarray experiment.

The principle of the technique is similar to DNA and protein microarrays and consists on the immobilization of the desired glycans onto a properly modified solid surface through a covalent or non-covalent binding. The array is obtained through the printing of micromolar carbohydrate solution by means of a robot.

The advantage, in the use of a microarray format, is that only few picoliters of glycans are required, allowing high-throughput analysis of several carbohydrate molecules and minimal amount of carbohydrate needed for each binding experiment, making most out of the precious material.

After the immobilization, the target proteins are incubated on the microarray to allow them to bind the exposed glycans before unbound proteins are washed from the surface. If necessary, fluorescent tag binding proteins are incubated subsequently in a similar fashion (**Figure 23**). Following the incubation, the slides are dried and scanned with a microarray confocal scanner laser. The fluorescence intensities represent the amount of ligand bound to the chip (the avidity-affinity between the ligand and the target). Varying the tag used to label the target protein, or its complementary, one could also detect the interaction through chemiluminescence or colorimetry.

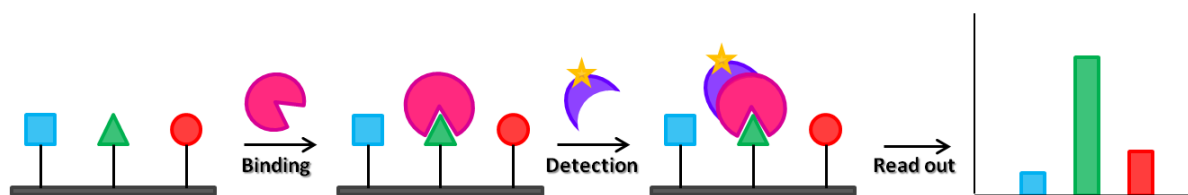


Figure 23: Exemplified microarray experiment for protein binding. Binding of the protein to the arrayed sugars, binding of the fluorescently labelled detection protein, read out by a fluorescence scanner and analysis.

A large number of different immobilization strategies have been used for sugar arrays, exploiting different reactive functionality, as previously described in 3.1.6., such as amine toward active ester or epoxy groups and various “click reactions” such as maleimide-thiols, azide-alkyne, etc.

Generally, the carbohydrates can be either isolated from natural sources or chemically synthesized.

A number of groups have been examining strategies for producing “natural glycan arrays”. The basic approach involves: a) isolating mixtures of glycans from natural sources such as cells, tissues, pathogens, milk, or urine, b) derivatizing the glycans with a linker/tag (if necessary) to facilitate purification and allow immobilization on array surface, and then c) separating the mixture into individual components or sub-fractions.

This approach offers a number of advantages: the organism synthesizes the glycans, in principle one can access the entire glycome, and one can focus studies on the glycans found in a particular target cell, tissue, or sample.

On the other hand, to be effective, this approach needs efficient and reliable methods to derivatize the glycans, powerful separation and purification techniques (impurities could interfere with the carbohydrates analysis not being ruled out¹⁴⁸), and methods to identify and characterize the unknown glycan structures.

In addition, each of these steps must be amenable to very small scale, since many individual glycans are only present in minute amounts.

On the other side chemical, chemo-enzymatic or enzymatic carbohydrates synthesis is also available as an alternative to isolating glycans from natural sources. The primary advantages are the control of the target structure being synthesized, the ability to produce larger quantities, if compared with the isolated ones, of homogeneous material and the possibility to increase sugars structural diversity^{134,148}. The chemical synthesis relies on the sequential coupling of appropriately protected carbohydrate building blocks¹³⁹. Following oligo-saccharide assembly, all protective

groups are removed and the linker is either installed or liberated, if it was present in protected form during the synthesis.

In chemical synthesis, the similar reactivity of the hydroxyl groups on the sugar ring requires complex blocking strategies with different protecting groups on the glycosyl acceptor, and a suitable leaving group at the anomeric position of the glycosyl donor. Although enzymatic synthesis provides an alternative, relying on the specificity of the enzymes to form the desired glycosidic linkage, the limited availability of glycosyltransferases continues to impede the generality of this approach¹⁴⁹. Nevertheless the need of libraries containing diverse carbohydrate structures stimulate the development of sophisticated techniques to chemically, enzymatically, and chemo-enzymatically rapidly synthesize glycan libraries. Solid-phase synthesis, carried out by Seeberger et al.¹⁵⁰, and OptiMer-based one-pot solution-phase method, presented by Wong and colleagues¹⁵¹, are examples of these techniques.

Among the synthetic carbohydrates, glycomimetics have been developed to antagonize the action of specific lectins in natural settings. They are designed mostly by trial and error processes, supported by molecular modeling of ligands and/or of ligand-lectin complexes^{152,153,154,155,156}. Such molecules find application as tools to interrogate the glycobiology of human lectins, which is still largely unknown in its molecular details, and can also be used as leads in drug discovery programs in fields ranging from antibacterial, antiviral and anti-inflammatory drugs. Drug discovery programs based on glycomimetics are greatly facilitated by the availability of glycomimetic arrays, which can be interrogated with individual lectins to identify specific leads.

Although the principle of carbohydrates microarray is the same of DNA and proteins, glycan arrays have revealed some specific aspects of sugar-protein interactions (i.e. multivalency). Biochemical studies of carbohydrates are complicated by the fact that the interactions are often weak¹⁴⁴, but thanks to the microarray format a surface higher concentration could be reached, mimicking sugar presentation on cell surfaces¹⁵⁷.

3.3.1. Multivalency and carbohydrates presentation

In all the interactions occurring in a natural environment, multivalency is one of the key principle for achieving strong and yet reversible interactions. The burr and its man-made analogous material (**Figure 24**), velcro, are good examples from daily life. The large amount of anchoring/coupling points, present on a side of the velcro allows, despite the weakness of the single interaction, a stronger final binding; therefore, the greater the surface, the stronger the binding.

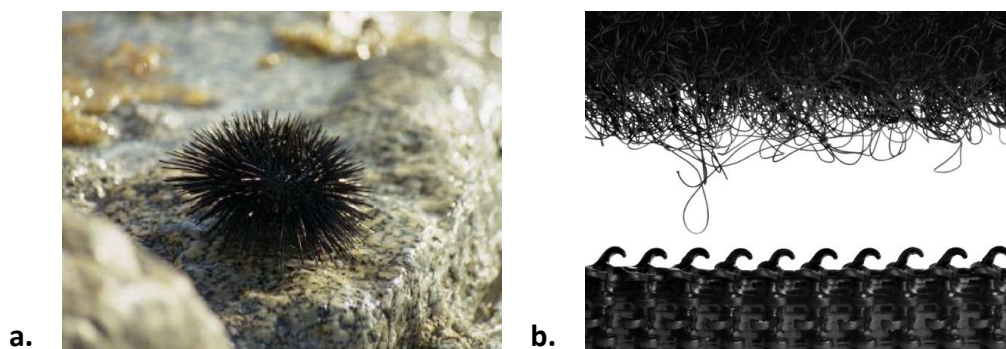


Figure 24: The principle behind the burr and nature-inspired velcro can be transposed to the molecular level.

On the molecular level, one can compare the hooks seen in the macroscopic example from nature with specialized molecular binding units (ligands) and the corresponding loops with the binding pockets in a complex molecule (receptor). Biologically speaking, such multivalent interactions between cells or with other organisms, such as bacteria and viruses, wherein the extensive interaction between a large number of individual binding partners plays a major role, are medically very important.

In contrast to weak monovalent binding, multivalent interactions offer the advantage of a multiple, and thus dramatically enhanced, binding on a molecular scale¹⁵⁸. In the case of glycans, since the individual protein–carbohydrate interactions are weak, it often takes a multitude of simultaneous interactions, i.e. multivalency, to produce a biological effect¹⁵⁹. Since blocking the carbohydrate binding proteins or lectins may be beneficial for treating certain diseases, the aspect of multivalency cannot be ignored. For this reason, the incorporation of multivalency into the design of inhibitors may be necessary to achieve sufficient inhibitory potency, and the development of a high-sensitivity analytical platform, that could monitor the behaviour of glycans moving from multi- to mono-valent conditions, could be an important breakthrough in carbohydrate research¹⁵⁷.

Mono- and oligosaccharides immobilized on a solid surface are likely to behave like cell-surface carbohydrates and bind biomolecules of interest in a specific manner, allowing the study of multiple interactions simultaneously. The high local concentration on the array slide mimics the multivalent presentation of glycans on proteins or cell surfaces, and allows for the detection of carbohydrate-protein interactions, which are typically intrinsically weak in a monovalent format as explained before^{160,161}.

Together with the multivalency aspect, presentation still remains the major bottle-neck for carbohydrate recognition in a microarray format^{134,148,162}. It has been observed that the type of linker used to immobilize the glycan on the surface may affect the ability of a glycan to be

recognized by its binding protein^{163,164}. Linker-dependent false-negative binding has been attributed to the influence of the spacer on the presentation of the glycan relative to the support surface. Ideally, the linker would present the glycan in the same way as it is found in natural conditions, but this is impossible with non natural linkers and surface.

As a consequence, the ability to immobilize a variety of different carbohydrates on the same surface, with proper spacing and orientation^{148,149, 165} plays a crucial role in the study of sugar-lectin interactions, that is translated in the success of any experiment, since the final performance of a microarray biochip strongly depends on parameters related to the immobilization process itself.

Polymeric coatings, yielding 3D matrixes rather than flat surfaces may significantly alleviate many of the presentation problems observed in glycoarrays¹⁶⁶. However, to the best of our knowledge, no 3D matrixes have ever been employed in the construction of glycoarrays. As a part of this thesis, a glycan array was built on a 3D polymeric matrix using our clickable polymer for ligand immobilization. The results of this work are discussed in **Chapter 7** of this thesis.

3.3.2. Glycan microarrays: tools for research and diagnostics

Soon after the first proof-of-principle glycan arrays had been constructed and used, the focus turned to applications addressing glycomics research (**Figure 25**).

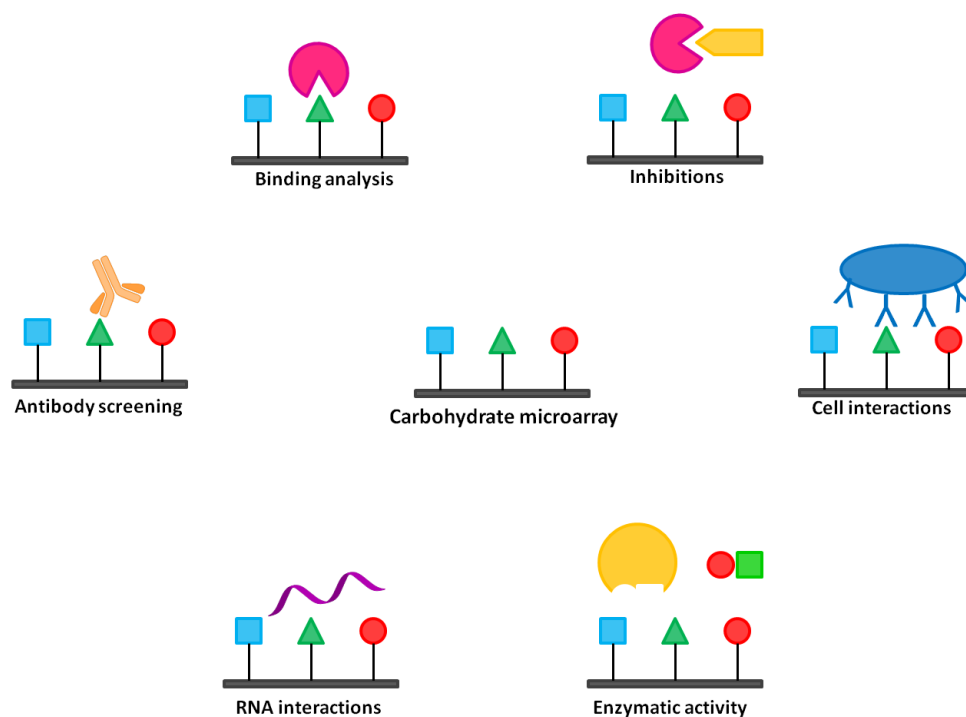


Figure 25: Different applications of carbohydrate microarrays.

Potential binders are added to the sugars on the microarray surface and the binding intensities are measured by a fluorescence reporter. Sugar binding preferences can be determined by comparing the spot fluorescence intensities. Protein–sugar interactions have been thoroughly established and provided valuable information regarding carbohydrate action in vivo.

Screening for inhibitors of carbohydrate-mediated interactions and determination of IC₅₀ values can be performed by co-incubation of the binding molecule with an inhibitor⁴¹.

In addition, kinetic constants can be calculated using carbohydrate microarrays¹⁶⁷. Binding intensities at various dilutions are measured and kinetic constants can be determined.

Since whole cells¹⁶⁸ and viruses bind⁹⁰ to carbohydrates on microarrays, sugar interactions of an entire organism can also be determined without purifying the carbohydrate-binding proteins. Carbohydrate binding bacteria can be detected in crude mixtures and isolated for detailed examination.

In an early, ground-breaking experiment, ten different proteins were tested against 200 arrayed sugars, using fluorescence detection⁹⁰. Several new interactions were identified due to the large number of sugars on the array. A detailed binding pattern for each protein was established, including fine differences in specificity. These experiments proved that carbohydrate microarrays are suitable for the high throughput investigation of most carbohydrates.

The new carbohydrate microarray system was exploited to analyze glycan dependent interactions of two HIV-1 envelope proteins, gp120 and gp41⁸⁹.

Carbohydrate microarrays were also used to investigate the action principle of different enzymes, such as glycosyl-, fucosyl-, galactosyl- and sialyl-transferases¹³⁴.

Microarrays also offer an attractive platform for diagnostic applications since many binding events can be screened in parallel. Bacterial adhesion to carbohydrate microarrays was investigated for *E. coli*, as the sugar based attachment to the urinary tract renders these bacteria into harmful pathogens¹⁶⁸. It was demonstrated that *E. coli* bacteria bearing a receptor protein (Fim H) that interacts with mannose, bind specifically to mannose on carbohydrate microarrays while bacteria lacking Fim H do not bind.

With the constant increase of carbohydrates research, also the analytical application has considerably grown. The official archive that collects more or less all the data obtained in the glycomics field is the “Consortium of Functional Glycomics”.

This project was born in the USA in 2001, promoted by the increasing quantities of research groups that focused their attention on carbohydrate interactions study, with funding coming from an

NIGMS Large-Scale Collaborative Project Award, also known as a 'glue grant'. At the beginning of the project, the program had the aim to define examples where protein-carbohydrate interactions mediate cell communication. To achieve these goals they initially focused their studies on:

1. the three major classes of mammalian glycan-binding proteins (GBPs): C-type lectins, galectin and SIGLEC;
2. immune receptors that bind carbohydrates: CD1, T cell receptor, and anti-carbohydrate antibodies;
3. GBPs of microorganism that bind to host cell glycans as receptors.

The Consortium of Functional Glycomics (CFG) comprises eight core facilities and more than 500 participating investigators, that work together to develop resources and services, and make them available to the scientific community free of charge. Its goal is to provide a networking forum and glycomics resources which enable investigators to reveal functions of glycans and glycan-binding proteins that impact human health and disease. The data generated by these resources are collected in databases accessible through the Functional Glycomics Gateway.

Furthermore, the CFG offers glycan microarrays screening services, a reagent bank, and free access to its extensive data repositories and molecule databases.

The Consortium also developed molecule databases for glycan-binding proteins, glycan structures, and glycosyltransferases, which integrate CFG-generated data and information from other publicly available databases. The available datasets, together with the molecule databases, are highly interconnected, representing an important step towards an integrated systems biology approach to glycobiology¹⁶⁹.

4. Lectins: Glycan Binding Proteins

Lectins (from *lectus*, the past participle of *legere*, to select or choose)¹⁷⁰ are defined as carbohydrate binding proteins, other than enzymes or antibodies, and exist in most living organisms, ranging from viruses and bacteria to plants and animals. Thanks to their involvement in diverse biological processes in many species, such as clearance of glycoproteins from the circulatory system¹⁷¹, adhesion of infectious agents to host cells, recruitment of leukocytes to inflammatory sites^{172,173}, cell interactions in the immune system, in malignancy and metastasis, their study is of upmost interest.

The first pure lectin, concanavalin A (Con A, from jack beans), was isolated in 1919 by Sumner¹⁷⁴, and its sugar specificity was then demonstrated¹⁷⁵.

Lectins interact with carbohydrates non-covalently, in a manner that is usually reversible and highly specific¹⁷⁶. Classical lectins contain two or more carbohydrate-binding sites; therefore, their interaction with sugars on the surface of erythrocytes results in the cross-linking of several blood cells and their subsequent precipitation. This phenomenon, known as cell agglutination, is a major attribute of the activity of lectins and has been used classically and routinely for their detection and characterisation (however it is now recognised that cell agglutination is not a defining feature of lectins¹⁷⁷). Both the agglutination and precipitation processes are inhibited by the carbohydrate for which the lectin is specific.

According to the monosaccharide ligand toward which they exhibit the highest affinity, lectins were first classified into five groups: mannose, galactose/N-acetylgalactosamine, N-acetylglucosamine, fucose and N-acetylneuraminic acid¹⁷⁸. However this classification, that ignores certain important monosaccharides such as mannose-6-phosphate and N-acetylgalactose-4-sulfate, is becoming obsolete.

Supported by marked differences in the fine specificities of lectins within a single category, and by the discovery of an increasing number of lectins, lacking of a high affinity toward simple saccharides, a new lectins classification was made; it is based on the lectins grouping, considering their similar sequences and structural organization. Furthermore, sequence similarity with known lectins provides a valuable guideline for the identification of new ones.

Most lectins belong to three classes: (1) simple, (2) mosaic (or multidomain) and (3) macromolecular assemblies.

(1) Simple lectins consist of a small number of subunits, not necessarily identical, each of molecular weight usually below 40 kDa. Each monomeric unit contains a carbohydrate-binding site. This class comprises practically all known plant lectins¹⁷⁹ and most members of the galectin family (formerly known as S-lectins), a group of β -galactoside specific animal lectins¹⁸⁰.

- (2) Mosaic lectins (or multidomain) are composite molecules consisting of several kinds of protein domains, only one of which possesses a carbohydrate-binding site. This class includes diverse proteins from different sources: viral hemagglutinins¹⁸¹ and animal lectins of C-, P- and I-types¹⁸².
- (3) Macromolecular assemblies are common in bacteria. They are filamentous organelles consisting of helically arranged subunits (pilins) assembled in a well-defined order¹⁸³.

A particular emphasis was addressed on legume lectins. Their abundance in plant seeds, their solubilities and their wide range of saccharide specificities make them good model systems, tools for elucidating protein-carbohydrate interactions as well as for biomedical and biotechnological applications.

4.1. Legume lectins

Legume lectins represent the largest and most thoroughly studied family of simple lectins. Concanavalin A (Con A), the lectin from the jack bean, is the prototype member of the family. The relative abundance of this protein in jack bean, the ease of its preparation and the large number of saccharides with which it can interact, have led to numerous studies on Con A, markedly accelerated by the discovery in 1969 that cells transformed by DNA tumour viruses or carcinogens were agglutinated by the lectin more readily than normal cells¹⁸⁴.

4.1.1. Structural features

Typically, legume lectins consist of two or four identical or near-identical subunits (protomers) of 25–30 kDa each, which are commonly single polypeptide chains of about 250 amino acids presenting one or two N-linked oligosaccharides. Each protomer typically contains a carbohydrate-combining site, a tightly bound Ca^{2+} and a transition metal ion, usually Mn^{2+} . Approximately 20% of the amino acid residues are invariant in all legume lectins and another 20% are similar. The conserved amino acids include several of those involved in the interaction with the saccharide and almost all the residues that coordinate the metal ions. The resolution of 3D-structures of about ten legume lectins has shown that each subunit is constituted largely (~ 60%) of β -strands mutually connected by loops. The tertiary structure is made up of two anti-parallel β -sheets, a six-stranded flat “back” and a seven-stranded curved “front”, connected by a five-stranded β -sheets, giving the well known “jellyroll” motif, also referred to as the “lectin fold”¹⁸⁵ (**Figure 26 a**).

The subunit structures of different legume lectins can be nearly superimposed, without considering proteins’ specificity. Despite their similarities at the primary, secondary and tertiary structural

monomeric level, legume lectins exhibit considerable variation in their quaternary structure: the monomers' association modes is affected by small differences in the amino acid sequences at the monomer-monomer interfaces and the presence/absence of glycosylation. In the case of lectins with "canonical" quaternary structure, such as Con A, PEA lectin, Favin and L. Ochrus, dimerisation involves anti-parallel side-by-side alignment of the flat six-stranded β -sheets of the two monomers, resulting in the formation of a continuous 12-stranded sheet that extends across the dimer interface.

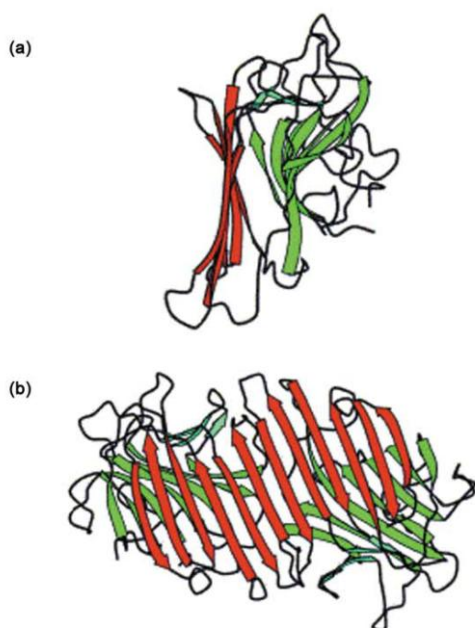


Figure 26: (a) representative tertiary structure of a legume lectine monomer; (b) dimeric structure of ConA.

Further association of two dimers gives the tetrameric assembly of, for example, Con A, observed in physiological conditions¹⁸⁶. As with most plant lectins, the quaternary structure, such as the one of ConA and PNA, depends on the pH (see paragraph on Concanavalin A). The lectin is a tetramer at physiological pH¹⁸⁷, and dissociates reversibly into dimers at acidic pH, where the exact value depends on the considered lectin (i.e for ConA is under 5.8, while for PNA is below 3.4¹⁸⁸).

4.1.2. Carbohydrate-binding site

During the past 25 years there has been significant progress in explaining the features of lectins involved in carbohydrate binding. X-ray crystallography of the proteins complexed with their ligands, site-directed mutagenesis experiments and molecular modelling have allowed the identification of the chemical groups belonging to both interacting species involved in the binding and of the types of bond formed. Studies of lectin-oligosaccharide complexes are especially interesting, providing the basis for the understanding of the proteins' interaction with natural

ligands. Generally, lectins show very good specificity for di-, tri- and tetrasaccharides, with association constants significantly higher than those for the corresponding monosaccharides.

Carbohydrate-binding sites are often superficial depressions on the surface of the protein. In all cases the combining site appears to be preformed¹⁸⁹, since few conformational changes occur upon binding. In all legume lectins, independently from their specificity, four invariant amino acid residues participate in the ligand binding, with an exception for ConA¹⁹⁰.

However, despite the conservation of key amino acids involved in the binding of the carbohydrate, different legume lectins can show different specificity. For instance, while Con A binds mannose and glucose, PNA, and SBA, for example, bind galactose. Therefore, while the multiplicity constellation of highly conserved amino acids provides the framework required for binding, specificity apparently arises from the variability of amino acid residues in other regions of the combining pocket¹⁹¹.

The Ca²⁺ and Mn²⁺ (or other transition metal) are situated around 4 Å apart and in close proximity to the sugar-combining pocket. Although not always directly involved in the carbohydrate binding, the cations help the positioning of the amino acid residues interacting with the glycoside.

Lectins bind carbohydrates through a network of hydrogen bonds and hydrophobic interactions. Van der Waals forces, although rather weak (usually a fraction of 4.2 kJ mol⁻¹ for each pair of atoms), are frequently numerous, contributing significantly to the overall binding¹⁷⁸. The steric disposition of hydroxyl groups in carbohydrates creates hydrophobic patches¹⁹² on the sugar surface that can interact with hydrophobic regions of the protein¹⁹³. Furthermore, tightly bound water molecules can in effect be considered as structural, i.e. an extension of the protein surface, playing a significant role in carbohydrate recognition, imparting in some cases exquisite specificity. In general, water molecules in the carbohydrate-binding region mimic the ligand to a substantial extent not only at the primary site, but also in the regions adjacent to it.

4.1.3. Physiological functions

Despite their long history, the true physiological role of legume lectins is still not well understood. Many hypotheses have been formulated in the course of the years but, at present, no physiological function for any legume lectin has been established with certainty. The difficulty to fully understand their precise role arises from several of their features. The defining characteristic of all lectins is their carbohydrate-binding ability. This activity has been preserved during evolution, suggesting that it is essential for the exploitation of their function.

In general, a single legume plant can contain a variety of lectins that may have evolved by gene duplication and become specialised for different roles in the plant¹⁹⁴. Furthermore, despite being concentrated in plant seeds, lectins are also present in different tissues, where their function

probably requires lower concentrations. One of the most validated theories on legume lectins' physiological role considers them as defence agents against predators¹⁹⁵. An essential feature of any active defence agent is the ability to recognise specifically the pathogen. Based on their carbohydrate-binding specificity and also considering their abundance in plant seeds and bark, lectins seem to possess all the necessary characteristics to exploit this function. Early investigators noted the similarities of lectins to antibodies and hypothesised that lectins might function as plant antibodies.

Furthermore, based on their carbohydrate-binding ability, lectins have also been thought to be involved in the establishment of symbiosis between nitrogen-fixing bacteria and plants¹⁹⁶. Legumes are able to associate specifically and form symbioses with soil bacteria of the rhizobia family, a phenomenon that makes them independent from soil nitrogen supplies. The nitrogen-fixing symbiosis is a multistep process that requires the formation of the root nodule, followed by the adhesion of the bacteria to the roots and, finally, the internalisation of the bacteria into the nodule¹⁹⁷. However, despite the fact that molecular genetics experiments support this hypothesised role of lectins as receptors for oligosaccharides produced during the symbiosis processes, several inconsistencies can be pointed out. First there is no proof of the presence of lectins and of the respective ligands on the two interacting species, and second, the correlation between the sugar specificity of legume lectins and their ability to recognise bacteria appears not to be particularly strong¹⁹⁸.

In other words, even if all the hypotheses born around the physiological functionality of legume lectins were considered, their exact biological role still remains unknown, but their specific saccharide-binding properties make them an ideal object for the study of protein–saccharide interactions¹⁹⁹.

4.2. Concanavalin A

As a part of this work I examined legume lectin Con A interacting with eight different glycomimetics, synthesized in the laboratory of Professor Anna Bernardi at University of Milan, through microarray analysis on a polymer-coated chip.

Concanavalin A, as briefly described before, belongs to the legume lectins family. It was the first pure lectin isolated in 1919 by Sumner¹⁷⁴ from the jack bean. This lectin generally binds to saccharides containing α -D-mannose or α -D-glucose residues but it could also recognize oligosaccharide sequences lacking these units. Con A has specific biological activities which depend on its binding to cell surface receptors. It preferentially agglutinates certain cells transformed by oncogenic viruses more than their untransformed counterparts, inhibits growth of malignant cells

in animals, and exhibits mitogenic activity. It has also been used in studies on the number and mobility of cell-surface receptors associated with cell–cell interactions¹⁹⁹.

The monomer of Con A is composed of 237 amino acid-residues that form 2 anti-parallel β -sheets. A curved ‘front’ β -sheet of 7-strands aligns with a flat ‘back’ β -sheet of 6-strands, these two are connected by another 5-strands ‘roof’ β -sheet from the front to the back. Two Con A monomers lay in an adjacent, anti-parallel and back-to-back manner, form a dimer. Two dimers form a tetramer in the same way (Fig. A)^{200,201}. Each monomer has the saccharide-binding site on the outer surface of the tetramer (spaced ca. 72 Å from each other¹⁵⁹), and the amino acids that participate in the interaction of Con A with the substrate are Tyr-12, Pro-13, Asn-14, Thr-15, Asp-16, Leu-99, Asp-208 and Arg-228. The structural organization of ConA is pH dependent: at physiological pH exists as a tetramer, otherwise, at pH lower than 5.8, as a dimer²⁰².

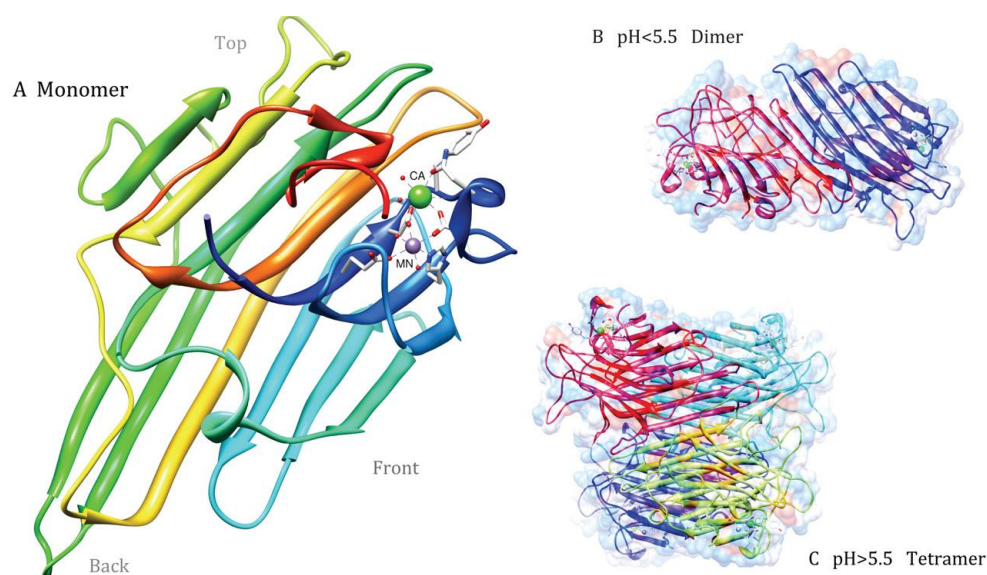


Figure 27: Molecular structures of Concanavalin A (ConA). (A) The primary and secondary structures of ConA, binding Mn^{2+} at S1 and Ca^{2+} at S2; (B) The crystal three-dimensional structure of ConA; (C) The quaternary structure of ConA.

Concanavalin A (ConA) is a Ca^{2+}/Mn^{2+} dependent. Each monomer contains a tightly bound manganese and calcium ion in the vicinity of the saccharide binding site. Each of the metal ions is coordinated by four amino acid side chains and two water ligands. In all four subunits the coordination of the manganese ion is octahedral, whereas the calcium ion has pseudo-octahedral geometry, with Asp10 binding in a bidentate manner capping the sixth vertex of the octahedron. In the case of the calcium ion, one of the water ligands forms a bridge between the metal and the main carbonyl chain of Asp208, thus stabilizing the unusual Ala207–Asp208 cis-peptide bond that is conserved in all known legume lectin crystal structures¹⁹⁹.

Concanavalin A has generated a rising attention for its anti-proliferative and anti-tumour activities towards various types of cancer cells. Con A has been reported to kill tumour cells targeting apoptosis, autophagy, anti-angiogenesis as well as immunomodulatory. These findings shed light on new perspectives of Con A as a potential anti-neoplastic agent for cancer therapeutics. However, the exact biological role of Con A remains unknown, but its specific saccharide-binding properties make it an ideal object for the study of protein–saccharide interactions¹⁹⁹.

5. High-performing microarray platform: solid support and polymeric matrix

5.1. Click-chemistry for surface modification: introduction of an alkyne functionality

The majority of reports present in the literature, that discuss the immobilization of probes onto a solid surface through “clickable” procedures, require multi-step approaches to introduce click functionalities (i.e. alkyne).

For example, Chaikof et al. in 2006¹⁰⁰ set up a procedure to introduce alkyne functionality onto a solid surface creating a self-assembled monolayer (SAM) through a short bi-functional PEG linker carrying alkyne and cycloaddition groups at opposite chain termini. The Diels-Alder reaction would allow the coupling of the short PEG with the maleimide functionalized glass slide commercially available, exposing in this way the alkyne functionality for copper-mediated bioconjugation (see Figure 16, paragraph 3.1.6.1.). The first coupling needs 12 hours of reaction time at room temperature, and the blocking of unreacted maleimide groups requires a further reaction with cysteine before “clicking” azido-probes. Pioneers in the area of clickable SAMs are Collman and Chidsey, who reported several important examples of SAMs functionalized by triazole linkages²⁰³. Their work primarily focused on gold surfaces, but was extended by other groups to different types of substrates such as silicon wafers or glass slides²⁰⁴.

Zhang et al. in 2006²⁰⁵ presented SAMs of carbohydrates on gold surface for surface plasmon resonance. They functionalized gold surface with a N,N'-(dithiodidecane-10,1-diyl)bispropiolamide (NDDA) that, besides a quite laborious synthesis, needs anhydrous ethanol solution in an overnight incubation step at 4°C to coat the surface.

Some years later Miura et al.²⁰⁶ published a work reporting on the functionalization of silicon, glass and quartz surfaces with a self-assembled monolayer of saccharides via click chemistry (**Figure 28**), through a silanization step for immobilizing the alkyne moieties onto the surface through a reaction with silanols.

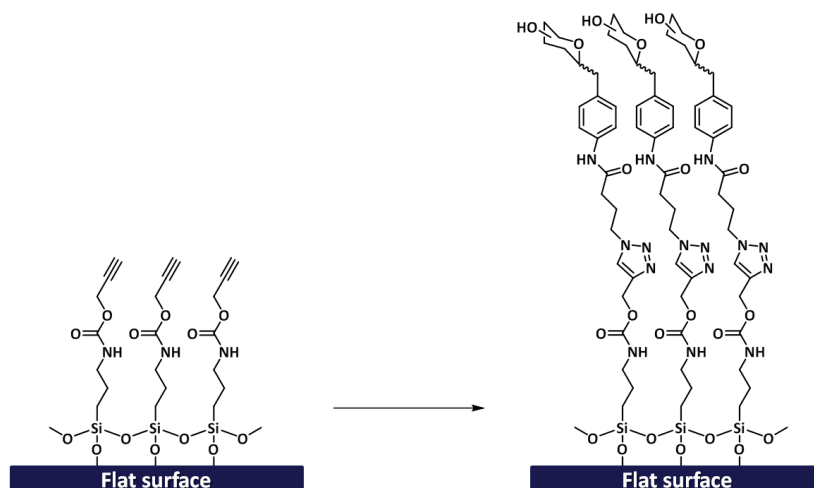


Figure 28: Schematic illustration of surface functionalization through the formation of carbohydrate self-assembled monolayers (SAMs) using click-chemistry as reported by Miura et al.²⁰⁶.

As most of the silanization processes reported in the literature, the SAMs formation needs at least 4 hours to be completed and the coating produced do not have the same antifouling character of a polymeric coating.

A number of works reported in the literature describe also the synthesis and characterization of polymeric coatings, that introduce functionalities promoting the regio-specific Huisgen cycloaddition^{207,208,209,210,211,212}. An example is given by the work recently published by Russel and co-worker in 2013 (**Figure 29**). They reported the synthesis of a novel alkyne-functionalized diblock copolymer (di-BCP), poly(methyl methacrylate-random-propargyl methacrylate)-block-poly(4-bromostyrene), synthesized by atom transfer radical polymerization (ATRP), and its use for the development of functionalized nanostructured materials via alkyne/azide click chemistry²¹³.

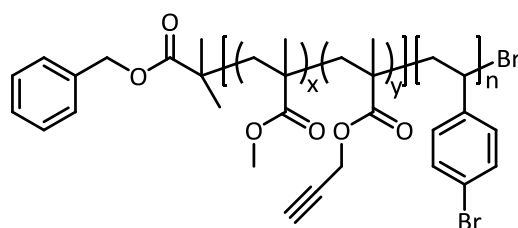


Figure 29: structure of the novel diblock copolymer (di-BCP) reported by Russel and co-worker²¹³.

However, in spite of the intense activity in the field of 'clickable' polymer coating, for the best of our knowledge, there are no examples in the literature of polymeric coatings obtained with processes as fast and robust like the one presented by this thesis.

5.1.1. Design of poly(DMA-PMA-MAPS): structure and characterization

In this work, a novel copolymer named poly(DMA-PMA-MAPS), obtained from the polymerization of N,N-dimethylacrylamide (DMA), 3-trimethylsilyl-prop-2-yn methacrylate (PMA) and 3(trimethoxysilyl)-propylmethacrylate (MAPS) was introduced (**Figure 30**).

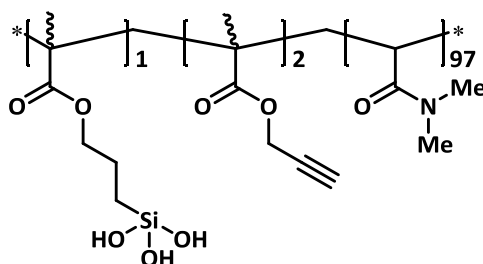


Figure 30: structure of poly(DMA-PMA-MAPS) The molar fraction of the monomers MAPS, PMA, and DMA monomers is 1, 2, and 97 respectively.

5.1.1.1. Synthesis of poly(DMA-PMA-MAPS)

The acryloyloxy-alkyne monomer was synthesized starting from commercially available trimethylsilylpropyn-1-ol reacting with metacryloyl-chloride in the presence of triethylamine (TEA) as the base (**Figure 31**), following a procedure reported by Ladmiral et al. (see materials and methods, paragraph)²¹⁴.

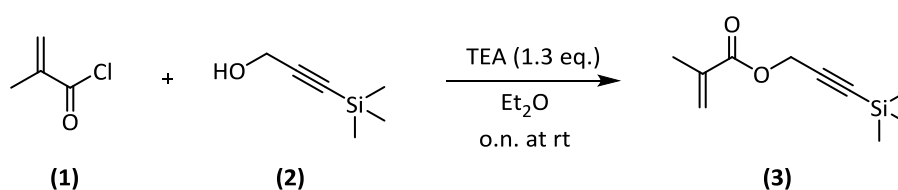


Figure 31: reaction scheme of the synthesis of protected alkyne monomer (PMA).

Poly(DMA-PMA-MAPS) was synthesized¹⁰ in THF via random free radical polymerization, thermally initiated by AIBN (azoisobutyronitrile) from the three monomers in different concentration (**Figure 32**), as described in materials and methods, and it was characterized through ¹³C-NMR.

The alkyne-monomer protected with TMS (compound (3), **Figure 31**) was used in the free radical polymerization due to the instability of the triple-bond under radical condition. After the polymerization, to provide available alkyne functionality for probes immobilization, a deprotection step was carried out in an aqueous solution of K₂CO₃ (pH≈9) as described in materials and method (paragraph 9.2.1.).

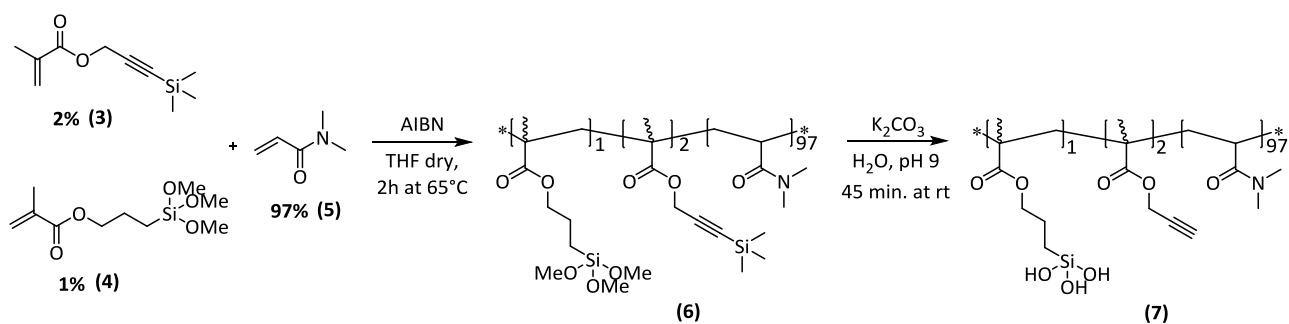


Figure 32: Synthesis of the poly(DMA-PMA-MAPS) copolymer. In brackets the molar fractions of the monomers (w/v).

5.1.1.2. Characterization of poly(DMA-PMA-MAPS)

¹³C-NMR poly(DMA-PMA-MAPS) analysis

¹³C-NMR analysis was made before and after the deprotection step, to highlight the presence and the absence of trimethylsilyl protecting group on alkyne moiety (**Figure 33**).

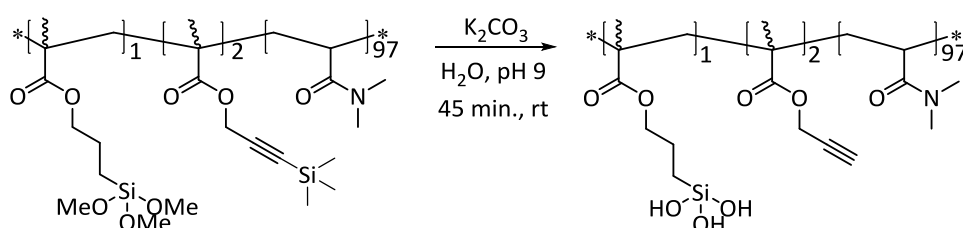


Figure 33: poly(DMA-PMA-MAPS) before and after the deprotection.

Furthermore two different solvents, DMSO (d_6) and $CDCl_3$, were used to resolve overlapping resonances of the signals of interest with the solvent signals. NMR samples were obtained by dissolving 50 mg of compound in 2.5 ml of solvent; ¹³C decoupled spectra were acquired at 100.62 MHz at room temperature and 64K point over 210 ppm were employed.

Polymer analysis before deprotection:

¹³C-NMR (400 MHz, $CDCl_3$), δ (ppm): 0.00 ($Si(CH_3)_3$); 36.65 (all CH_2); 45.62 ($OCH_2C\equiv$) 50.94 ($Si(OCH_3)_3$); 53.32 (OCH_2CH_2) 174.95 (all CO).

¹³C-NMR (400 MHz, DMSO), δ (ppm): -0.31 ($Si(CH_3)_3$); 36.08 (all CH_2); 44.78 ($OCH_2C\equiv$) 50.10 ($Si(OCH_3)_3$); 52.76 (OCH_2CH_2) 173.89 (all CO).

Polymer analysis after deprotection:

^{13}C -NMR (400 MHz, CDCl_3), δ (ppm): 36.65 (all CH_2); 45,62 ($\text{OCH}_2\text{C}\equiv$); 52.40 (OCH_2CH_2); 75.92 ($\equiv\text{CH}$); 174.95 (all CO).

^{13}C -NMR (400 MHz, DMSO), δ (ppm): 36.08 (all CH_2); 44.79 ($\text{OCH}_2\text{C}\equiv$); 52.02 (OCH_2CH_2); 77.63 ($\equiv\text{CH}$); 78.31 ($\text{C}\equiv\text{CH}$); 174.96 (all CO).

Decoupled ^{13}C NMR spectra, run in CDCl_3 , of protected (**Figure 34**, bottom) and deprotected (**Figure 34**, top) polymers are shown in **Figure 34**. The deprotection step was confirmed by the disappearance of the peaks at 50 and 0 ppm, which correspond to the methoxy and trimethylsilyl (TMS) groups respectively. Furthermore, the integration of the two signals at 45.31 ppm and 52.08 ppm (belonging to the methylene signals of the PMA and MAPS moieties respectively) in the deprotected sample (**Figure 34**, top) show a ratio of 2:1, confirming the molar fraction ratio of the monomers in the copolymer to be as desired. The resulting PMA peak is very close to 2% (1.75%) of the total methylene signal at about 36 ppm. The presence of alkyne moieties was also confirmed to be in the desired ratio through a ^{13}C decoupled NMR spectrum run in DMSO. The two peaks of the methyne moiety appear around 76 and 78 ppm, exactly under the CDCl_3 peak (data/spectra not shown).

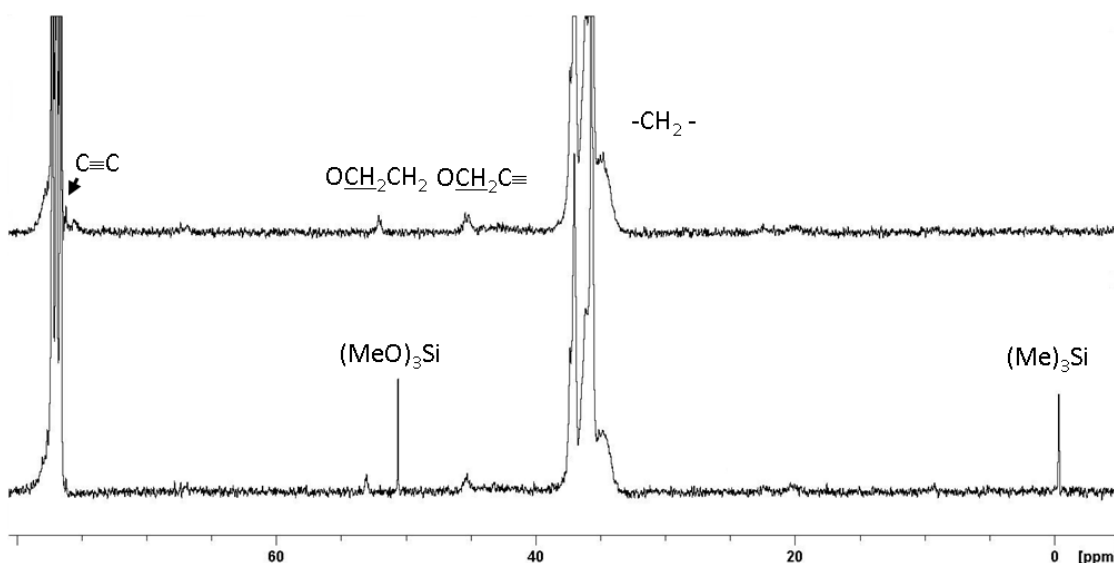


Figure 34: ^{13}C decoupled NMR spectra of protected (bottom) and unprotected (top) polymer, run in CDCl_3 .

Gel Permeation Chromatography

The polymer was analysed by Gel Permeation Chromatography in tandem with an UV-detector ($\lambda=214\text{nm}$). The polymer molecular weight was obtained by using a calibration curve (made of polyacrylamide standards). Poly(DMA-PMA-MAPS) sample was diluted using the GPC mobile phase (GPC buffer: 100 mM NaCl, 50 mM NaH_2PO_4 , pH 3, 10% v/v Acetonitrile) to a concentration of 2.66 mg/ml and the sample ($V=20\ \mu\text{l}$) was run three times through the GPC-UV system to test for reproducibility ($v=0.3\ \text{ml/min}$). The GPC-MALLS analysis of poly(DMA-PMA-MAPS) reveals a polymer molecular weight (M_w) of $4.2 \times 10^4\ \text{g/mol}$ ($\approx 40\ \text{kDa}$), and its polydispersity is about 2.6. Both values are in the same range of the previous synthesized poly(DMA-NAS-MAPS).

Poly(DMA-PMA-MAPS) is similar in composition and in behaviour to its predecessor poly(DMA-NAS-MAPS). In fact, the difference stands only in 2 % of the total monomers. It was demonstrated by the work of this thesis that the replacement of NAS with PMA does not change the ability of the copolymer to form a coating on a silicon oxide surface as demonstrated by a detailed characterization of the coating carried out by Dual Polarization Interferometry (DPI) and Contact Angle (CA) analysis discussed in Section **5.1.2.**

5.1.2. Poly(DMA-PMA-MAPS) coating: characteristics and advantages

This new polymer, as previously described, is similar to a ter-polymer introduced by our group in 2004 to allow the formation of a hydrophilic 3D coating on a solid surface by a simple “dip and rinse” procedure¹⁰. Due to its self adsorbing properties, the coating was obtained by simply immersing the slide in an aqueous solution of the copolymer (10mg/ml) at room temperature, and after 30 minutes an ultrathin polymer film was generated. To remove the polymer excess the slides were rinsed in D.I. water and dried under nitrogen flow. The coated substrates were then cured at 80°C for 15 min to fix the polymer through formation of siloxane bridges (**Figure 35**).

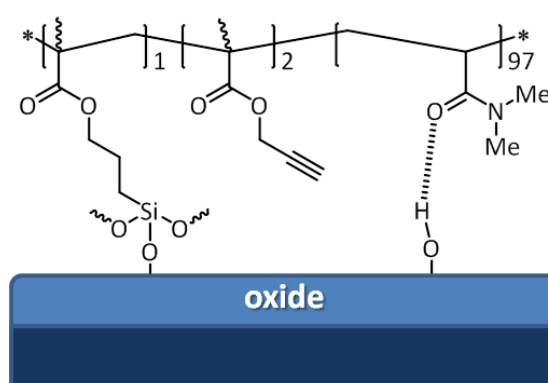


Figure 35: Schematic representation of the chemical structure of the copolymer poly(DMA-PMA-MAPS) coating on a SiO₂ surface. The drawing illustrates the binding mechanism of the polymer to the SiO₂ surface. Dimethylacrylamide (DMA) residues form hydrogen bonds whereas silanol (MAPS) groups react with silanols on the surface and stabilize the coating by covalent attachment via formation of siloxane bridges. The alkyne functionality provided by the PMA group promotes the covalent attachment by reacting with azide groups on probe molecules.

The polymer introduced by this work provides a number of advantages in the coating formation over commonly used approaches. Similarly to poly(DMA-NAS-MAPS), also this polymer physisorbs on the surface through formation of H-bond between its backbone and surface silanols. Following adsorption, 3(trimethoxysilyl)-propylmethacrylate (MAPS) binds covalently to the solid surface through formation of siloxane bridges, stabilizing the coating. The thin layer of hydrophilic polymer provides a solution-like environment that is of fundamental importance to obtain a high-performance in microarray analysis.

The novelty of this polymer relies on the presence of a different functionality, compared to poly(DMA-NAS-MAPS), for the covalent binding of probes. Instead of the succinimide (NHS) active esters provided by the NAS monomer, an alkyne moiety was introduced, using the 3-trimethylsilylprop-2-yn methacrylate (PMA) monomer in the random radical polymerization.

The presence of the alkyne functionality allows the binding of azide-modified probes (from small molecules, such as glycomimetics, to peptides and antibodies) by the well-known Cu(I) catalyzed 1,3-dipolar azide-alkyne Huisgen cycloaddition. Therefore, the regio-specific and bio-orthogonal reaction in microarray analysis could be investigated in depth. The proposed coating approach is advantageous as it provides a fast, simple and versatile method to obtain an alkyne functionalized solid surface in a solution-like environment.

Surface characterization: Contact Angle measurements (CA)

Contact angle is measured using a contact angle goniometer, in this case using water as liquid and following the so called *sessile drop method*. A high resolution camera captures the profile of a water drop on a solid substrate and a software is employed to analyze the contact angle value.

In case of microarray analysis an hydrophilic surface exhibiting a contact angle of about 30°-40° is to be preferred as it ensures probe spots not to spread out on the surface or to merge and, at the same time, it guarantees a proper probe tethering.

In the case of poly(DMA-PMA-MAPS) Si/SiO₂ coated surface, the contact angle was measured both before and immediately after the coating deposition onto silicon/silicon oxide surface, to monitor and quantify changes of the surface hydrophilicity resulting from the presence of a surface polymer layer. The water contact angle could not be measured on an uncoated silicon chip after 10 minutes of oxygen plasma treatment because of its extremely high hydrophilicity (i.e. complete wetting). Thanks to this characteristic, the formation of a polymer coating was clearly detectable because the water droplet contact angles increased on the coated surface from 0° to 33° ± 0.78 ° (the obtained contact angle value is the average of five measurements each on five different coated chips).

The surface hydrophilicity of poly(DMA-PMA-MAPS) was found to be similar to that of poly(DMA-NAS-MAPS): the contact angle value on a poly(DMA-PMA-MAPS) coated surface showed an hydrophilic feature with a 33° ± 0.78 angle, while poly(DMA-NAS-MAPS) coated surface showed a contact angle value of 31° ± 0.48 (**Figure 36**).

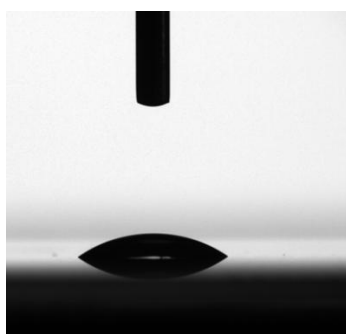


Figure 36: image of a water-drop on a poly(DMA-PMA-MAPS) coated Si/SiO₂ surface.

Surface characterization: Dual Polarization Interferometry (DPI)

The coating was also characterized using dual polarization interferometry (DPI), which is an optical surface analytical technique that provides multiparametric measurements of surface coatings providing information on their molecular dimension (layer thickness), packing (layer refractive index, density) and surface loading (mass)²⁴.

From the DPI analysis it was possible to characterize the polymeric coating by obtaining information in its thickness, mass and density as shown in **Table 1**.

The obtained thickness values revealed the swelling capability of poly(DMA-PMA-MAPS) and confirmed its straight similarity with poly(DMA-NAS-MAPS).

	Thickness (nm)	Mass (ng/mm²)	Density (g/cm³)
Poly-(DMA-PMA-MAPS)	15.31 ± 3.21	1.98 ± 0.14	0.14 ± 0.04
Poly-(DMA-NAS-MAPS)	13.6 ± 3.8	1.4 ± 0.01	0.105 ± 0.03

Table 1: Thickness, mass and density of the poly(DMA-PMA-MAPS) and poly(DMA-NAS-MAPS) coating obtained from DPI analysis.

The similarity between the two polymers, poly(DMA-NAS-MAPS) and poly(DMA-PMA-MAPS), is expected as only a 2% of the total monomers has been changed from one polymer to the other. Furthermore the monomer in question is not involved in the covalent interaction with the substrate.

Polymer binding capacity: wash-off experiments. Density of the immobilized probes as a function of the spotting concentration

In order to assess the density of molecules bound to the polymer coated slide, a simple experiment was carried out based on the measurement of fluorescence after spotting, immobilization and washing of the azido-modified dye, Cyanine-3 (**Figure 37**).

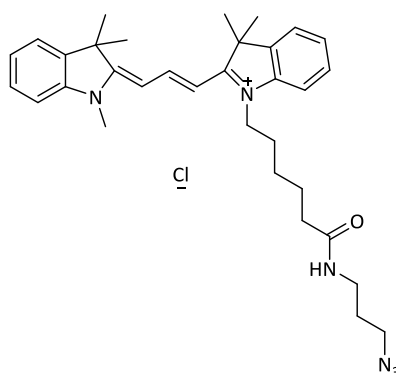


Figure 37: Cy3-N₃ chemical structure.

From the attachment density of the dye, estimated through a fluorescence calibration curve it was possible to evaluate the distance between the bound molecules, which is representative of the distance between immobilized glycans. This parameter is a very important characteristic of glycan arrays, because, as mentioned above, carbohydrate-protein interactions depend critically on multivalent presentation. Indeed, when a glyco-chip is challenged with a multivalent target, such as most lectins, depending on the probe density of the chip different mechanisms can contribute to the affinity measured. If the distance between the immobilized molecules is larger than the distance of two binding sites on the protein, the multivalency of the chip works through statistical rebinding of the target, which reduces the *off* rate. When the distance between probes decreases below a critical threshold reaching the distance between two binding sites on the protein, two probes on the chip can simultaneously engage two binding sites (chelation) and this normally results in a measurable decrease of the dissociation constants ($K_{d,surf}$), i.e. in an increase of the apparent affinity of the protein.¹⁶⁷

Following an approach described in the literature by Wong and coworkers for a glycan monolayer array on glass¹⁶⁷, Cyanine 3 carrying an azido linker, was printed at concentrations ranging from 1 pM to 1 mM on poly(DMA-PMA-MAPS) coated Si/SiO₂ slides in 14 replicates using the optimized “click-protocol” described below. The slide was immediately imaged at 543 nm with a confocal scanner laser. After 12 hours of incubation in a dark humid chamber, the slides were washed with dimethylformamide (DMF) for 10 minutes to remove unbound molecules, dried under a nitrogen

flow and imaged again to assess the binding efficiency. At a fixed laser power and photomultiplier gain (60% and 70% respectively) not all the spots could be visualized: the lowest detectable spotting concentration was 0.5 μM . Since the concentration (C) and the volume (V) of the Cy3 dye spotted are known, the number of molecules covalently bound to the surface (N_p or $N_{\text{molecules}}$) is the product of the number of Cy3 printed and the ratio of the prequench (Q_{pre}) to postquench (Q_{post}) spot fluorescence intensities, where N_A is Avogadro's number (**Equation 2**). Spot diameters vary from 55 to 280 μm , depending on the concentration the printed dye (**Figure 37**, Cy3- N_3).

$$N_p = \frac{C \cdot V \cdot N_A \cdot Q_{post}}{Q_{pre}}$$

Equation 2: equation for the calculation of the effective number of molecules (N_p) covalently bound to the surface.

The distance between molecules on the surface can be estimated as the distance d between the center of two tangential circumferences, with radius $d/2$ and an area $N_p/\text{spot area}$, obtained as the fraction of the total area (spot area, **Figure 38a**) occupied by a single immobilized molecule. This estimate results from an approximation of the 3D matrix to a 2D arrangement. The thickness (≈ 15 nm) of the polymer layer is indeed negligible, considering the size of the spot area (in the range of $61,5 \cdot 10^3 - 2,4 \cdot 10^3 \mu\text{m}^2$). Clearly, when the concentration of immobilized probes on the surface decreases the distance between two molecules in the same spot increases.

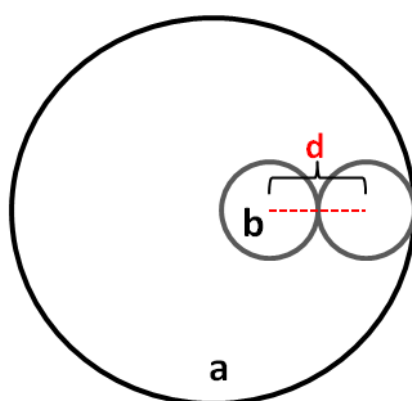


Figure 38: (a) corresponds to the spot total area, while (b) is the area occupied by each single molecule, which was calculated dividing the total area (a) by the total number of immobilized molecules (or N_p). The distance between the centers of two tangential circumferences (d) corresponds to the distance of two near molecules inside the spot, and it is equal to the diameter of the area occupied by each molecule.

As shown in **Figure 39**, at spotting concentrations $\geq 600 \mu\text{M}$ the binding sites on the surface appear to be saturated and the maximum binding capacity (or maximum binding density) of the polymer is $\approx 2,2 \cdot 10^{14}$ molecules/cm², corresponding to an average distance between two probes of 8 Å. At lower spotting concentrations, the number of molecules immobilized on the surface (N_p) is proportional to the spotting concentration. At the lowest detectable concentration (0.5 μM) the probe density is $5.07 \cdot 10^{12}$ molecules/cm² and the average distance between two molecules inside a spot can be estimated to be 50 Å (**Table 2**).

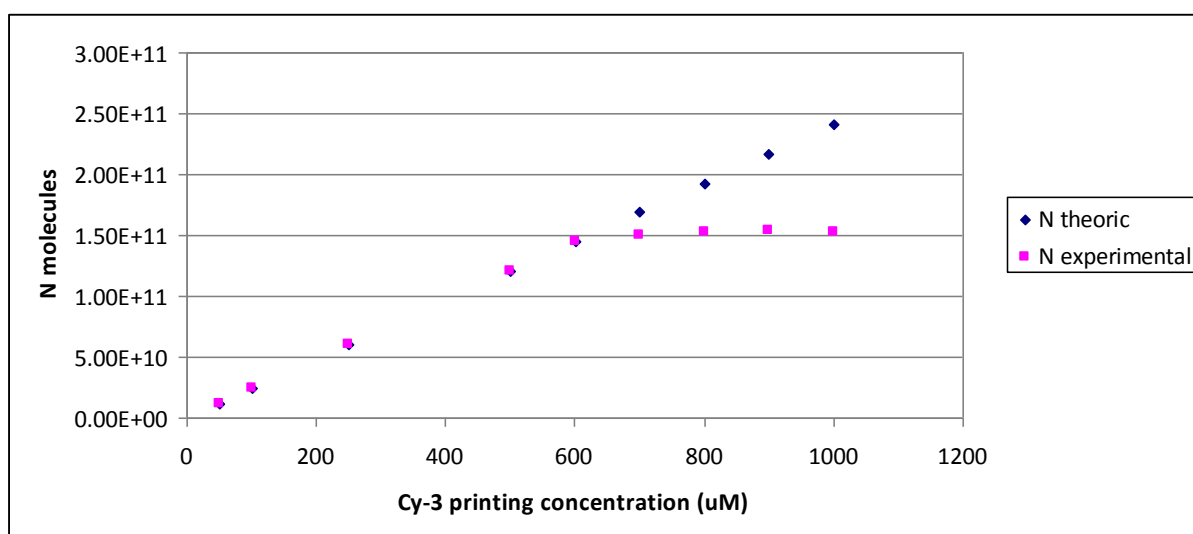


Figure 39: number of the azide modified Cyanine-3 immobilized onto the Si/SiO₂ surface, as measured by the “wash-off experiments”.

Cy3 printing conc. (μM)	Density (N_p/cm^2)	Distance (Å)
0.5	$5.07 \cdot 10^{12}$	50
1	$6.84 \cdot 10^{12}$	43
5	$1.22 \cdot 10^{13}$	32
10	$1.50 \cdot 10^{13}$	29
50	$2.98 \cdot 10^{13}$	21
100	$4.12 \cdot 10^{13}$	18
500	$1.96 \cdot 10^{14}$	8
600	$2.19 \cdot 10^{14}$	8

Table 2: Probe density and average distance between Cyanine3 molecules on the surface as a function of their printing concentration.

The maximum density ($\approx 2 \cdot 10^{14}$ molecules/cm²) obtained on the poly(DMA-PMA-MAPS) 3D matrix is higher than value described for standards in the glycan array field. For instance, in the seminal paper by Wong et al. cited above¹⁶⁷, the binding capacity of the system was reported to be $\approx 1 \cdot 10^{14}$ molecules/cm², two times lower than on this polymeric format. The higher density of immobilized probes onto the 3D matrix results in a higher sensitivity of the platform at lower spotting concentration of the probe (see **6.1.1**).

5.2. High-performing support selection

Commercially available Si/SiO₂ slides were chosen as support to maximize the intensity of the fluorescence detected on the surface. As previously shown (in paragraph 3.1.2), the optical interference phenomenon induced by layers of different refractive index of well-defined thickness (100 nm) maximizes photo-absorption of the dye molecules in the vicinity of the surface and enhances the light emitted towards the detector^{45,56}. To demonstrate the advantage of using this substrate, a comparison of fluorescence intensity on glass and Si/SiO₂ slides was made.

Both glass and Si/SiO₂ slides were coated with poly(DMA-PMA-MAPS) and a 50 μM solution of Cy3-azide (**Figure 37**), in DMF:H₂O (1:1), was printed by means of a piezoelectric spotter (SciFlexArrayer S5, Scienion, Berlin Germany) and the click reaction performed under the conditions previously optimized (section 7.1.). After overnight incubation in a humid chamber, both slides were washed 10 minutes in dry DMF under nitrogen flow and imaged with a fluorescence scanner. Each image was taken with the scanner set at the same laser power (70%) and photomultiplier gain (60%).

The spots on Si/SiO₂ (**Figure 40b**) showed more intense fluorescence signals relative to the glass slide (**Figure 40a**). The fluorescence detected for the same amount of dye was higher by a factor of 4 (**Figure 40c**) on the silicon slide as a result of constructive interference between the radiations reflected at the silicon/silicon oxide interface and that reflected from the surface of the slide. The optimal enhancement is obtained with a silicon oxide thickness of 100 nm on the silicon surface, as reported in the literature⁴⁵.

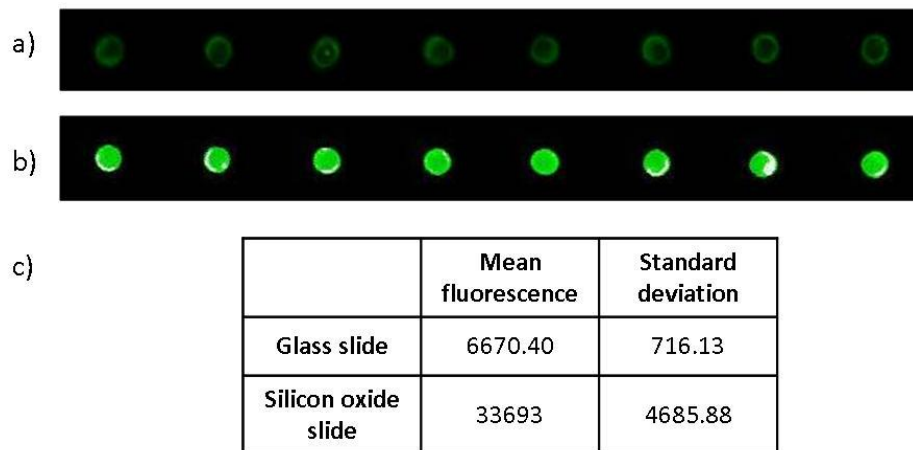


Figure 40: Fluorescence signals of Cy3-azide 50 μ M on poly-(DMA-PMA-MAPS) coated glass slides (a) and silicon oxide chip (b); (c) mean fluorescence of the above Cy3-azide spots and relative standard deviation.

6. Glycan microarrays

6.1. Fluorescence bioassay: a qualitative analysis of carbohydrates-lectin interaction

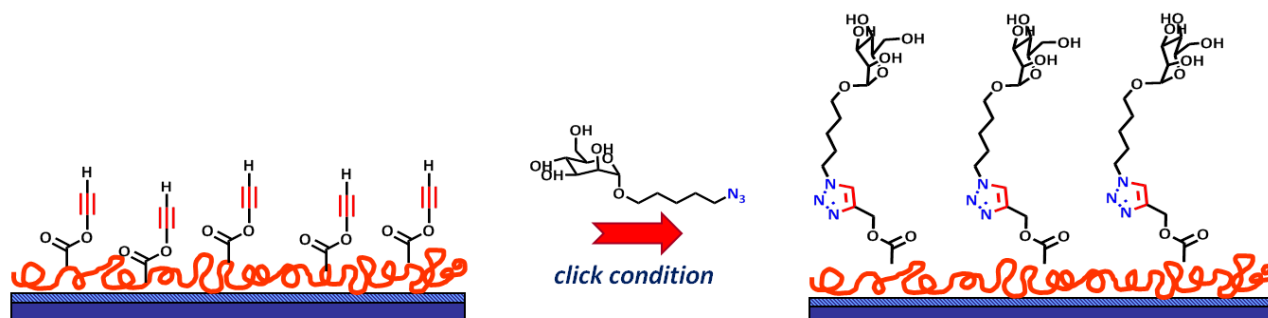


Figure 41: scheme of glycans immobilization on the clickable polymeric matrix, adsorbed on Si/SiO₂ surface, here presented for the construction of a high-performance microarray analysis.

The novel substrate was first tested in glycan microarray analysis (**Figure 41**). In collaboration with the group of Prof. Anna Bernardi, at the University of Milan, we set up a procedure for the screening of a small library of glycomimetics. Eight α -mannose derivatives, interacting with the legume lectin Concanavalin A (Con-A) were spotted on polymer coated slides. Con-A was chosen for its high affinity toward α -mannose derivatives^{215,216}.

At first, to prove the successful immobilization and accessibility of the selected glycomimetics onto the polymeric matrix, we compared the behaviour of amino-modified α -mannose derivatives (**Table 3**, compounds **2a** and **10a**) on both, epoxysilane (**Figure 42a**) and poly(DMA-NAS-MAPS) (**Figure 42b**) coated Si/SiO₂ slides. The probes were attached through a reaction between the free amino terminal group at 1 mM concentration and the epoxy or succinimidyl ester on the surface.

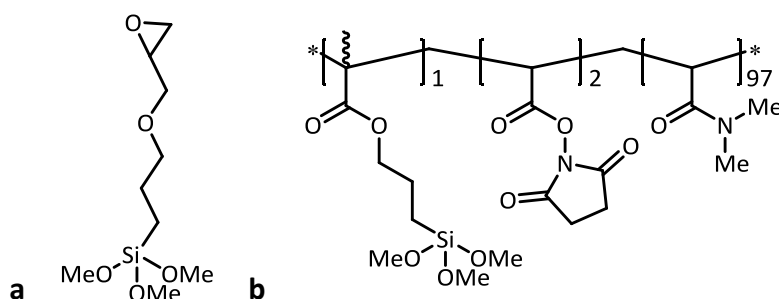


Figure 42: (a) epoxysilane and (b) poly(DMA-NAS-MAPS) structures.

The solvent used to obtain a good immobilization of the sugars onto the two modified surfaces was phosphate buffer saline (PBS, pH 7.4). A synthetic β -galactose with an amino linker (**11a**, **Table 3**) was employed as the negative control to confirm the specificity of the binding with the target in solution. After spotting, the slides were incubated overnight in a humid chamber and the free reactive groups (active ester and epoxide) were blocked with ethanolamine (1 hour at room temperature). The slides were incubated with biotinylated-ConA (0.1mg/ml) and after an incubation step with streptavidin labelled with fluorophore Cy3, they were scanned by means of a confocal scanner laser. The results are shown in **Figure 43**.

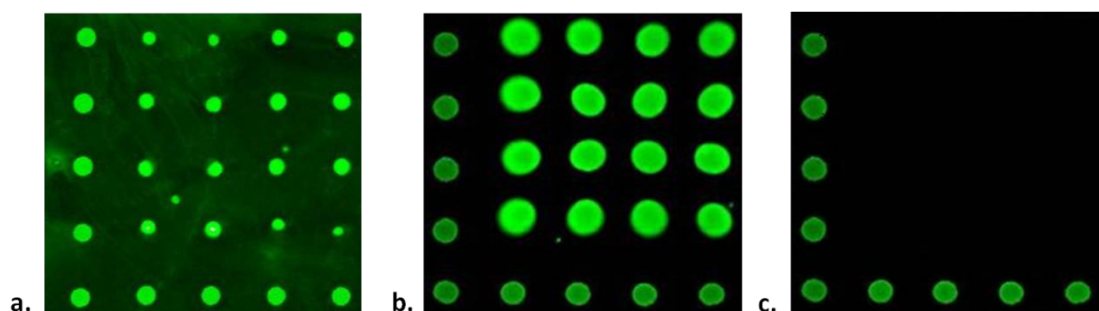


Figure 43: Fluorescence of the spots of α -mannose derivative **10a** (**Table 3**) on (a) epoxysilane monolayer and (b) poly(DMA-NAS-MAPS) Si/SiO₂ coated surfaces. (c) β -galactose (**11a**, **Table 3**) negative control on poly(DMA-NAS-MAPS).

As shown in **Figure 43**, poly-(DMA-NAS-MAPS) coating, due to its higher binding capacity and antifouling properties, provided better results in terms of spot fluorescent intensity, and signal-to-noise ratio if compared to the epoxysilane monolayer coating. Therefore, these results confirmed that this polymeric coating provides major technical advantages in glycan microarray technology and allows good accessibility to the immobilized small glycan molecules. These observations prompted us to develop the new alkyne functionalized ter-polymer coating.

With the synthesis and characterization of poly(DMA-PMA-MAPS) and its use in the coating formation, a new surface with the desired alkyne functionality was ready to be tested in the screening of the affinity of different α -mannose derivatives (**Table 3**, **2-9**) immobilized through a copper-catalyzed cycloaddition, for the legume lectin Con A.

All the glycomimetics shown in **Table 3** share a common azide linker of the same length on the anomeric position. They were synthesized in the laboratory of Prof. Bernardi. A positive (**10b**) and negative (**11**) control were also introduced, while the azido-modified dye (**1**) was used as a positional reference.

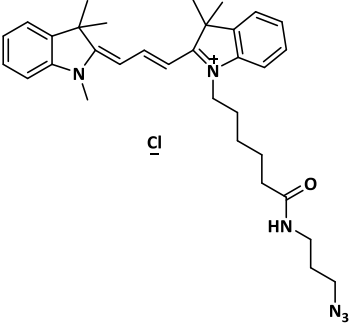
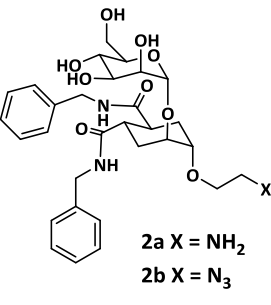
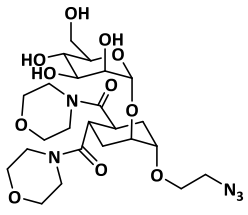
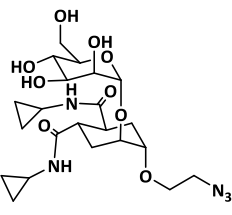
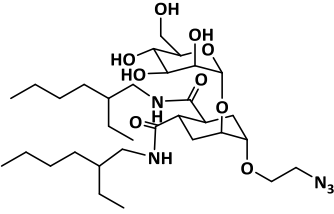
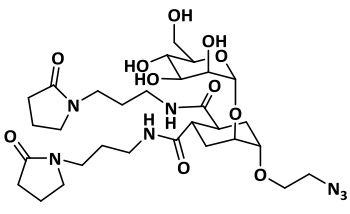
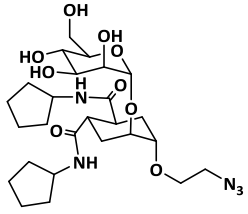
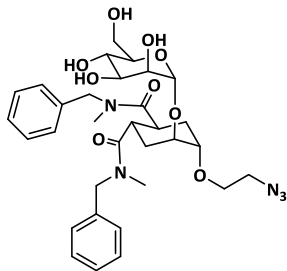
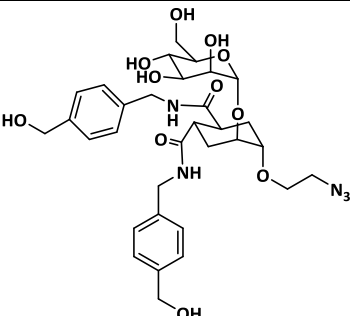
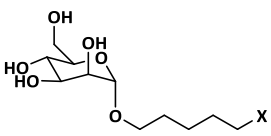
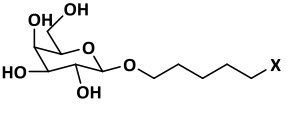
1	2	3	4
	 <p>2a X = NH₂ 2b X = N₃</p>		
5	6	7	8
			
9	10 (α-mannose)	11 (β-galactose)	
	 <p>10a X = NH₂ 10b X = N₃</p>	 <p>11a X = NH₂ 11b X = N₃</p>	

Table 3: Chemical formula of: azide cyanine dye (1), α-mannose derivatives (2-9) positive (10, α-mannose) and negative (11, β-galactose) controls.

After careful optimization of the relative concentration of glycans and CuSO₄/ascorbic acid in the spotting solution (kept at constant 1:5 ratio) on the new polymeric surface, an intense fluorescence signal was obtained upon interaction of immobilized glycans with biotinylated lectin detected through interaction with streptavidin labelled with cyanine 3 (**Figure 44**). The conditions were optimized using mannose derivative (**2b**) in four different concentrations (from 0.05 mM up to 0.5 mM) and incubating the array with the same concentration of biotinylated-Con A (0.75 μg/ml) that was optimized in a separate experiment. Con A concentration was screened starting from 100 μg/ml to 10 ng/ml, and 0.75 μg/ml was selected as the most suitable concentration for a first qualitative screening. The results showed that decreasing the concentration of the immobilized probe down to

0.05 mM, improved spot morphology and provided high signal to noise ratio in the hybridization with Con A. (**Figure 44**).

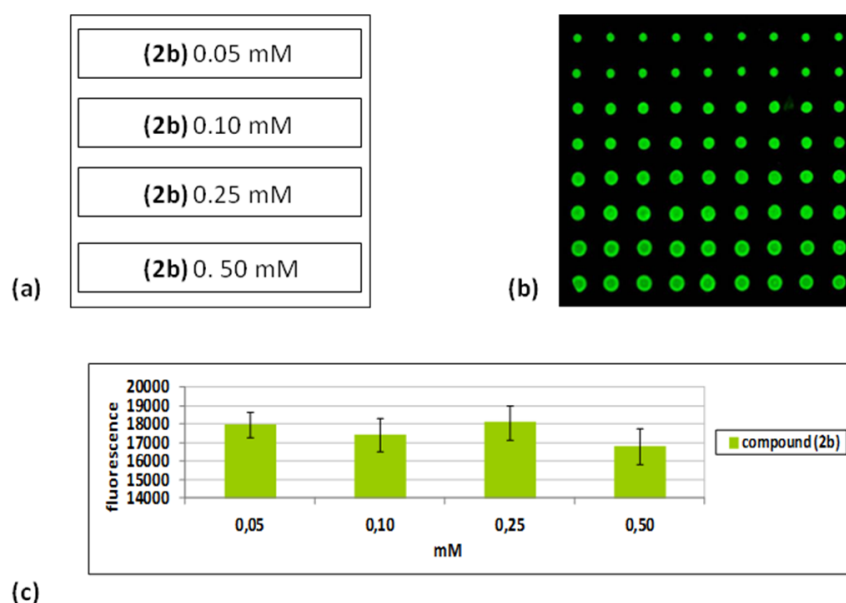


Figure 44: (a) Microarray spotting scheme. (b) Fluorescent image of the microarray spots labelled with Cy3 (c) Plot of relative fluorescence intensities. The bars are the average of the intensity of the 18 spots of each subarray.

The glycans were spotted onto the coated surface by means of a piezoelectric spotter. The optimized printing solution was composed of 0.05 mM glycan, 2.5 mM CuSO_4 and 12.5 mM sodium ascorbate. After overnight incubation in a humid chamber, the slides were incubated with solutions of protein (0.1 $\mu\text{g}/\text{ml}$) in Lectin Binding Buffer (50mM HEPES, 5 mM $\text{MnCl}_2 \cdot 6\text{H}_2\text{O}$, 5 mM $\text{CaCl}_2 \cdot 2\text{H}_2\text{O}$, pH 7.4). The biotinylated Concanavalin A was visualized after an incubation step with Streptavidin-Cy3, 2 $\mu\text{g}/\text{ml}$ in PBS (Phosphate Buffer Saline, pH 7.4) by means of a confocal laser scanner. The quantification of the spot fluorescence intensity provided a rough estimate of the affinity between the lectin and each glycan. The lectin concentration was decreased (from 0.75 to 0.1 $\mu\text{g}/\text{ml}$) to highlight the differences between sugar-lectin affinities. In fact, in order to be significant, a microarray analysis must be run using a lectin concentration below saturation level, that on these arrays is reached using a 0.5 $\mu\text{g}/\text{ml}$ Con A concentration.

After optimization of the experimental conditions, the eight compounds (shown in **Table 3**), together with the negative (β -galactose, **11b**) and the positive (α -mannose, **10b**) control were spotted and screened. The positive control is needed as an internal quality control of the Con A-glycan interaction, while the negative control (β -galactose, **11b**) is needed to confirm the specificity of the lectin recognition. The spots of Cy3 dye (**1**, **Table 3**) were used as to guide the image processing (**Figure 45**).

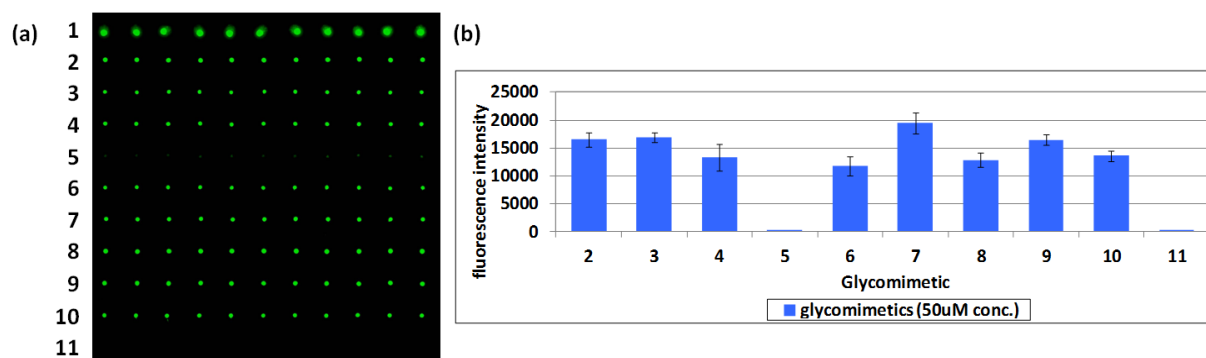


Figure 45: Mean fluorescence intensity of the glycomimetics of **Table 3** (11 replicates per line, 50 μM) incubated with 0.1 $\mu\text{g}/\text{ml}$ of biotinylated Con A (0.943 nM) and revealed with Cy3 labelled streptavidin, (a) image of the glycomimetic microarray; (b) histogram of spot fluorescence intensity of 11 spot replicates.

The surface-immobilized glycans, incubated with 100 ng/ml (0.943 nM) of biotinylated ConA and detected with Cy3-labelled streptavidin, show a variable degree of fluorescent intensity (**Figure 45, b**) depending on their affinity for Con A. The interaction between α -mannose derivatives and Con A was specific as confirmed by the lack of fluorescence on the spots of β -galactose (**11**), the negative control. The plot (**Figure 45, b**) reports the fluorescence intensity observed for different glycan spots. Except for ligand **5** (**Table 3**), all the mannosides of this study, as well as the control **10** (**Table 3**), have similar affinities for Con A, as expected from their strong structural similarities. On the contrary, ligand **5** does not seem to interact, possibly due to steric hindrance from the large, lipophilic amide groups. This analysis provided only a qualitative estimation of the affinity between the α -mannose derivatives immobilized onto the surface and the selected lectin, but showed that the technology can be applied to these small molecules with good results and sensitivity. The next step, we evaluated equilibrium constant for the surface interactions, following an approach described by Wong et al. in 2007¹⁶⁷.

6.1.1. Determination of the surface equilibrium constant ($K_{D,surf}$): quantitative estimation of carbohydrates-lectin affinity

As reported in the literature, in all the interactions occurring in a natural environment, multivalency is one of the key principle for achieving strong and yet reversible interaction. In contrast to weak monovalent binding, multivalent interactions offer the advantage of a multiple, and thus dramatically enhanced, binding on a molecular scale¹⁵⁸. In the case of glycans, since the individual protein-carbohydrate interactions are weak, it often takes a multitude of simultaneous interactions, i.e. multivalency, to produce a biological effect¹⁵⁹.

Thanks to the high local concentration of surface-immobilized glycans on microarray format, it is possible to reproduce the mechanism and the behavior of cell-surface glycoconjugates^{217,218} during lectin's binding that occurs through multiple, simultaneous interactions. The observed discrepancies between the values of K_D obtained in solution and on surface for sugar protein pairs could be ascribed to the high local concentrations of the carbohydrates present in a single spot, which may generate a multivalent interaction with the lectin. This effect has been reported by others in different experimental conditions²¹⁹.

6.1.1.1. Microarray experiment: $K_{D,surf}$ and glycans multivalent presentation

The influence of the multivalence presentation of carbohydrates on this new platform, which combines the higher sensitivity provided by the Si/SiO₂ surface with a good surface quality, was investigated. The surface chemistry proposed by this work allows an easy immobilization of probes in an oriented manner thanks to the regio-selectivity of the click chemistry reaction in a solution-like environment thanks to the use of the poly(DMA-PMA-MAPS) coating. The impact of these features on the interaction with Con A was investigated at different glycan immobilization densities. By carrying out a series of hybridization experiments at different concentration of Con-A, a quantitative characterization of the glycomimetic affinities were obtained, allowing the measurement of the surface dissociation constant ($K_{D,surf}$). In particular, the high-sensitivity of the platform proposed allows the study of carbohydrates-lectin interactions at both high (50 μ M) and low (0.5 μ M) glycan surface density, in conditions where most of the conventional solid phase assays fail to provide a detectable signal.

A fundamental example in the literature, obtained on a glass-immobilized hydrogel matrix¹⁶⁷, reports that the maximum binding capacity towards ConA was reached at carbohydrate printing concentrations around 100-10 μ M. In these conditions, multivalency is responsible for the high-affinity ($K_{D,surf}$ in the scale of nano-molar) recorded. At these printing concentrations the ligands are

displayed at a distance lower than the distance between two lectin's binding sites ($\approx 72 \text{ \AA}$ for Con A¹⁵⁹). A significantly weaker affinity was found in a more diluted ($< 10 \mu\text{M}$) presentation.

Therefore, in this work, each glycomimetic was first analyzed at $50 \mu\text{M}$ and $10 \mu\text{M}$, obtaining $K_{D,\text{surf}}$ values in high-density conditions. The results confirmed the considerations reported in literature¹⁶⁷ on the high-affinity obtained thanks to a multivalent effect. The experiment was performed in parallel : nine slides were spotted with $50 \mu\text{M}$ and $10 \mu\text{M}$ aqueous solutions of the glycomimetics **2-11** (11 replicates) (**Table 3**), in the optimized condition previously reported ($\text{CuSO}_4 : \text{Ascorbic acid} = 2.5 \text{ mM} : 12.5 \text{ mM}$). The chips were incubated with Con A solutions of increasing concentration, from 47.2 pM up to 469.3 nM . By scanning the surface, a mean fluorescence value was obtained for each of the glycomimetic spot replicates. For each glycan, average values of fluorescence were plotted against Con A concentrations (logarithmic scale) and the curve was fitted as a sigmoidal/growth function. Typical curves of high (**3**) and low affinity (**5**) glycomimetics spotted at $50 \mu\text{M}$ concentration are shown in the graphs below (**Figure 46**).

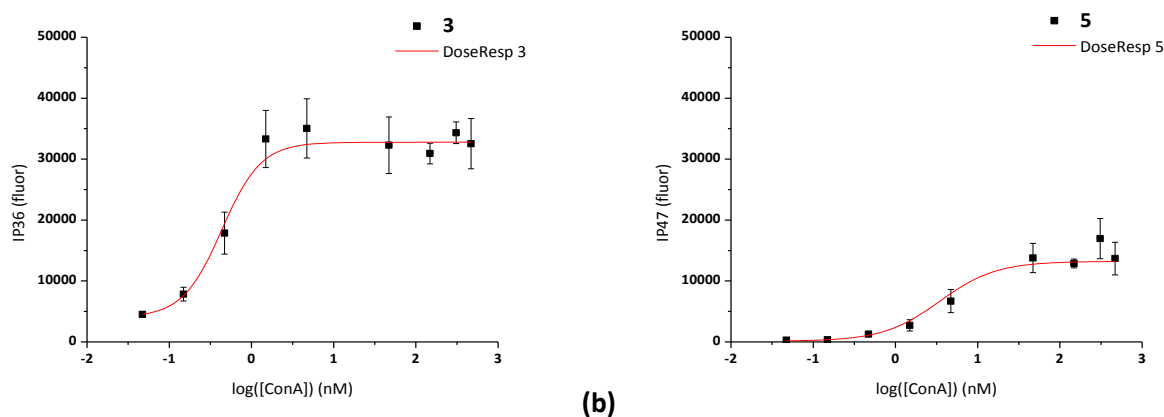


Figure 46: Fluorescence vs $\log([\text{ConA}])$ in a sigmoidal/growth graph. Both the glycomimetics (**3** and **5**) were spotted at $50 \mu\text{M}$ printing concentration. The bars represent the standard deviation of each fluorescence mean value. (a) Trend of a glycan with higher affinity for ConA (0.34 nM) (b) trend of a glycan with a lower affinity with the lectin (5.33 nM).

From these curves it was possible to extrapolate a value of EC_{50} (the half maximal Effective Concentration) for each molecule. EC_{50} refers to the Con A concentration at which half of the probes on the surface are occupied by the target. The values of EC_{50} reported in **Table 4** represent the surface equilibrium constant $K_{D,\text{surf}}$, and provide a quantitative estimation of the affinity between the glycomimetics and the considered lectin, when the interaction occurs on a surface at a given ligand density.

Glycomimetic	50 μM^{a} * $K_{\text{D,surf}}$ (nM)	10 μM^{b} * $K_{\text{D,surf}}$ (nM)
2	0.26	1.01
3	0.34	0.79
4	0.67	1.71
5	5.33	N/A
6	0.88	1.77
7	0.40	0.98
8	0.34	0.85
9	0.43	0.75
10	0.90	1.33

a. probe density $\approx 3 \cdot 10^{13}$, distance 21 Å; b. probe density $\approx 1,5 \cdot 10^{13}$, distance 29 Å

Table 4: $K_{\text{D,surf}}$ values obtained for each glycomimetic printed at 50 μM and 10 μM concentration.

To obtain $K_{\text{D,surf}}$ reported in **Table 4**, all the data obtained were fitted with OriginPro8 using a growth/sigmoidal function fixing the parameter $p=1$ and the parameter $A1=0$.

The experimentally found $K_{\text{D,surf}}$ values are considerably lower than K_{D} reported in the literature for interactions taking place in solution²²⁰ and, although they are in the same range of the values determined by other authors based on surface interactions²²¹, they are substantially lower. A possible reason for the observed difference could be a better multivalent presentation of immobilized glycans provided by the polymeric matrix. The tri-dimensional coating creates, during lectin incubation, a solution-like environment, improving the accessibility of the probes, with an oriented immobilization fashion, by the analyte in solution. Furthermore, between 50 μM and 10 μM glycans concentration a high-multivalent presentation is available (the ligand's distance is lower than the distance between two ConA binding sites, ≈ 72 Å) so, no significant difference in affinity could be notice ($K_{\text{D,surf}}$ are of the same order).

6.1.1.2. *Microarray experiment: $K_{\text{D,surf}}$ at lower glycans' surface density*

Thanks to the high sensitivity of the platform presented in this thesis and motivated by the results previously shown, we have investigated the close dependence of the K_{D} on the glycans density in the interaction with ConA.

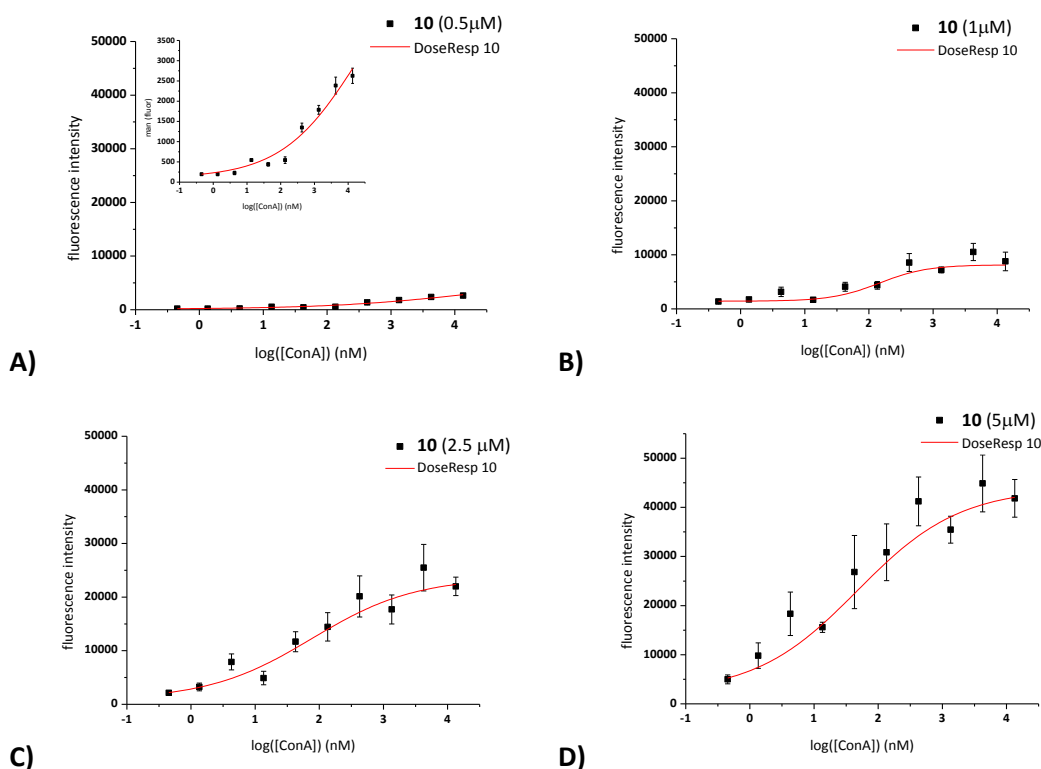


Figure 47: The four curves represent dose response curves obtained changing the glycans density immobilized on the surface. In particular, these graphs represent the behaviour of glycomimetic **10b** (Table 3) at different printing concentrations interacting with increasing concentrations of Con A (from 0.450 nM up to 13.4 μ M). The bars represent the standard deviation of each mean fluorescence. A) **10b** printed at 0.5 μ M B) **10b** printed at 1 μ M C) **10b** printed at 2.5 μ M and D) **10b** printed at 5 μ M. (For the probe density and distances expected at these printing concentrations, see Table 2)

The behaviour of α -mannose (**10**) and the α -mannose derivative (**9**) has been investigated more in depth. Both glycans were printed on a poly(DMA-PMA-MAPS) coated Si/SiO₂ surface at four different concentrations (from 5 μ M to 0.5 μ M), and incubated with a wide range of Con A solutions (from 0.450 nM up to 13.4 μ M). In Figure 47, typical dose response curves of fluorescence versus Con A concentrations at various glycan surface densities are depicted for **10**. Similar curves were obtained for **9**.

By extrapolating $K_{D,surf}$ from these curves, it is clear that as the glycan surface density decreases, the affinity also decreases (Table 5), thus supporting the hypothesis that the surface affinity between the analyzed carbohydrates and the lectin is dominated by multivalency effects. It is worth noting that, due to the high immobilization density achieved on the 3D matrix, the probe distance is expected to remain lower than the distance between two binding sites of ConA (≈ 72 Å) at all the printing concentration (between 21 Å, when the glycans are spotted at 50 μ M concentration and 50

Å when they are spotted at 0.5 μM concentration). Thus chelation should be allowed under all the examined situations. However, in a clear illustration of the importance of multivalency in determining the strength of sugar-protein interactions, the increased local density of the probes is still producing a measurable effect (over one order of magnitude), presumably *via* statistical rebinding mechanisms.¹⁵⁹

Carbohydrate	Printing conc. (μM)	molecular distance (Å)	*K _{D,surf} (nM)
10	0.5	50	756
10	1	43	146
10	2.5	36	77
10	5	32	47
9	0.5	50	171
9	1	43	93
9	2.5	36	6.7
9	5	32	1.5

Table 5: Dependence of K_{D,surf} values of α-mannose derivatives **9** and **10** on printing concentration.

6.2. Conclusion: poly(DMA-PMA-MAPS)-Si/SiO₂ platform in glycan arrays

In this work we introduce a new polymer obtained from the polymerization of N,N-dimethylacrylamide (DMA), *3-trimethylsilanyl-prop-2-yn methacrylate* (PMA) and 3(trimethoxysilyl)-propylmethacrylate (MAPS), poly(DMA-PMA-MAPS) and describe its use in the formation of a functional coating for microarray. The backbone of the polymer bears alkyne moieties that allow binding azide-modified glycans to the surface by "click" chemistry. This attachment mode offers a number of advantages in the immobilization of glycans, such as high grafting efficiency, oriented immobilization and insensitivity to functionalities present in natural glycans (bio-orthogonality). The solution-like environment provides by a swelling of the dimethylacrylamide backbone (≈ 15 nm) when in contact with a buffer solution, as well-demonstrated by the DPI measurements, dramatically increases the availability of the probes immobilized onto the surface and their accessibility to the target in solution, that could better interact. This is clearly noticeable in the very low values of $K_{D,surf}$ observed using this novel platform if compared with the ones reported in literature¹⁶⁷. Furthermore, the higher sensitivity to the fluorescence signal provided by the novel Si/SiO₂ microarray substrate offers significant advantages over conventional glass slides allowing analysis at lower glycan printing concentration.

7. Antibody microarrays

7.1. Oriented antibody microarrays: high-performing biosensor

In the last decade, a wide variety of different biosensors emerged. Sensor specificity relies strongly on the properties of the immobilized detection element, which has stimulated the use of antibodies (Abs) or fragments thereof. In 1971 Abs were used for the first time in an enzyme-linked immunosorbent assay (ELISA) to quantitatively detect analytes²²². Abs with better affinities and higher stabilities have been selected to improve biosensor performance. Further sensor optimization was directed towards surface preparation of biosensors aiming to promote specific binding and suppress non-specific binding. For this purpose site-specific coupling and immobilization of antibodies, and proteins in general, are of great interest²²³.

Antibodies are a class of glycoproteins with a well-defined Y-shape structure as depicted in section 3.2.1.1. (**Figure 20**). Since only two binding sites on the top of the Y-shape are present, it can be highly advantageous to orient these molecules to improve performance of a bio-sensor.

To preserve the biological recognition activity of the immobilized antibody an ideal immobilization method, under mild conditions (aqueous buffer solution), should enable the binding at a solely single point providing a tail-on orientation, which promotes antigen binding. Many immobilization strategies adopt this tail-on orientation to improve the functionality of the antibodies by exploiting the presence of carbohydrate moieties on a precise position on the stem (Fc) region^{127,128,129,130,131}.

Since the azido functionality is not present in nature, inspired by the work of Zeglis et al., we set up a procedure that allows a site-specific modification of the constant region (Fc) of any desired antibody (IgG) through an enzymatic pathway, which exploits the presence of a terminal galactose on the side chain (see **Figure 20**, paragraph 3.2.1.1). This modification would allow an exclusively tail-on orientation, leaving the two binding sites free for the interaction. This feature is extremely important to construct high-performing biosensors^{122,224}.

As it will be discussed below, the modification procedure proposed in this work, although time-consuming, is still more convenient than other procedures used for providing tail-on orientation that require the use of the recombinant proteins A, G or L. These proteins specifically interact with the Fc portion, but the wide range of interactive immunoglobulins (IgGs) increases the possibility of non specific interactions, which could lead in a high-background. Furthermore, the few binding sites available on the protein for the Fc binding will provide a biosensor with a low binding efficiency²²⁵.

On the contrary, the oriented immobilization obtain on the antifouling polymeric coating proposed by this thesis provides excellent signal-to-noise ratio in a solution-like environment with a good

binding efficiency, offering improved accessibility of the antibody's binding site by the target in solution.

The enzymatic modification process was inspired by a work published in 2013 by Zeglis et al.¹³² and described in depth in the Introduction (paragraph 3.2.1.1). The authors report on an enzymatic modification of the galactose moiety present on the Fc antibody portion using a system based on an unnatural UDP-galactose substrate azido-modified and a substrate-permissive mutant of β -1,4-galactosyltransferase, GalT(Y289L), first designed, engineered, and expressed by Ramakrishnan and Qasba¹³³. They proposed this approach for the site-specific radio-labeling of antibodies, combining both enzyme-mediated GalNAz incorporation and bio-orthogonal, strain-promoted, copper-free azide/alkyne cycloaddition click chemistry¹³².

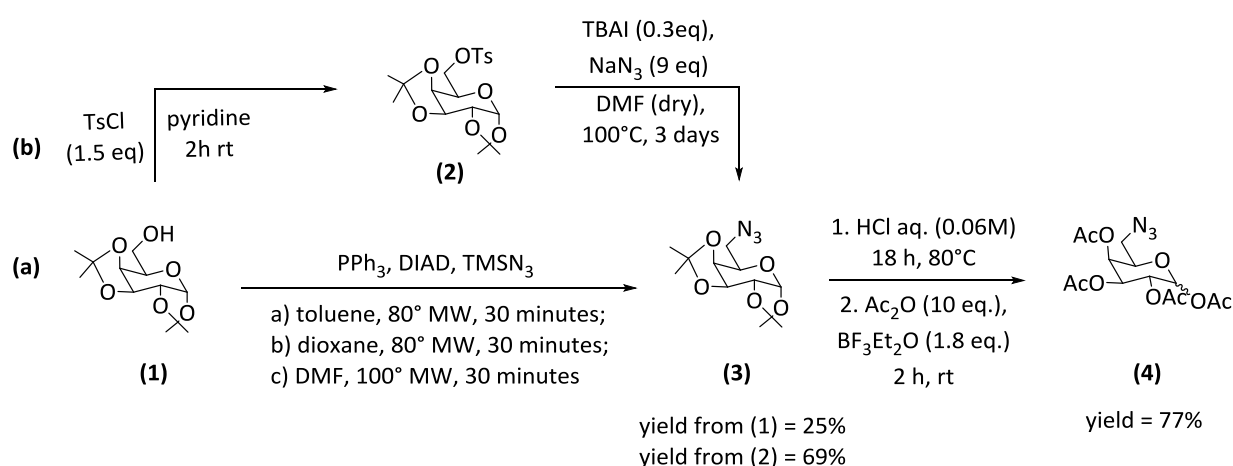
Motivated by the great potential of antibody microarrays as a rapid and effective diagnostic tool, we focused our attention on this antibody site-specific enzymatic modification to optimize antibody microarrays, using a covalent, regio-specific and oriented, copper-mediated, "click" chemistry immobilization. In this thesis the procedure proposed by Zeglis¹³² (now available as a SiteClick Antibody Labelling Kit sold by Life Technologies) was reproduced using commercially available enzyme, β (1-4)-galactosyl-transferase, and replacing the UDP-2-azidogalactose used by Zeglis with the UDP-6-azidogalactose, that is synthetically simpler and expected to display a better reactivity in surface immobilization procedures because it is less sterically hindered.

7.1.1. Synthesis of UDP-GalNAz

Part of the strategy adopted for the synthesis of UDP-6-azidogalactose came from the procedure reported by Bosco et al.². They developed a new strategy to tag glycoproteins carrying terminal GlcNAc using commercially available bovine $\beta(1,4)$ -galactosyltransferase (GalT) and UDP-6-azidogalactose.

The azide functionality was introduced at the C-6 position of the galactose ring because it was demonstrated by Bosco and co-workers that a modification, such as azide or even biotin, appended to the C-6 position of UDP-galactose could maintain the sugar as a substrate for human GalT, without the need for a mutant enzyme². Mainly two strategies for the chemical synthesis pyrophosphate UDP-azidogalactose can be exploited. The first one, essentially developed by Hindsgaul's group²²⁶, is based on the reaction between an activated galactose moiety with an uridine diphosphate. Through this methodology the desired product could be obtained rapidly but in anomeric mixtures and in low yield. The second methodology, here partially adopted, was first developed by Moffatt and Khorana²²⁷ and improved by Wittmann and Wong²²⁸. They proposed, together with the use of nucleoside-5'-phosphoromorpholidates in the synthesis of pyrophosphate derivatives (i.e. UDP-GalNAz), the use of 1-H tetrazole as catalyst in phosphomorpholidate coupling reactions, reporting an efficient synthesis of GDP-Fucose, GDP-Mannose, and UDP-Galactose.

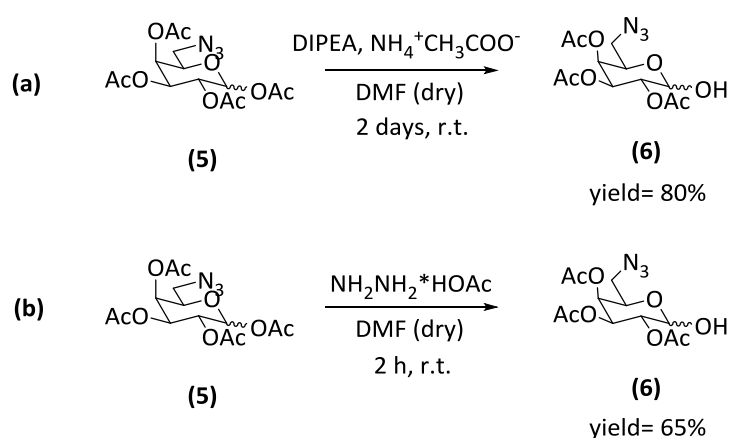
First, as reported in Scheme 1, the 6-azido-6-deoxygalactose (3) was prepared from commercially available (1) passing through the tosylate (2) using NaN_3 in large molar excess (9 eq.).



Scheme 1: two reaction schemes: (a) the one-pot Mitsunobu reaction with the three different solvents studied under microwave condition, and (b) the classical nucleophilic substitution passing through the formation of tosyl derivative (2).

Also the Mitsunobu reaction of (1) with TMSN_3 ²²⁹ was tested, under microwave condition, testing toluene, dioxane and dimethylformamide as the solvent (**Scheme 1**), but it was discarded for scale-

up because of the high amount of by-products formed and the cost of the reagents. Once the azido functionality was introduced, the diisopropylidene azido-galactose was fully deprotected and the sugar was re-protected using acetates as protecting group (**Scheme 1, 4**), which is more stable compared to the trimethylsilylether protection used by Hindsgaul's group²²⁶. The anomeric position was deprotected within a 2 hours reaction (**Scheme 2b**) using hydrazine-acetate, prepared in situ by dissolving hydrazine-monohydrate in dry methanol, in the presence of 1 eq. of acetic acid, under nitrogen atmosphere for 30 minutes, and added drop-wise to a DMF solution of (4) cooled to 0°C. The purified product (5) was obtained in a 65% yield. This is to compare with the procedure described by Bosco et al. with AcONH₄ (**Scheme 2a**), which, although the high yield (80%), requires 2 days and lead to a 80 % yield to reach the completion.

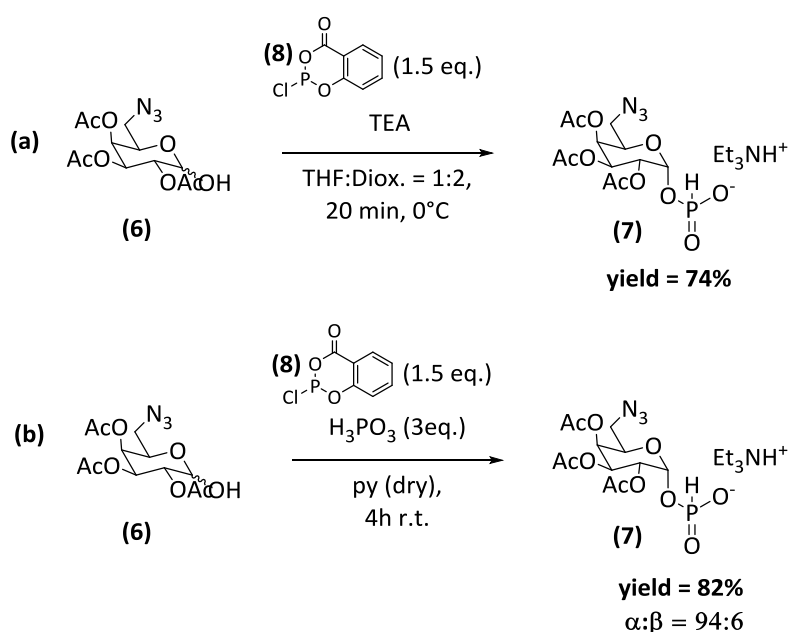


Scheme 2: two reaction conditions for achieve the anomeric deprotection. (a) procedure reported by Bosco et al.², (b) our procedure²³⁰.

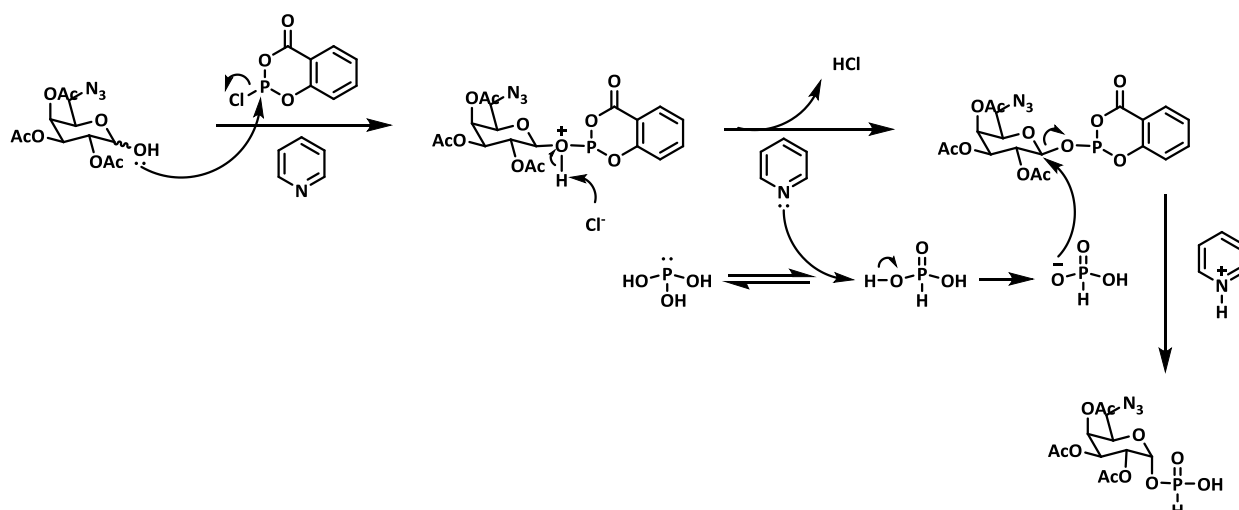
Once the anomeric position was deprotected it could be activated as the H-phosphonate (7) (**Scheme 3**).

As reported in the literature^{231, 232}, depending on the phosphorylating agent used it is possible to favor the β - or α -anomer. In particular, using 2-chloro-4H-benzodioxaphosphorin-4-one (**8**, **Scheme 3**)²³¹ the configuration of the anomeric centre could be controlled and almost only α -anomer of (7) was isolated.

The authors reported the phosphite formation using a mixture of THF/Dioxane in the presence of triethylamine and 2-chloro-4H-benzodioxaphosphorin-4-one (8) (also called salicylchlorophosphite), **Scheme 3a**. In our hands, the reaction worked better under conditions optimized by L. Morelli²³⁰, in which a 82% yield of (7) could be reached in 4 hours, in dry pyridine using a mixture of (8) and H_3PO_3 (**Scheme 3b**). The reaction mechanism proposed for our strategy is reported in **Scheme 4**.

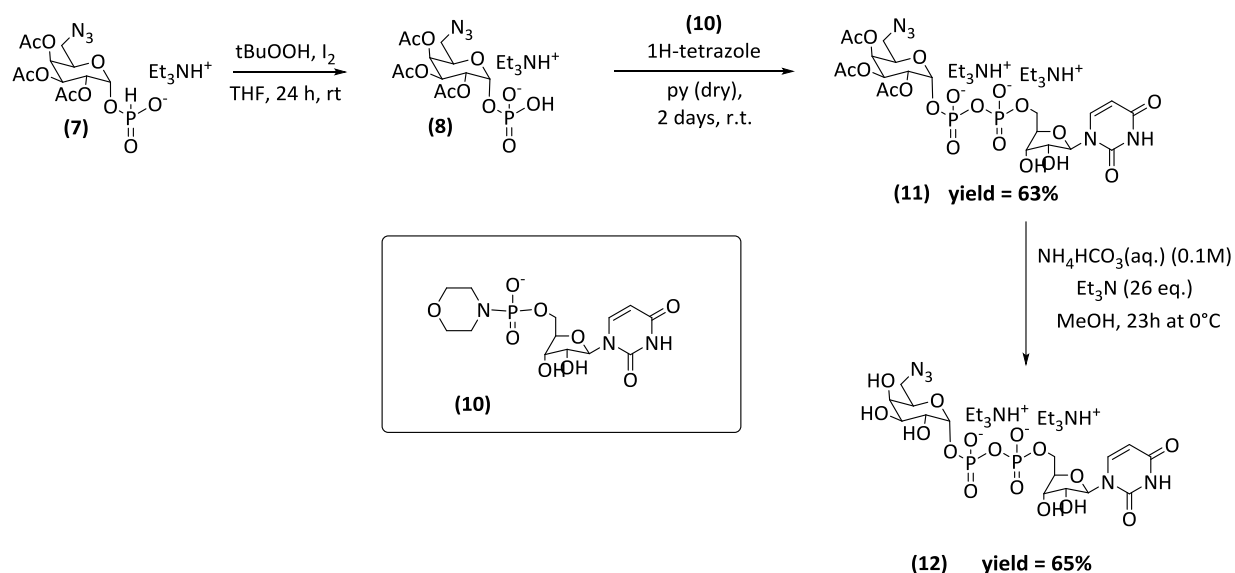


Scheme 3: reaction scheme for the synthesis of phosphite derivative. (a) is the protocol presented in the article Bosco et al., while (b) is the protocol we followed, condition from L. Morelli²³⁰.



Scheme 4: mechanism of salicyl-chlorophosphate (8) in the formation of the phosphate-salt (9).

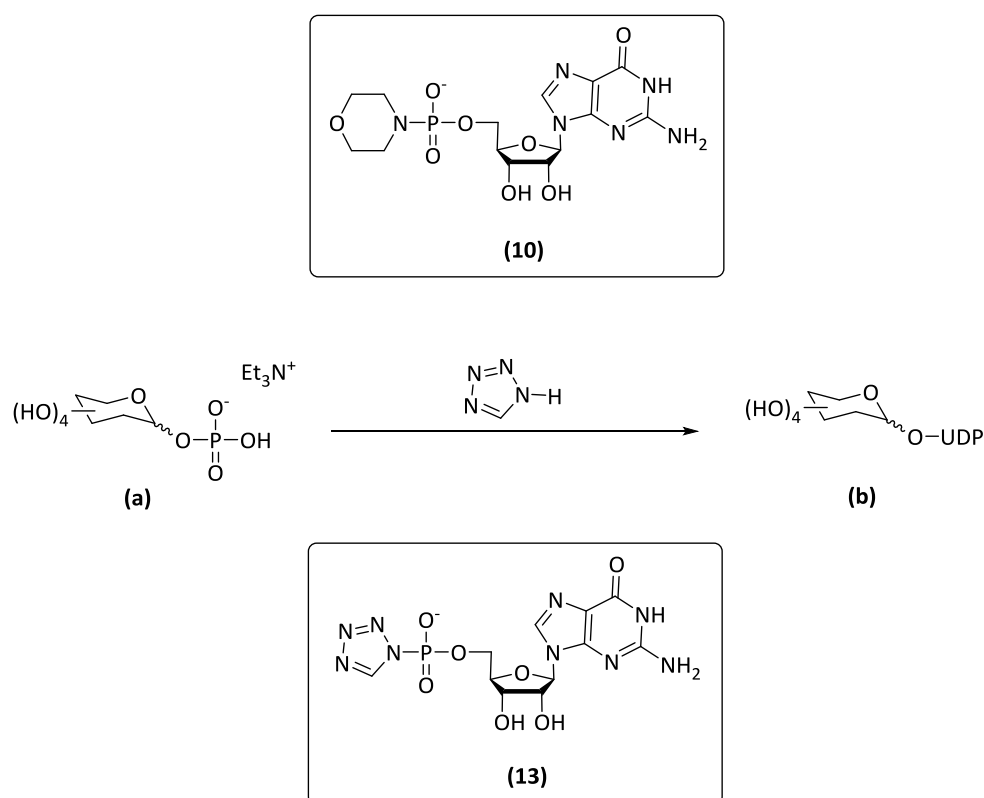
After the phosphite derivative (7) oxidation to the phosphate (9) was obtained under the conditions reported by Bosco et al., in the presence of $t\text{BuOOH}$ and I_2 in catalytic amount (**Scheme 5**). For the formation of phosphodiester bridge, uridine-5'-phosphormorpholidate was used to yield, after purification and deprotection in mild condition, the Gal-T substrate compound (10) in only its α -anomeric conformation.



Scheme 5: scheme of the last steps for the synthesis of the UDP-6-azidogalactose (12) in its α -conformation.

The use of 1-*H*-tetrazole as catalyst in phosphomorpholidate coupling reactions was well-explained in the work published by Wittmann and Wong²²⁸. 1-*H*-Tetrazole (pK_a 4.9) is commonly used for the

activation of phosphoramidites²³³ and accelerates coupling during oligonucleotide synthesis by the phosphotriester method²³⁴. It turned out that this heterocycle is also an efficient catalyst for the phosphoramidate coupling. When used to activate phosphoramidites, tetrazole is known to act as both an acid and nucleophilic catalyst, and tetrazolophosphane derivatives (13, **Scheme 6**) have been identified as reactive intermediat²³⁵. Compared with the activation of phosphomorpholidates by acetic acid (pKa 4.75), tetrazole (pKa 4.9) activation of phosphomorpholidates accelerates the reaction much more than the acid, suggesting a nucleophilic catalysis mechanism in addition to the simple acid catalysis.



Scheme 6: reaction scheme of sugar nucleotide derivative formation *via* phosphoramidate coupling catalyzed by 1-*H*-tetrazole. (a) sugar phosphate derivative, (b) sugar nucleotide derivative and (13) phosphotetrazolide intermediate.

The activation mechanism proposed by Wittmann et al.²²⁸ (that carried out the coupling reaction with different additives and followed the course of the reaction by ³¹P-NMR spectroscopy), is that the tetrazole activates uridine-5'-phosphomorpholidate (10) (**Scheme 6**) by protonation of the leaving group nitrogen and presumably by nucleophilic catalysis *via* the highly reactive phosphotetrazolide (13) (**Scheme 6**), which reacts with sugar phosphate (**Scheme 6, a**) to give the sugar nucleotide derivative (**Scheme 6, b**) (i.e. UDP-Gal).

The main difficulty of the whole reaction process consisted in the purification of the phosphite and phosphate derivatives (from compound (7) to compound (12)) with the C-18 reverse phase column using only water as eluent, as reported by Bosco et al.². The purification of (7) phosphite derivative and (8) phosphate derivative was carried out using C-18 biotage column with water as eluent in the presence of TEA (1%) to stabilize the product as a salt, but the purification yield ($\approx 30\%$) were low, probably due to its instability and its possible interaction with silica. So, to avoid loss of precious products (in particular 11 and 12 di-phosphate derivatives), the acetylated UDP-6-azidogalactose (11) and the final product (12) were purified by means of HPLC chromatography using a semi-preparative C-18 column. The eluent used was a NH_4HCO_3 50 mM buffer (pH 7.4). The introduction of the HPLC chromatography enhanced dramatically the final purification yield affording compound 11 in 63% yield from 10, and 12 in 65% yield from 11 (higher than the 46 and 53% yield respectively reported by Bosco et al.).

7.1.2. Antibody site-specific modification

An UDP-azido galactose was synthesized (as described in the experimental section 9.2.2) by introducing the azido functionality on C-6 instead of C-2; the enzymes used for the antibody modification were the commercial available β -(1,4)-galactosidase and β -(1,4)-galactosyltransferase. The original galactose, which was cleaved in acidic condition in the presence of β -(1,4)-galactosidase (Figure 48, step 1), was replaced with the unnatural UDP-6-azido-galactose (Figure 48, step 2) using β -(1,4)-galactosyltransferase to catalyze the conjugation. In the first step (Figure 48, step 1), the enzyme β -(1,4)-galactosidase works in acidic condition (sodium acetate, 10 mM, pH 5), whereas in the second step the enzyme β -(1,4)-galactosyltransferase requires the use of a slightly alkaline buffer (TRIS·HCl, 50 mM, pH 7.4) and the presence of $MnCl_2$ (20mM) and Alkaline phosphatase (2U) (Figure 48, step 2). The nucleoside diphosphatases generated during the reaction are potent glycosyltransferase inhibitors, therefore the presence of alkaline phosphatase would prevent product inhibition by hydrolyzing the UDP moiety.

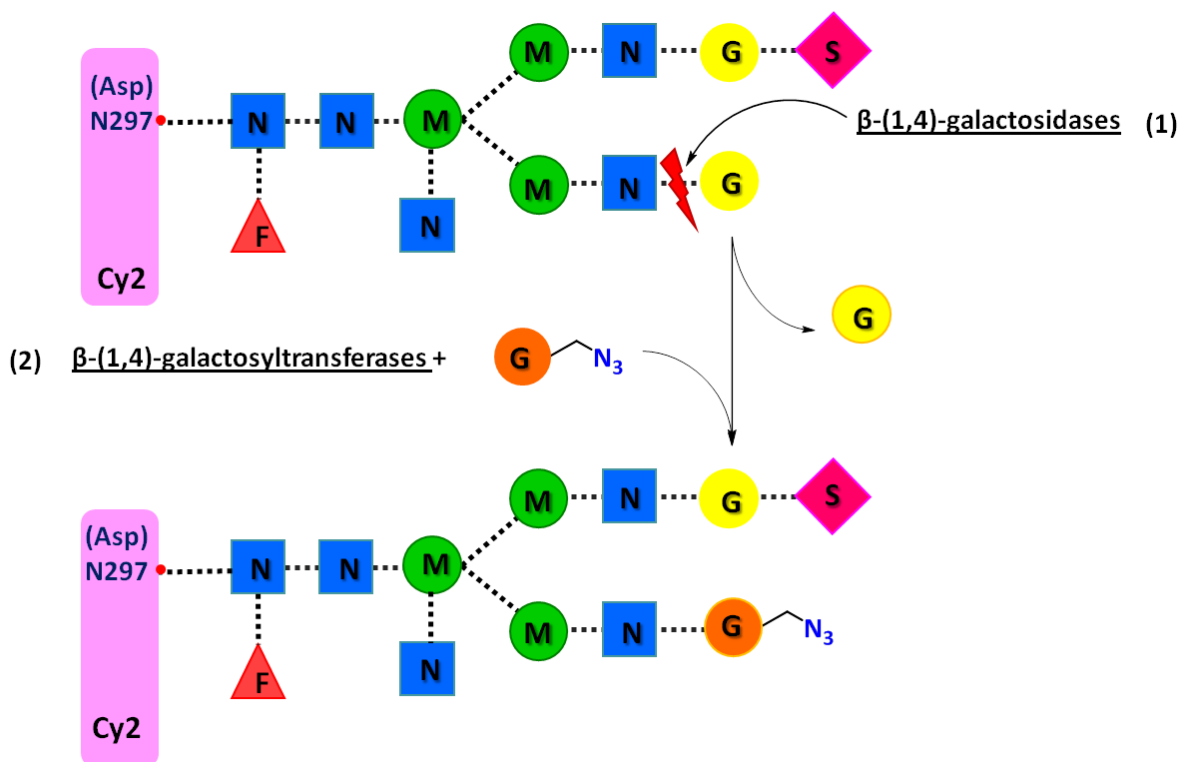


Figure 48: Scheme of the enzymatic site-specific modification of the antibody. (1) Cleavage of the GlcNAc-Gal bond through β (1,4)-galactosidase in sodium acetate buffer (10 mM, pH 5). The reaction was left overnight (\approx 12 hours) at 30°C. (2) Attachment of the unnatural UDP-6-azidogalactose using UDP-6-azido-galactose and β (1,4)-galactosyltransferase in TRIS·HCl buffer (50

mM, pH 7.4), in the presence of Alkaline phosphatase (2 U) and $\text{MnCl}_2 \cdot 4\text{H}_2\text{O}$ (20 mM). The reaction was left at 37°C overnight.

7.1.3. Antibody immobilization

7.1.3.1. Copper-mediated click-chemistry and its biocompatibility

Instead of using strain-promoted click reaction, we decided to use copper catalyzed cycloaddition to exploit its higher reactivity over copper-free azide/alkyne cycloaddition click chemistry. In fact, strain-promoted cycloaddition still remains 10-times slower than copper catalyzed terminal alkyne cycloaddition¹⁰⁴.

The main drawback of using a transition metal as catalyst to modify a protein is its toxicity caused by the Cu(I)-mediated generation of reactive oxygen species (ROS) from O_2 , that would damage biomolecules and cells²³⁶.

To overcome this problem, additives known to improve the biocompatibility of the reaction such as THPTA, BTTA and bis-L-histidine are currently used. These molecules are water-soluble ligands for Cu(I) that offer the advantages of both, accelerating the cycloaddition reaction and acting as reductants, helping the protection of biomolecules from ROS¹⁰⁶. Inspired by the work of Hong et al.¹⁰⁶, we focused on the use of THPTA catalyst, a water-soluble member of the tris(triazolylmethyl)amine family. The performance of this system was found to be sensitive to the nature of the solvent and to the overall copper concentration. The copper-catalyzed bioconjugation reaction was carefully optimized. The key factors to achieve a fast reaction are the following¹⁰⁶:

- a) Ascorbic acid is the preferred reducing agent, due to its convenience and effectiveness in generating the catalytically active Cu(I) oxidation state.
- b) Copper concentrations should generally be between 50 and 100 μM (use used 100 μM). The lower limit is necessary to achieve a sufficient concentration of the proper catalytic complex which incorporates more than one metal center, while more than 100 μM is not necessary to achieve high rates.
- c) At least 4 equivalents of THPTA relative to CuSO_4 should be employed^{104,106}. The purpose is to intercept and quickly reduce reactive oxygen species generated by the ascorbate-driven reduction of dissolved O_2 without compromising the CuAAC reaction rate.
- d) Compatible buffers include phosphate, carbonate, or HEPES in the pH 6.5-8.0 range, while Tris buffer should be avoided as the tris(hydroxymethyl)aminoethane molecule is a competitive and inhibitory ligand for Cu.

- e) Ascorbic acid should not be added to copper-containing solutions in the absence of the ligand (THPTA). So, it would be better first mix CuSO_4 with the THPTA ligand, add this mixture to a solution of the azide and alkyne substrates, and then initiate the CuAAC reaction by the addition of ascorbic acid to the desired concentration.

7.1.3.2. Optimization study using IgG from porcine serum (p-IgG)

Once a modification protocol was devised, the activity was focused on the optimization of the immobilization conditions. To this purpose we have used, as a model protein, an anti-rabbit immunoglobulin from porcine serum (hereafter reported as p-IgG).

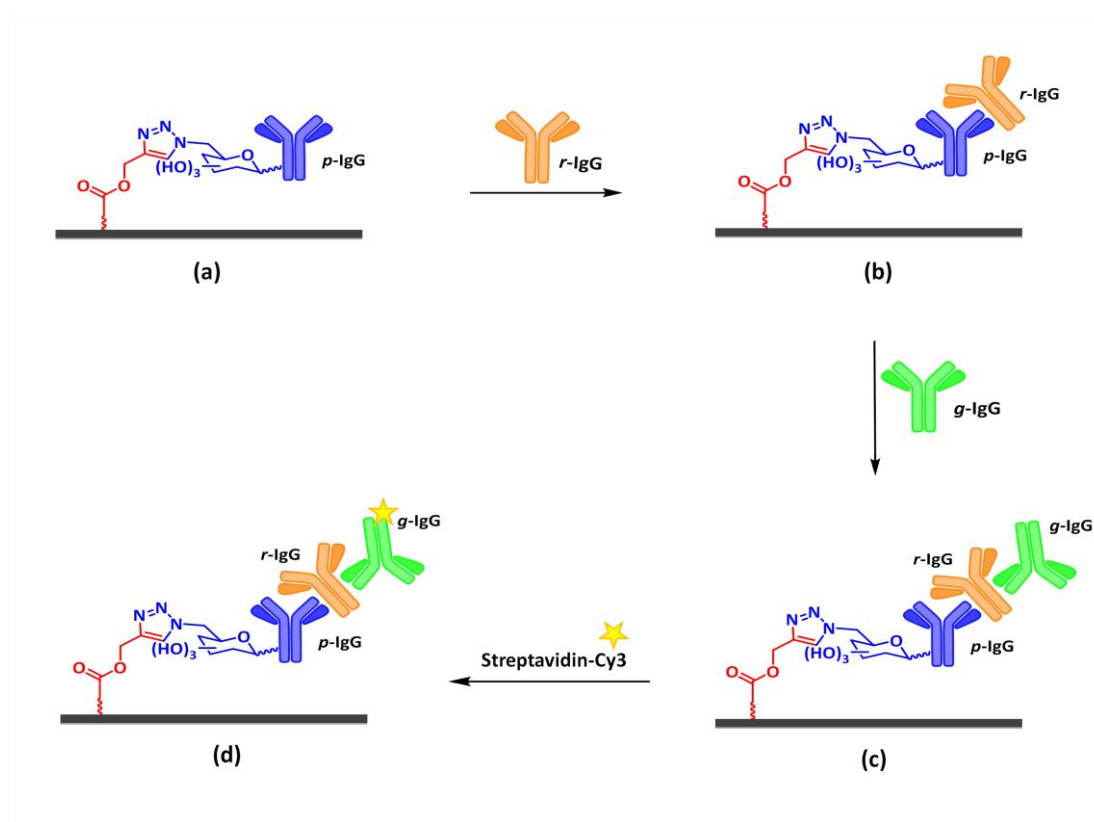


Figure 49: Scheme of the sandwich assay of the anti-rabbit immunoglobulin from porcine serum (p-IgG), where r-IgG is the antigen (anti-pig immunoglobulin from rabbit) and g-IgG is the biotinylated secondary antibody from goat (anti-rabbit). The last step (d) is the incubation with streptavidin labelled Cy3, to allow the fluorescence detection by a confocal scanner laser.

Starting from the consideration that the density of triple bonds on the surface, accessible for the interaction with the azide-probe, is not known, and considering that the amount of copper catalyst to be used strictly depend on this parameter, it was not possible to set up a protocol with an exact amount of catalyst calculated in theory.

Therefore, it was decided to start from the condition employed previously for glycans immobilization (paragraph 6.1) and to optimize this recipe: a solution containing antibody (0.6 mg/ml), CuSO_4 (2.5 mM) and ascorbic acid (12.5 mM) in TRIS HCl 50 mM buffer (pH 7.4) was arrayed on a poly(DMA-PMA-MAPS) coated Si/SiO_2 surface. In parallel, an experiment on poly(DMA-NAS-MAPS) coated surface was run, printing the same antibody (0.6 mg/ml) without modification, leading to a random immobilization *via* amine. After an overnight incubation of both chips in a humid chamber, the slides were washed and. A blocking-step with ethanol-amine was needed to block the unreacted active esters only for poly(DMA-NAS-MAPS) coated slides. Then, as depicted in **Figure 49b**, the chips were incubated with a solution (100ng/ml) of antigen (r-IgG), for 2 hours in dynamic conditions at room temperature. After a washing step an incubation with the secondary biotinylated antibody (g-IgG) was carried out (1 $\mu\text{g}/\text{ml}$ in PBS, 1 hour at rt in static condition) (**Figure 49c**), to allow fluorescence detection of the spots through the incubation with a streptavidin-Cy3 labelled (2 $\mu\text{g}/\text{ml}$ in PBS, 1 hour at room temperature in static condition) **Figure 49d**.

After the first washing step (10 min., PBS buffer) for the poly(DMA-PMA-MAPS) slide, and a blocking step of 1 hour with ethanolamine for the poly(DMA-NAS-MAPS) slide, the mass of p-IgG- N_3 and p-IgG immobilized on the corresponding chip were quantified through label-free IRIS analysis. This technique, as described in section 3.1.2., is a microarrays sensing technique that utilizes optical interferometry with a buried reference plane to detect binding of biomolecules on a Si/SiO_2 biochip with a 500 nm layer of silicon oxide⁵⁶.

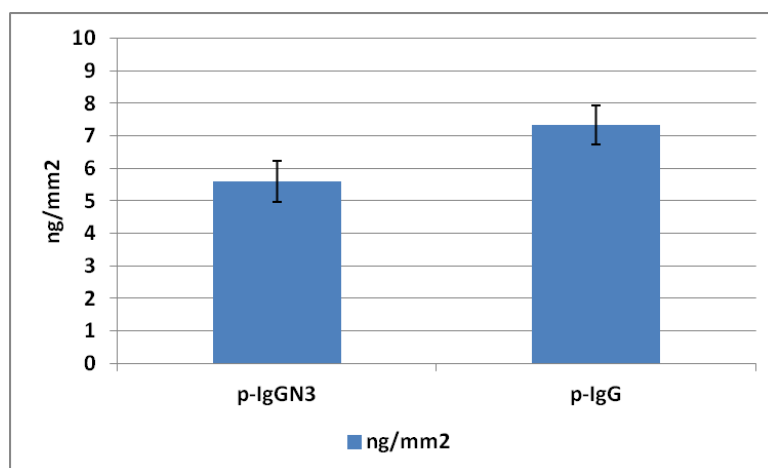


Figure 50: quantification of mass immobilized onto poly(DMA-PMA-MAPS) surface, p-IgG- N_3 , and poly(DMA-NAS-MAPS), p-IgG, respectively.

The mass determined, expressed as ng of antibody per mm^2 , in each immobilization strategy is reported in **Figure 50**. The immobilization of azido p-IgG resulted in a lower amount (5.6 ± 0.6 ng/mm^2) of antibody compared to the random immobilization *via* amine p-IgG (7.34 ± 0.64 ng/mm^2). In the following steps the chips were incubated with the antigen (r-IgG immunoglobulin from

rabbit) and with a biotinylated secondary antibody (g-IgG, biotinylated immunoglobulin from goat). The amount of captured antigen (r-IgG) was detected thanks to a final incubation with streptavidin-Cy3 allowing fluorescence detection using a confocal scanner laser. The mean fluorescence reported in **Figure 51a** confirms the presence of a lower amount of the p-IgG-N₃ (8000 ± 826) compared to the unmodified p-IgG (12000 ± 1332), each immobilized on a surface modified by the specifically reactive polymer. The fluorescence signals normalized by the mass of the immobilized p-IgG demonstrate that there is no signal gain using the oriented antibody (**Figure 51b**). So, in spite of the oriented immobilization, an apparently similar interaction affinity was observed.

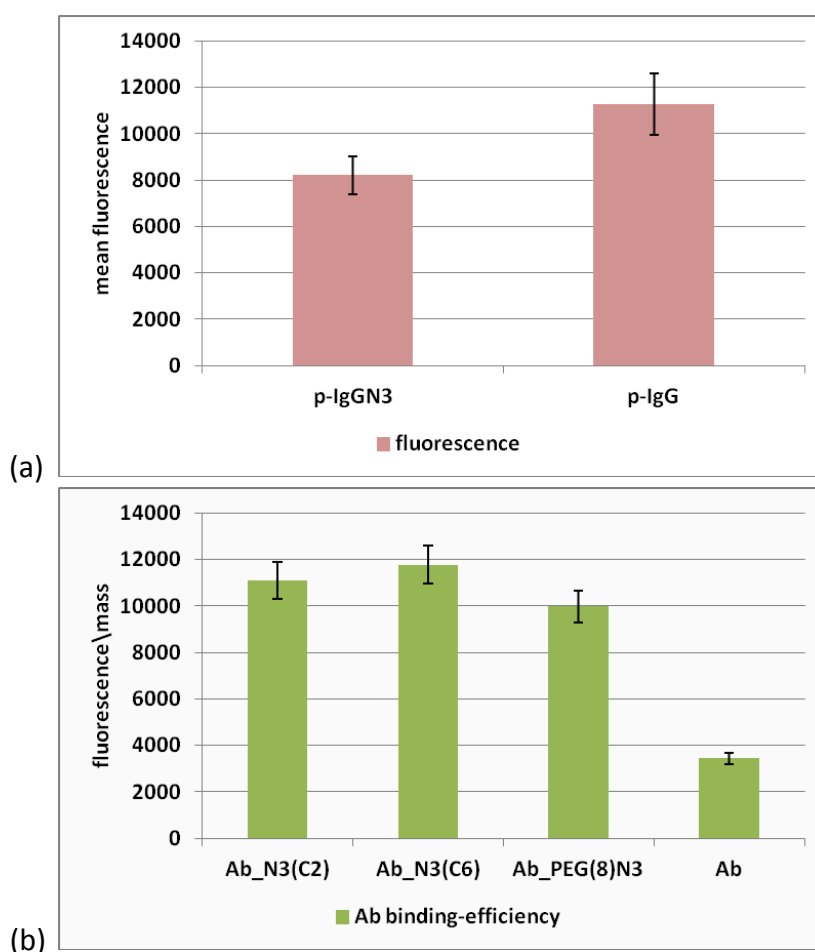


Figure 51: (a) mean fluorescence data for the two immobilized antibodies following a site-specific (p-IgG-N₃), *via* azide/alkyne cycloaddition, immobilization and a randomly (p-IgG), *via* amine, immobilization. (b) binding-efficiency obtain relating the immobilized amount with the recorded mean fluorescence signal.

Optimization of click condition using IgG-pegylated-N₃ (from porcine serum)

In the procedure described in paragraph 7.1.3.2., no precautions were taken toward oxidation and the antibody was used without THPTA protecting ligand, appropriate buffer and optimal reaction

time, etc. These conditions led to a low apparent affinity of the antibody under investigation. Therefore the entire procedure was revised. A new immobilization protocol implying random modification of the antibody, using a bifunctional polyethylene glycol (Azido-PEG₈-NHS ester) as the linker, was developed. The use of a bifunctional reagent with an azide moiety on one side and an active ester at the other end, allows introducing a larger number of azide groups by exploiting the numerous lysine amino-acids, present on the antibody.

A 5 mg/ml solution of p-IgG (from porcine serum) in PBS buffer (pH 7.4), reacted at room temperature for 2 hours in the presence of 4 equivalents of NHS-PEG₈-N₃ linker. Once the reaction was completed, the unreacted PEG was removed on centrifugal filter (Amicon Ultra 0.5 ml, Ultracel-30K) and the buffer was changed to sodium phosphate buffer (50 mM, pH 7.4) to facilitate the following click-reaction.

We compared the p-IgG-PEG₈-N₃ with the unmodified p-IgG on Si/SiO₂ surfaces coated with poly(DMA-PMA-MAPS) and poly(DMA-NAS-MAPS) respectively.

At the same antibody printing concentration (0.6 mg/ml), the following conditions were tested for the azido-modified p-IgG in sodium phosphate buffer (50 mM, pH 7.4):

1. CuSO₄ 2.5 mM, ascorbic acid 12.5 mM ([Cu]:[AAc]=1:5);
2. CuSO₄ 2.5 mM, THPTA 10 mM, ascorbic acid 12.5 mM ([Cu]:[THPTA]:[AAc]=1:4:5);
3. CuSO₄ 100 μM, THPTA 400 μM, ascorbic acid 6.25 mM ([Cu]:[THPTA]:[AAc]=1:4:62).

The unmodified p-IgG was spotted, at the same concentration (0.6mg/ml), in sodium phosphate buffer (50 mM, pH 7.4) on poly(DMA-NAS-MAPS) coated Si/SiO₂ surface.

After the spotting, the slides were left in a humid chamber for the immobilization step. Two different reaction times (1 hour, 12 hours) were initially tested to check if the introduction of the ligand protector, THPTA, could accelerate the immobilization rate also on a solid surface.

After the reaction was completed, the chips were washed 10 minutes with PBS, incubated with the antigen (r-IgG) and with the biotinylated-secondary antibody (g-IgG). The final incubation with streptavidine-Cy3 in PBS, allowed fluorescence detection, using a confocal scanner laser, and quantification of the captured antigen (r-IgG).

The same exact conditions were used for the immobilization of the unmodified p-IgG on poly(DMA-NAS-MAPS). On this surface a blocking-step was carried out before the incubation with the antigen. This was necessary to block all the remaining active esters that could be still reactive thus avoiding any secondary/aspecific interaction with the surface¹⁰. In the graph below (**Figure 52**) a comparison

of the fluorescence obtained at the end of the assay in experiments run at different reaction times (1 and 12 hours) is depicted.

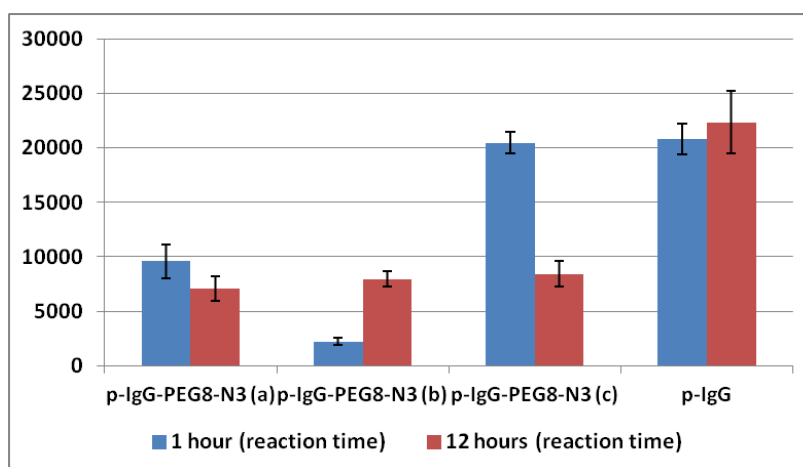


Figure 52: The three reaction conditions for the immobilization of the randomly modified p-IgG-PEG₈-N₃ are signed as (a) CuSO₄ 2.5 mM, ascorbic acid 12.5 mM ([Cu]:[AAc]=1:5), (b) CuSO₄ 2.5 mM, THPTA 10 mM, ascorbic acid 12.5 mM ([Cu]:[THPTA]:[AAc]=1:4:5) and (c) CuSO₄ 100 μM, THPTA 400 μM, ascorbic acid 6.25 mM ([Cu]:[THPTA]:[AAc]=1:4:62). Both p-IgG-PEG₈-N₃ and p-IgG were left react 1 hour (blue bars) and 12 hours (pink bars), in a humid chamber before starting the experimental protocol.

From the results it was evident that the presence of the ligand THPTA was essential to protect the antibody from possible damage. The experiment also provided information on the correct amount of reagents to be used. In the presence of THPTA the reaction time must be shorter, therefore a higher amount of the reducing agent (ascorbic acid) was required (≈ 62 equivalents)^{104,106}. Furthermore, an unnecessary long-time of reaction leads to an increase of the toxic effect of the copper catalyst. As described by others, an increased exposure to O₂ also enhances the production of reactive oxygen species (ROS) that are known to be prejudicial for biomolecules and cells¹⁰⁴.

For these reasons, similar experiments were performed to investigate reaction immobilization time in a humid chamber in two different reaction conditions. The same p-IgG-PEG₈-N₃ amount (0.6 mg/ml) in sodium phosphate buffer (50 mM, pH 7.4) was reacted in the presence of copper, THPTA and ascorbic acid at different concentrations but maintaining an “excess” of the reducing agent (ascorbic acid), as reported:

1. CuSO₄ 2.5 mM, THPTA 10 mM and ascorbic acid 125 mM ([Cu]:[THPTA]:[AAc]=1:4:50);
2. CuSO₄ 100 μM, THPTA 400 μM and ascorbic acid 6.25 mM ([Cu]:[THPTA]:[AAc]=1:4:62).

Six poly(DMA-PMA-MAPS) coated Si/SiO₂ surfaces were arrayed with p-IgG-PEG₈-N₃ in the two different reaction condition, and six poly(DMA-NAS-MAPS) coated Si/SiO₂ surfaces were arrayed with the unmodified p-IgG. In order to study the influence of the different reaction times, two chips for each coating were incubated for 5, 10, 20, 30, 60 minutes whereas the classical 12 hours protocol was used to compare the classical condition of immobilization on the active ester coated surface.

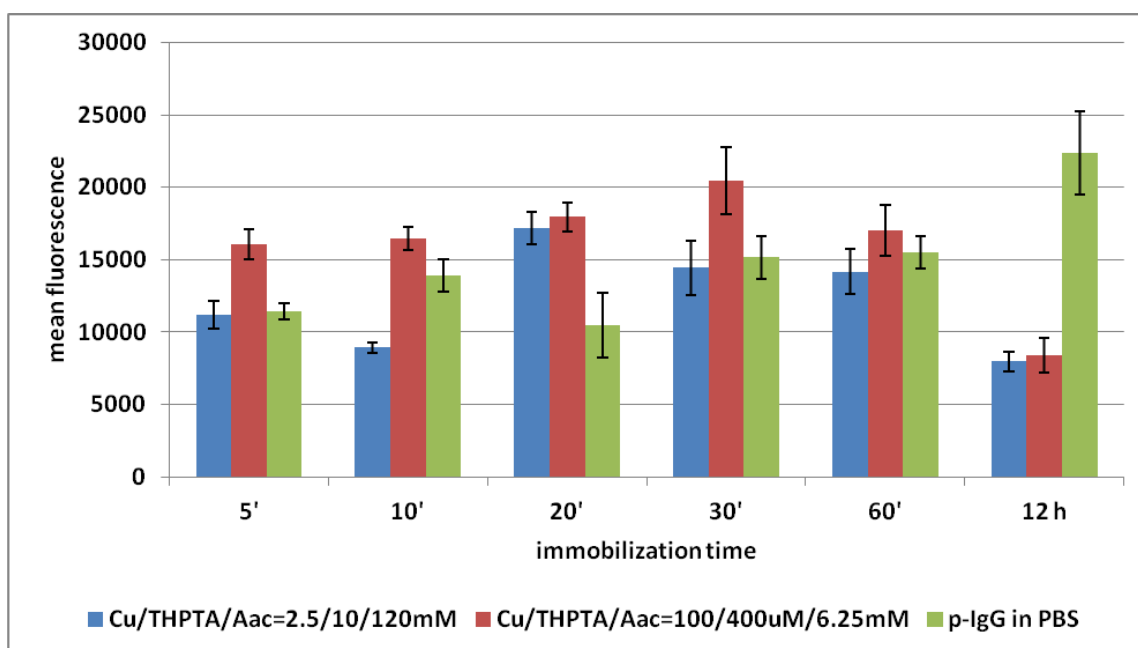


Figure 53: mean fluorescence intensities obtained from the different immobilization conditions of p-IgG-PEG₈-N₃ (blue: CuSO₄ 2.5 mM, THPTA 10 mM and ascorbic acid 120mM; red: CuSO₄ 100 μM, THPTA 400 μM and ascorbic acid 6.25 mM) on poly(DMA-NAS-MAPS), of unmodified p-IgG, green, on poly(DMA-NAS-MAPS), depending on the immobilization time.

As it can be observed from the above histogram (**Figure 53**), the best results among the p-IgG-PEG₈-N₃ conditions were obtained using copper catalyst at 100 μM concentration. A higher catalyst amount is therefore not necessary, confirming the data reported by Hong et al.¹⁰⁶. Considering the immobilization via 1,3-dipolar Huisgen cycloaddition, a higher immobilization yield was obtained in 30 minutes, whereas, extending the reaction time (from 1 to 12 hours), was not advisable probably due to antibody stability problem. On the other hand, the random immobilization *via* amine active ester reaction on a poly(DMA-NAS-MAPS) coated surface, has the drawback of requiring a longer immobilization time. However it still remains competitive when random immobilization conditions are used. The real advantage of the “click” approach lies in its site-specific immobilization. If the azide functionalities are randomly introduced there are no reasons to use of the more sophisticated click approach.

7.2. Interleukin-6 bioassay: the advantage of orientation

In order to evaluate the advantages provided by the oriented immobilization, we deeply explored the advantages of a site-specific modification on the Fc region of an antibody, coupled with the use of a quickly and regio-specific immobilization onto a polymeric coated surface, that features a solution-like environment (paragraph 5.1.2.).

To validate the methodology and highlight its advantages, a sandwich microarray test for the detection of interleukin-6 (IL-6) was developed²³⁷. Among the most intensively studied protein biomarkers, cytokines are implicated in the initiation and development of almost every major life-threatening disease. They play a prominent role in cancer, neurodegenerative diseases, cardiovascular diseases, sepsis and many other pathologies²³⁸. Although enzyme-linked immunosorbent assay (ELISA) is the gold standard for the measurement of individual cytokine concentration, the key to successful identification of biomarkers is the simultaneous detection of multiple cytokines with high sensitivity. IL-6 was chosen as a model of a typical inflammatory biomarker to be detected with high sensitivity, thus demonstrating the advantages provided by an oriented immobilization of the capturing antibody in a microarray based immunoassay.

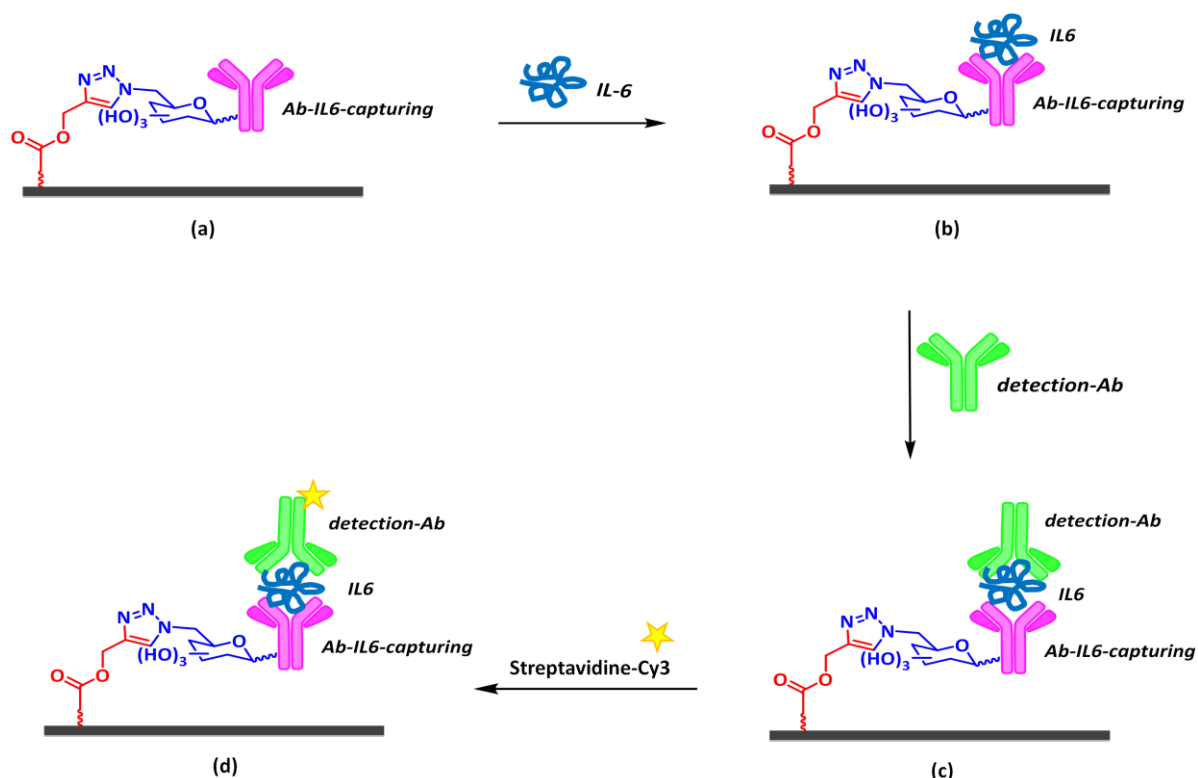


Figure 54: Scheme of the IL-6 test. (a) First the immobilization of the capturing antibody occurred via oriented copper mediated 1,3-dipolar Huisgen cycloaddition; then (b) the interaction with the target in solution (IL-6) occurs and (c) the detection-Ab was used to allow a final fluorescence detection through (d) streptavidin-Cy3.

The IL-6 capturing antibody was modified both site-specifically, using the procedure described above and detailed in “materials and method” (chapter 9), and randomly, using 4 equivalents of the azido-PEG linker (NHS-PEG₈-N₃), exploiting the abundance of lysine (-NH₂ terminal) on the antibody structure.

Furthermore, to validate the enzymatic procedure here proposed to modify antibodies with an azide moieties, the enzymatic path developed in this thesis was compared with the one proposed by the commercial kit, named Site-Click Antibody Labelling from Life Technologies. With the commercial kit a 2-azidogalactose was introduced on Fc region of the antibody using a mutant enzyme, GalT(Y289L)¹³³.

With both enzymatic pathways, the advantage of surface oriented immobilization was demonstrated. This immobilization strategy leaves the two binding-sites available for the interaction with the antigen (IL-6) in solution (comparison with the pegylated antibody). In addition, the higher binding-efficiency obtained by introducing an unnatural galactose carrying a less hindered azido functionality on C-6, instead of on C-2, was demonstrated.

Three azido modified IL-6 capturing antibodies were spotted at the same concentration (0.35 mg/ml) in sodium phosphate buffer (50 mM, pH 7.4) onto poly(DMA-PMA-MAPS) coated slides. The reagents for 1,3-dipolar cycloaddition were used in the optimized condition previously determined: CuSO₄ 100 μM, THPTA 400 μM and ascorbic acid 6.25 mM. CuSO₄ and THPTA were first mixed for 10 minutes, and then added to the solution containing the modified antibodies. Finally, just before the spotting, ascorbic acid was added to initiate the reaction.

A slide coated with poly(DMA-NAS-MAPS) was spotted with 0.35 mg/ml of the unmodified IL-6 capturing antibody in the 50mM sodium acetate, buffer, pH 4, to compare oriented and random immobilization via active ester/amine reactivity.

After the spotting step, the alkyne modified slides were left in the humid chamber for 30 minutes and then washed for 10 minutes in PBS, whereas poly(DMA-NAS-MAPS) slides were first blocked with ethanol-amine.

Before starting the incubation, the mass of the immobilized antibody was measured using IRIS, a label-free technique briefly described in paragraph 3.1.2.. The mass quantification allows relating the efficiency of the Ab-antigen interaction (fluorescence of the bioassay) to the mass (ng/mm²) of antibody effectively immobilized. This relation helps to understand the importance of an oriented immobilization of the capturing bioprobe. In particular it was demonstrated that a higher amount of immobilized probe does not necessary lead a higher amount of antigen captured on the surface confirming the importance of an immobilization strategy that favors at most the tail-on antibody orientation.

In the histogram below the amount of the immobilized IL-6 capturing antibody is depicted (**Figure 55**).

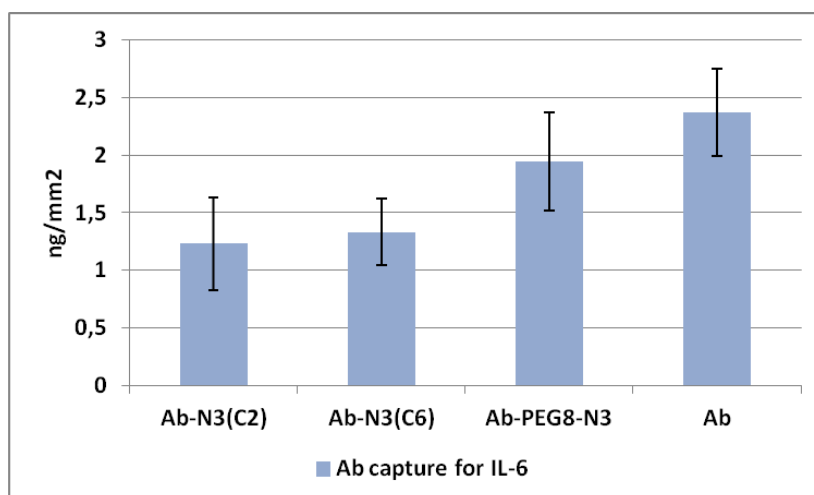


Figure 55: the different amount (ng/mm²) of antibody captured IL-6 (Ab) immobilized onto the respective coated surface. The azido modified were all immobilized on poly(DMA-PMA-MAPS) coated surface, while the unmodified Ab was immobilized on poly(DMA-NAS-MAPS) surface.

After the incubation with the antigen (IL-6, 2ng/ml), with the biotinylated secondary antibody (detection-Ab) and with streptavidin-Cy3, a fluorescence signal was obtained and normalized to the mass of probe to provide a graphic of normalized fluorescence/(ng/mm²), **Figure 56**.

Considering the results obtained (**Figure 56**), the advantage of an oriented antibody immobilization is evident. The dramatic decrease in the efficiency of the antibody when randomly immobilized via amine, also compared with the pegylated antibody, is probably due to the higher sensitivity of this antibody toward the orientation of its binding-sites.

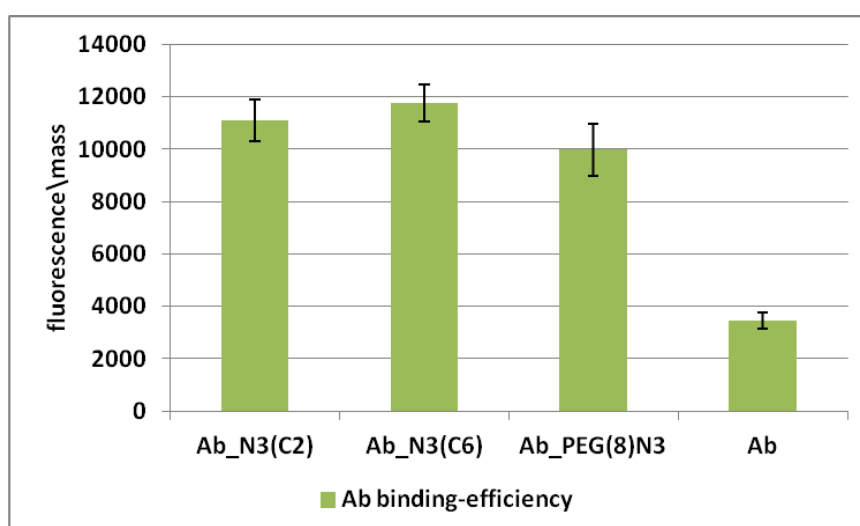


Figure 56: the binding-efficiency of each modified and unmodified antibody for IL-6 capture printed on their properly modified surface.

The importance of the orientation to achieve good binding efficiency of the target was demonstrated by this experiment. Independently from the approach used for the functionalization, the site specific azido-modified antibodies show a higher amount of antigen captured per mass unit compared to the antibodies randomly immobilized. Even though a higher immobilization yield is achieved with the native antibody on poly(DMA-NAS-MAPS), this does not result in a higher capture efficiency in this specific bioassay. The PEG modified antibody, Ab-PEG₈-N₃, thanks to its multiple anchoring points was also immobilized with high efficiency: $1.94 \pm 0.43 \text{ ng/mm}^2$, a value close to that of the unmodified one ($2.37 \pm 0.38 \text{ ng/mm}^2$). However the bio-recognition efficiency provided by the site-specific azido modified antibodies was higher when compared with the non oriented antibodies due to a more efficient antibody-antigen interaction. Furthermore, thanks to the azido functionality, the immobilization occurred in only 30 minutes as opposite to several hours required by the poly(DMA-NAS-MAPS) surface.

7.3. Conclusion. Poly(DMA-PMA-MAPS)-Si/SiO₂ platform in antibody microarrays: the role of probes orientation

In conclusion, in this work we have developed a simple methodology to increase the performance of microarray analysis by combining the superior optical and physical characteristics of a Si/SiO₂ surface with a simple and robust coating procedure using a polymer that allows a click chemistry reaction to bind biomolecules to the surface. The polymer forms a thin film which reproduces a solution-like environment. The alkyne functionality of the polymer leads to a regiospecific probe immobilization by fast copper mediated 1,3-dipolar Huisgen cycloaddition.

This new functionalization approach was used for the immobilization of an azido site-specific modified antibody in a regiospecific manner. The antibody tail-on orientation was found to enhance the molecular recognition efficiency toward the antigen in solution. The results shown in this chapter confirm the general knowledge that antibody microarrays take advantage from orientational control of the immobilized probe. An enzymatic approach based on the use of commercially available enzyme, was successfully applied to the site specific protein modification with an azido moiety.

A sandwich assays for interleukin-6 (IL-6) (**Figure 54**) was developed to demonstrate the advantage of an oriented antibody immobilization compared to a random immobilization strategy, exploiting both an azido PEG modified antibody (Ab-PEG₈-N₃) and the amino functionality naturally presents in the protein.

The proposed conjugation approach offers the advantage of insensitivity to pH buffer and side reactions of the triazole formed, expanding its application toward every antibody.

Furthermore, the polymeric coating reproduces a solution-like environment when in contact with a buffer solution that results in a swelling of the dimethylacrylamide back-bone of about 15 nm (paragraph 5.1.2). This coating feature coupled with the oriented immobilization mode increases the availability of the probes immobilized onto the surface and their accessibility to the target. The binding-efficiency of the oriented antibody was found to be higher than that of randomly attached antibodies.

All these advantages, combined with the superior characteristics of the surface (Si/SiO₂) pave the way for the construction of a high-performing antibody microarray platform. Further studies are ongoing, to improve the covalent attachment of the site-specifically modified antibody to consolidate the strategy for the oriented covalent immobilization of antibodies.

8. Conclusions

In this work we introduce a new polymer obtained from the polymerization of N,N-dimethylacrylamide (DMA), *3-trimethylsilylprop-2-yn methacrylate* (PMA) and 3(trimethoxysilyl)propylmethacrylate (MAPS), poly(DMA-PMA-MAPS) and describe its use in the formation of a functional coating for glycan and antibody microarray analysis. By combining physisorption and chemisorption, an ultra-thin hydrophilic 3D coating covalently grafted onto glassy solid surface could be obtained in less than one hour. The dimethylacrylamide (DMA) back-bone interacts with the surface by weak non covalent interactions (i.e. H-bond, Van der Waals or hydrophobic forces) allowing the whole polymer to get closer to the surface, while the pending hydrolyzed silanol monomers (MAPS) promote condensation of the polymer with surface silanols or between contiguous chains providing coating stabilization.

The backbone of the polymer bears alkyne moieties, which allow binding of azido-modified probes by "click" chemistry. This attachment mode offers a number of advantages in the immobilization process, such as high grafting efficiency, oriented immobilization and insensitivity to functionalities present in natural probes (bio-orthogonality). The high local concentration of probe molecules on the polymer and the hydrophilic character of the coating increase the availability of the immobilized probes and their ability to interact with the target in solution.

Additionally, this work introduces a new silicon/silicon oxide (Si/SiO₂) substrate with superior optical properties in order to obtain a high-performing platform for microarray analysis. This support allows to enhance the signal fluorescence intensity by a factor of 4, which is vital for microarray sensitivity⁵⁶. This layered substrate is widely available, inexpensive and compatible with established glass surface chemistries, it has a low roughness and provides a tuneable wavelength enhancement by changing the thickness of the oxide onto the silicon substrate.

The advantages of the technology were demonstrated in glycan and antibody microarray analysis.

In the first application, glycan microarrays, eight different α -mannose derivatives carrying an azido functionality on their linker could be covalently immobilized onto poly(DMA-PMA-MAPS) Si/SiO₂ coated surface in a regio-selective manner, and their interaction with the legume lectin Concanavalin A was studied. Thanks to the high sensitivity of the solid support (Si/SiO₂) and to the high binding-capacity of the polymeric coating, carbohydrate-lectin interactions were studied at low glycan density. Furthermore, besides the classical qualitative fluorescence analysis, a quantitative analysis was carried out to determine surface dissociation constants ($K_{D,surf}$) of each glycomimetic under investigation. A detailed investigation on the influence of multivalency on

carbohydrate-lectin affinity could be made by calculating surface dissociation constant ($K_{D,surf}$) for each glycomimetic at decreasing glycan printing concentration.

In the second application, the new polymer coating was used for the regio-specific immobilization of azido site-specifically modified antibodies. The antibody tail-on orientation was found to enhance the molecular recognition efficiency toward the antigen in solution. The proposed new approach was inspired by a work of Zeglis et al.¹³² that has been reported for the site-specific radio-labelling of antibody. The results shown confirmed the general knowledge that an orientational control of the probes is recommended to provide a high-performing antibody microarray analysis. An enzymatic approach based on the use of a commercially available enzyme was successfully applied to the site specific modification of an antibody azido moiety.

A sandwich assays for interleukin-6 (IL-6) was developed to demonstrate the advantage of oriented immobilization compared to random immobilization.

This click conjugation approach offers the advantage of insensitivity to solvent and to buffer pH. Furthermore, the hydrophilic character of poly(DMA-PMA-MAPS) coupled with the oriented immobilization mode, increases the availability of immobilized probes onto the surface and their accessibility to the target in solution.

In conclusion, a new robust, sensitive, versatile and easy-to-make microarray surface was presented, combining the feasibility of poly(DMA-PMA-MAPS) 3D matrix, the versatility of the click chemistry and the superior optical characteristics of the Si/SiO₂ solid surface used.

9. Materials and methods

List of Abbreviations

AIBN	Azoisobutyronitrile
Azido-PEG	Polyethylene glycole azide
BSA	Bovine serum albumine
ConA	Concanavalin A
CuAAC	Copper-catalyzed Azide-Alkyne cycloaddition
Cy-3	Cyanine-3
DI water	Deionized water
DCM	Dichloromethane
DMA	<i>N, N</i> -Dimethylacrylamide
DMF	dimethyl-formamide
DMSO	Dimethylsulfoxide
EC50	Half maximal effective concentration
DPI	Dual polarization interferometry
GalNAz	Azido galactose
GalT	β (1,4)-galactosyltransferases
GPC	Gel Permeation Chromatography
$K_{D,surf}$	Surface dissociation constant
HEPES	4-(2-hydroxyethyl)-1-piperazineethanesulfonic acid
HPLC	High-performance liquid chromatography
IL-6	Interleukin-6
LBB	Lectin binding buffer
MALLS	Multi-Angle Laser Light Scattering
MAPS	3-(trimethoxysilyl) propyl methacrylate
MS	Mass Spectrometry
MW	Molecular Weight
Q H ₂ O	MilliQ Water
NAS	<i>N</i> -Acryloyloxysuccinimide
NHS	<i>N</i> -hydroxysuccinimide
NHS-PEG ₈ -N ₃	<i>N</i> -hydroxysuccinimide-polyethylene glycole-azide
PBS	phosphate buffer saline
PEG	Polyethylene glycole
Py	pyridine

PMA	3-trimethylsilyl-prop-2-ynyl methacrylate
Rf	Retardation factor
SAMs	Self-Assembled Monolayers
Si/SiO ₂	Silicon/silicon oxide
TEAB	triethylaminetetra
THF	Tetrahydrofuran
THPTA	Tris(3-hydroxypropyltriazolylmethyl)amine
TLC	Thin liquid chromatography
Tris	Trizma Base /2-Amino-2-(hydroxymethyl)-1,3-propanediol
UDP	Uridine 5'-Diphosphate
UMP	Uridine 5'-Monophosphate

9.1. Materials

Dichloromethane (DCM), methanol (MeOH), and triethylamine (TEA) were dried over calcium hydride; THF was distilled over sodium. Reactions requiring anhydrous conditions were performed under nitrogen or argon where indicated.

1,2,3,4-di-*O*-isopropylidene-D-galactopyranose and 2-Chloro-4H-1,3,2-benzodioxaphosphorin-4-one (97%) were purchased from ABCR (Karlsruhe, Baden-Württemberg, Germany). Cy-3 azide was purchased from Lumiprobe GmbH (Feodor-Lynnen Strasse 23, 30625 Hannover, Germany). The SiteClick Antibody Labelling was purchased from LifeTechnologies (part of the Thermo Fisher Scientific Inc., Waltham, MA, USA). The Amicon filters were purchased from Millipore (Merk s.p.a., Milan, Italy).

ELISA MAXTM standard set Human IL-6 was purchaseTM from BioLegend (San Diego, CA, USA).

The bifunctional polyethylene glycol (Azide-PEG₈-NHS ester) was purchased from Jena Bioscience GMBH (Jena, Germany).

Tetrazole solution (0.45 M in CH₃CN), tert-Butyl hydroperoxide solution (≈5.5 M in decane), Uridine 5'-monophosphomorpholidate-4-morpholine-N,N'-dicyclohexylcarboxamidine salt and all other chemicals, the enzymes (β -(1,4)-galactosidases and β -(1,4)-galactosyltransferases), the immunoglobulins (IgG anti-rabbit from porcine serum, IgG anti-pig from rabbit and biotinylated IgG anti-rabbit from goat), dry and deuterated solvents (CDCl₃, MeOD, D₂O), were purchased from Sigma Aldrich (St. Louis, MO, USA) and used without further purification.

Silicon oxide chips with a 100 nm thermal oxide layer were bought from Silicon Valley Microelectronics (Santa Clara, CA, USA), IRIS chips with a 500 nm thermal oxide layer were a kind gift from Prof. Selim M. Unlu from Boston University, MA (USA) and silicon oxynitride AnaChipTM

were brought from Fairfield. An Agilent 1200 series liquid chromatography system, (Agilent Technologies, Santa Clara, CA, USA) was used to carry out GPC. GPC columns were from Schodex (New York, NY, USA); MALLS system was purchased from Wyatt Technology (Santa Barbara, CA, USA). The piezoelectric spotter SciFlexArrayer S5 was brought from Scienion (Berlin, Germany) with its related software program, the microarray scanner ProScanArray was purchased from Perkin Elmer (Boston, MA, USA) along with its ScanArray express software, and the Analight Bio 200 with its Analight Explorer software were purchased from Fairfield Group (Stockholm, Sweden). IRIS instrumentation was a prototype developed in collaboration with the laboratory of Prof. Selim M. Unlu at Boston University, MA (USA), and it consists of a CCD camera (Retiga 2000R from QImaging), and an ACULED VHL surface-mount LED package (Perkin-Elmer), which has four independently driven LEDs with peak emission wavelengths of 455nm, 518, 598nm, and 635nm. IRIS images were acquired and fitted with ZoirayAcquire software, then the data were analyzed with ZoirayProcess software. For each protein, signals from 35 replicate spots were averaged.

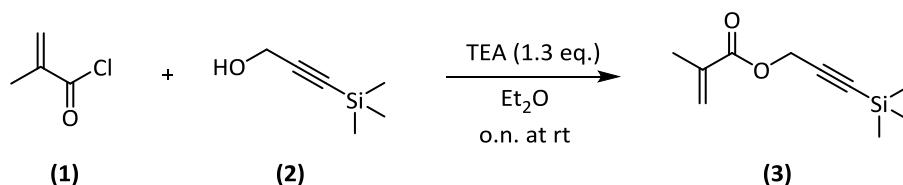
The HPLC chromatography was carried out using a manual injection (Rheodyne valve) connected to a pump JASCO 887-PU, a detector equipped with a preparative cell UVIDEC100-VI that is connect with a Data Station LKB 2210 1-channel recorder. The semi-preparative column used is a Phenomenex (Jupiter 10u Proteo 90A, size 250x21 10 mm) purchased from Phenomenex (Bologna, Italy).

^1H , ^{13}C and ^{31}P spectra were recorded at 400MHz on a Bruker AVANCE-400 instrument. Chemical shifts (δ) for ^1H , ^{13}C and ^{31}P spectra are expressed in ppm relative to an internal standard (CDCl_3 : 7.26 for ^1H and 77.16 for ^{13}C ; CD_3OD : 3.31 for ^1H and 49.00 for ^{13}C , D_2O : 4.79 for ^1H). Signals were abbreviated as s, singlet; br s, broad singlet; d, doublet; t, triplet; q, quartet; m, multiplet. Mass spectra were obtained with a ThermoFisher LCQapparatus (ESI ionization), or iontrap ESI Esquire 6000 from Bruker, or a Microflex apparatus (MALDI ionization) from Bruker, or Apex II ICR FTMS (ESI ionization—HR-MS). Thin layer chromatography (TLC) was carried out with pre-coated Merck F254 silica gel plates. Flash chromatography (FC) was carried out with Macherey-Nagel silica gel 60 (230–400 mesh).

9.2. Experimental section

9.2.1. Poly(DMA-PMA-MAPS) synthesis and characterizations

Synthesis of 3-trimethylsilyl-prop-2-ynyl methacrylate (PMA)

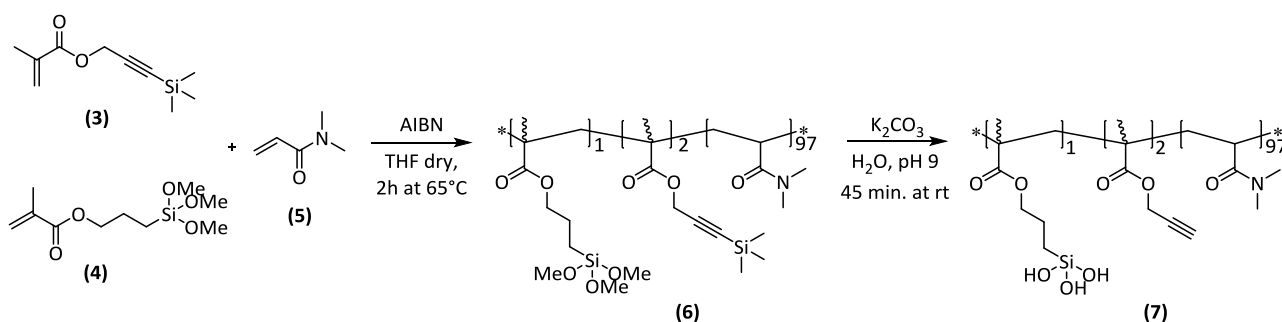


3-(trimethylsilyl)prop-2-yn-1-ol (2.31 ml, 15.6 mmol) and triethylamine (2.83 ml, 20.27 mmol) were dissolved in Et₂O (20 ml) and cooled to -20°C. A solution of methacryloyl chloride (2) (1.81 ml, 18.56 mmol) in Et₂O (10 ml) was added drop wise over 1 hour. The mixture was stirred at -20°C for 30 minutes and then overnight at room temperature. Ammonium salts were removed by filtration and the volatiles were removed under reduced pressure.

The yellow oil residue was purified by flash chromatography (EtP:Et₂O=50:1, R_f= 0.39) and the product (3) was obtained in 81% yield.

¹H-NMR (400 MHz, CDCl₃): δ = 0.18 (s, 9H, Si(CH₃)₃); 1.97 (m, 3H, CH₃C=CH₂); 4.76 (s, 2H, OCH₂); 5.62 (m, 1H, C=CHH); 6.17 (m, 1H, C=CHH).

Synthesis of copoly(*N,N*-dimethylacrylamide (DMA)- 3-trimethylsilyl-prop-2-ynyl methacrylate (PMA)- 3-(Trimethoxysilyl)propyl methacrylate (MAPS)), (poly(DMA-PMA-MAPS)).



The polymer was synthesized via a random radical polymerization in anhydrous tetrahydrofuran with a 20% w/v total monomer concentration. The DMA (5) was filtered on aluminium oxide to remove the inhibitor. The molar fraction of the monomers DMA (5), PMA (3) and MAPS (4) was 97:2:1.

The DMA and PMA monomers were dissolved in dry tetrahydrofuran (THF) in a round-bottom flask equipped with condenser, magnetic stirring. The solution was degassed by alternating argon purges with a vacuum connection, over a 10-min period. MAPS (4) and α,α' -Azobisisobutyronitrile (AIBN) (this latter at 2mM final concentration) were added to the solution, which was then warmed to 65 °C and maintained at this temperature under a slightly positive pressure of argon for 2 h.

After the polymerization was completed, the solution was first diluted to 10% w/v with dry THF and the polymer (6) precipitated by adding petroleum ether (10 times the reaction volume). The product, a white powder, was filtered on Buckner funnel and dried under vacuum at room temperature.

¹³C-NMR (400 MHz, CDCl₃), δ (ppm): 0.00 (Si(CH₃)₃); 36.65 (all CH₂); 45,62 (OCH₂C \equiv); 50.94 (Si(OCH₃)₃); 53.32 (OCH₂CH₂) 174.95 (all CO).

¹³C-NMR (400 MHz, DMSO), δ (ppm): -0.31 (Si(CH₃)₃); 36.08 (all CH₂); 44.78 (OCH₂C \equiv); 50.10 (Si(OCH₃)₃); 52.76 (OCH₂CH₂) 173.89 (all CO).

The protective trimethylsilyl groups were removed in water under basic condition, using K_2CO_3 (9mM) at pH 9. The reaction mixture was stirred at room temperature for 1h, then the polymer (7) was dialyzed, lyophilized and the white powder obtained was stored at $-20\text{ }^\circ\text{C}$.

^{13}C -NMR (400 MHz, $CDCl_3$), δ (ppm): 36.65 (all CH_2); 45,62 ($OCH_2C\equiv$); 52.40 (OCH_2CH_2); 75.92 ($\equiv CH$); 174.95 (all CO).

^{13}C -NMR (400 MHz, DMSO), δ (ppm): 36.08 (all CH_2); 44.79 ($OCH_2C\equiv$); 52.02 (OCH_2CH_2); 77.63 ($\equiv CH$); 78.31 ($C\equiv CH$); 174.96 (all CO).

Polymer characterization by Gel Permeation Chromatography

The size of each polymer was characterized using Gel Permeation Chromatography in tandem with an UV-detector ($\lambda=214\text{nm}$).

A JASCO 880 PU liquid chromatography system, consisting of an isocratic pump to control mobile phase flow throughout the system connected to a JASCO UVIDEC-100-III UV detector. ChromNAV Chromatography Data System -JASCO was used to analyze the sequence of sample injection and to calculate the calibration curve of polyacrylamide standards.

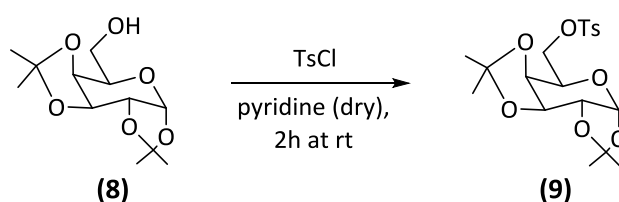
The GPC setup consists of four Shodex aqueous GPC columns in series: OHpak SB-G (guard column), OHpak SB-804M HQ, OHpak SB-803 HQ, and OHpak SB-802.5 HQ. Each column is packed with a poly-hydroxymethacrylate gel and connected in series with a decreasing exclusion limit. The columns were maintained at 40°C throughout each run using a thermostated column compartment. After the polymer sample is fractionated by GPC, the sample flows into a UV-detector. The molecular weight of the polymer was obtained by using a calibration curve.

Copoly(DMA-PMA-MAPS) (7) sample was diluted using the GPC mobile phase (GPC buffer: 100 mM NaCl, 50 mM NaH_2PO_4 , pH 3, 10% v/v Acetonitrile) to a concentration of 2.66 mg/ml and the sample was run three times through the GPC-UV system to test for reproducibility. Each run injected 20 μL of sample to be analyzed and the flow rate through the system was held at a constant 0.3 mL/min.

9.2.2. Total synthesis of Uridine 5'-(6-azido-6-deoxy- α -D-galactopyranosyl) diphosphate bis-triethylammonium salt (UDP-6-azidogalactose).

^{13}C -NMR, ^{31}P NMR and MS characterizations of the compounds here reported could be found in the referential article: M. Bosco, S. Le Gall, C. Rihouey, S. Couve-Bonnaire, M. Bardor, P. Lerouge, X. Pannecouke, *Tetrahedron Letters*, 2008, 49, 2294-2297.

1,2,3,4-di-O-isopropylidene-6-tosyl-6-deoxy- α -D-galactopyranose (9)



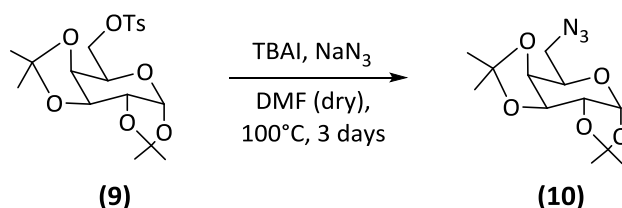
In a round bottom flask (250ml) the protected galactose (8) was introduced (3.0g, 11.5 mmol). After drying under vacuum for 20 minutes the galactose (8) was put under nitrogen atmosphere. Dry pyridine (115 ml, 0.1M) was added and the obtained mixture was stirred until a homogeneous solution was obtained. The tosyl-chloride (3.4g, 17.25 mmol) was then added and the reaction mixture was left 2 h under stirring at room temperature.

The reaction was controlled through TLC (Hex:AcOEt=7:3, Ammonium molybdate/Cerium sulphate).

Once the reaction was completed the solvent was removed under reduced pressure and re-dissolved in AcOEt. The crude was washed with HCl 1N, with a saturated NaHCO_3 solution and brine. The collected organic phases were dried over Na_2SO_4 anhydrous and the solvent was removed under reduced pressure.

The obtained product (9) was used without further purification (quantitative yield).

1,2,3,4-di-O-isopropylidene-6-azido-6-deoxy- α -D-galactopyranose (10)



The 6-tosyl galactose (9) (2.9 g, 7 mmol) was dried under vacuum and, under nitrogen atmosphere, dry DMF (7 ml, 1M) was added. Once the galactose was completely dissolved TBAI (775.8 mg, 2.1 mmol) and NaN₃ (2.73g, 42 mmol) were added.

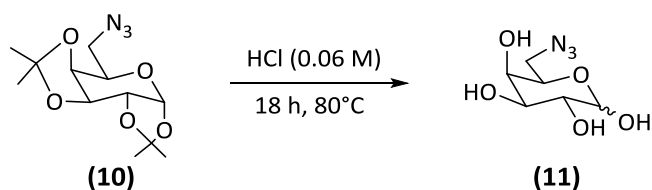
The mixture was stirred for 3 days at 100°C under nitrogen atmosphere.

The reaction was monitored through TLC (Hexane: AcOEt = 7:3). Once the reaction was completed the solvent was partially removed under vacuum and the reaction mixture was diluted with AcOEt and washed three times with distilled water. The collected organic phases were dried over anhydrous Na₂SO₄ and the solvent was removed under reduced pressure.

The crude was purified through flash chromatography (Hexane: AcOEt = 9:1, R_f = 0.4), and the 6-azidogalactose (10) was obtained in 69% of yield.

¹H-NMR (400MHz, CDCl₃) δ : 5.54 (d, 1H, J₁₋₂ = 5 Hz, H-1), 4.62 (dd, 1H, J₂₋₃ = 7.8 Hz, H-3), 4.34 (broad dd, 1H, H-4), 4.19 (dd, 1H, J₂₋₃ = 7.8 Hz, H-2), 3.90 (ddd, 1H, J₅₋₆ = 7.9 Hz, J_{5-6'} = 5.4 Hz, H-5), 3.50 (dd, 1H, J_{6-6'} = 12.7 Hz, J₆₋₅ = 7.9 Hz, H-6), 3.36 (dd, 1H, J_{6-6'} = 12.7 Hz, J_{6'-5} = 5.4 Hz, H-6'), 1.55 (s, 3H, C-CH₃), 1.46 (s, 3H, C-CH₃), 1.34 (s, 6H, C-CH₃).

6-azido-6-deoxy- α -D-galactopyranose(**11**)



The 6-azidogalactose (**10**) (1.72 g , 6.6 mmol) was dissolved in 60 ml of HCl aqueous solution (0.06 M) and left at 80°C under stirring for 18 hours. The reaction was followed through TLC.

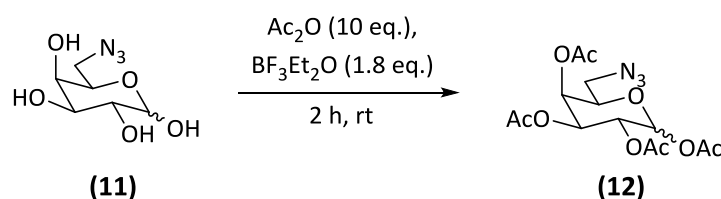
(Hexane:AcOEt = 8:2 was used to control the presence of the starting material, while a polar eluant, DCM:MeOH = 8:2, was used to monitor product (**11**) formation).

Once the reaction was completed the mixture was frozen, lyophilized and the crude was purified with flash chromatography (DCM:MeOH = 8:2).

The purified product (**11**) was obtained in quantitative yield.

$^1\text{H-NMR}$ (400 MHz, D_2O) δ : 5.26 (d, 1H, $J_{1-2} = 3.8$ Hz, H-1 α), 4.60 (d, 2H, $J_{1-2} = 7.9$ Hz, H-1 β), 4.18 (m, 1H, H-5 α), 3.95 (m, 1H, H-4 α), 3.89 (m, 2H, H-4 β), 3.85-3.76 (m, 4H, H-5 β , H-3 α , H-2 α), 3.67-3.43 (m, 11H, H-3 β , H-6 β , H-6 β' , H-6 α , H-6' α , H-2 β).

1,2,3,4-tetra-O-acetyl-6-azido-6-deoxy- α -D-galactopyranose(12)



The deprotected 6-azido-galactose (11) (1.35 g, 6.6 mmol) was dissolved under nitrogen atmosphere in Ac_2O (6.3 ml, 60 mmol). The reaction mixture was cooled to 0°C and $\text{BF}_3\cdot\text{Et}_2\text{O}$ (1.47 ml, 11.88 mmol) was added. The reaction was stirred for 30 minutes at 0°C and the trend of the reaction was controlled through TLC (Hex:AcOEt = 6:4, $R_f = 0.5$).

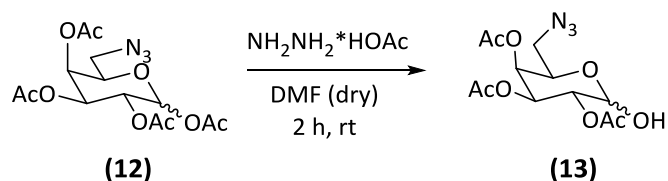
Once the reaction was completed the mixture was diluted with 150 ml of DCM. The diluted solution was washed three times with NaHCO_3 saturated solution and one time with brine. The organic phase was dried over anhydrous Na_2SO_4 and the solvent was removed under reduced pressure.

The crude was purified by flash chromatography (Hex:AcOEt = 7:3, $R_f = 0.35$).

The product (12) was obtained with 77 % of yield.

$^1\text{H-NMR}$ (400MHz, CDCl_3) δ : 6.40 (d, 1H, H-1 α), 5.71 (d, 1H, $J_{1-2}=8.4$ Hz, H-1 β), 5.48 (1H, H-4), 5.40 (d, 1H, H-3), 5.36-5.32 (dd, 1H, H-2 β), 5.10 (dd, 1H, $J_{1-2}=3.3$ Hz, $J_{2-3}=10.3$ Hz, H-2 α), 4.22 (broad ddd, 1H, H-5 α), 3.94 (broad ddd, 1H, H-5 β), 3.53 (dd, 1H, $J_{6-6'}=12.6$ Hz, $J_{6-5}=7.3$ Hz, H-6 β), 3.45 (dd, 1H, $J_{6-6'}=12.8$ Hz, $J_{6-5}=7.6$ Hz, H-6 α), 3.22 (dd, 2H, $J_{6-6'}=12.8$ Hz, $J_{6-5}=5.3$ Hz, H-6 α and β), 2.20 (s, 3H, $\text{CH}_3\text{-COO}$), 2.15 (s, 3H, $\text{CH}_3\text{-COO}$), 2.07 (s, 3H, $\text{CH}_3\text{-COO}$), 2.02 (s, 3H, $\text{CH}_3\text{-COO}$).

2,3,4-tri-O-acetyl-6-azido-6-deoxy- α -D-galactopyranose(12)



The acetylated 6-azido-galactose (12) (1.39 g, 3.7 mmol) was dissolved in 14 ml of dry DMF under nitrogen atmosphere and the solution was cooled to 0°C. At the same time in a 5 ml round bottom flask the monohydrate hydrazine (233.6 μ l, 4.81 mmol) was dissolved in 1.6 ml of dry MeOH and acetic acid (212.5 μ l, 3.7 mmol) was slowly added to obtain hydrazine acetate. After 30 minutes the MeOH solution of hydrazine acetate was added drop wise to the DMF solution of the sugar at 0°C. The reaction mixture was left 15 minutes at 0°C, then let to warm to room temperature and stirred for 2 hours.

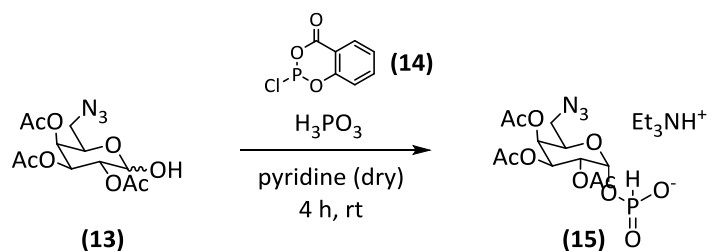
The reaction was control by TLC (Hex:AcOEt = 6:4).

Once the reaction was completed it was first diluted with AcOEt and washed with a solution of 1N HCl, a saturated NaHCO₃ aqueous solution and final with brine. The organic phase was dried over anhydrous Na₂SO₄ and the solvent was removed under reduced pressure.

The crude was purified with flash chromatography (Hex:AcOEt = 6:4) and a mixture of alpha and beta anomer (13) was obtained in 65 % yield.

¹H-NMR (400MHz, CDCl₃) δ : 5.57 (d, 1H, H-1 α), 5.45 (dd, 1H, J₄₋₃= 3.3 Hz, J₄₋₅=1.1 Hz, H-4), 5.43 (dd, 1H, J₃₋₂= 10.6 Hz, J₃₋₄= 3.3 Hz, H-3), 5.19 (dd, 1H, J₂₋₃ = 10.5 Hz, J₃₋₄= 3.6 Hz, H-2), 4.41 (dd, 1H, J_{5-6'} = 4.3 Hz, J₅₋₆ = 8.3 Hz, H-5), 3.46 (dd, 1H, J_{6-6'} = 12.8 Hz, J₆₋₅ = 8.2 Hz, H-6), 3.23 (dd, 1H, J_{6'-6} = 12.7 Hz, J_{6'-5} = 4.5 Hz, H-6'), 2.20 (s, 3H, CH₃-COO), 2.12 (s, 3H, CH₃-COO), 2.02 (s, 3H, CH₃-COO).

2,3,4-tri-O-acetyl-6-azido-6-deoxy- α -D-galactopyranosyl phosphite Et₃N salt (15)



Phosphorous acid (H_3PO_3 , 115 mg, 1.40 mmol) was co-evaporated three times with dry toluene and left under vacuum over night. The day after it was dissolved in dry pyridine to obtain a 2 M solution. The H_3PO_3 solution was added drop-wise into a dry pyridine solution of the 6- azido-galactose (13) (155 mg, 0.47 mmol), at room temperature under nitrogen atmosphere. The reaction mixture was cooled to 0°C , and salicyl chloro phosphite (14) (143 mg, 0.71 mmol) was added. The reaction mixture was left stirred at room temperature until the starting material has been consumed (4 hours).

The reaction was control with TLC (DCM:MeOH=7:3, 1% of TEA).

Work up:

Once the reaction was completed, a 1 M buffer solution of $\text{Et}_4\text{N}^+\text{HCO}_3^-$ (TEAB, pH 8.5) was added (4ml/mmol of galactose). The mixture was then diluted with DCM and washed three times with a 0.5 M buffer solution of TEAB (tetraethylammonium bicarbonate, 1M aqueous solution). The collected organic phases were dry over Na_2SO_4 (anhydrous) and the solvent was removed under reduced pressure.

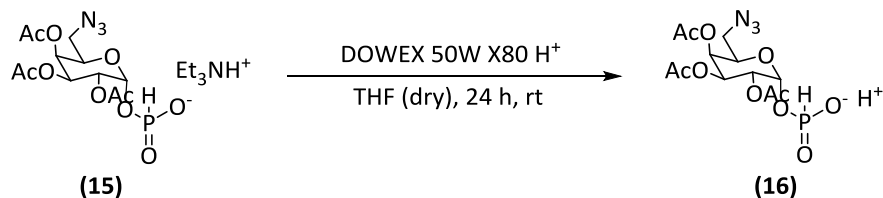
The crude was purified by automated chromatography on silica gel (using a gradient from pure CH_2Cl_2 to 20% of MeOH in X min), in the presence of 1% of TEA), and the product (15) was obtained in 84% yield.

$^1\text{H-NMR}$ (400MHz, CD_3OD) δ : 6.92 (d, 1H, $J_{\text{P-H}} = 635.2$ Hz, P-H), 5.80 (dd, 1H, $J_{\text{H-P}} = 8.8$ Hz, $J_{1-2} = 3.6$ Hz, H-1 α), 5.48 (d, 1H, $J_{4-3} = 3.0$ Hz, H-4), 5.40 (dd, 1H, $J_{3-4} = 3.2$ Hz, $J_{3-2} = 10.8$ Hz, H-3), 5.15 (dd, 1H, $J_{2-3} = 10.5$ Hz, $J_{2-1} = 3.4$ Hz, H-2), 4.43 (m, 1H, H-5), 3.50 (dd, 1H, $J_{6-6'} = 12.9$ Hz, $J_{6-5} = 7.7$ Hz, H-6), 3.30 (dd, 1H, $J_{6'-6} = 12.8$ Hz, $J_{6'-5} = 5.2$ Hz, H-6'), 3.22 (q, 6H, $J = 7.3$ Hz, $(\text{CH}_3\text{CH}_2)_3\text{NH}^+$), 2.20 (s, 3H, $\text{CH}_3\text{-COO}$), 2.10 (s, 3H, $\text{CH}_3\text{-COO}$), 1.98 (s, 3H, $\text{CH}_3\text{-COO}$), 1.40 (t, 9H, $(\text{CH}_3\text{CH}_2)_3\text{NH}^+$).

$^{31}\text{P-NMR}$ (121.5 MHz, CD_3OD) δ : 1.41 (s, 1P, P-H).

2,3,4-tri-O-acetyl-6-azido-6-deoxy- α -D-galactopyranosyl phosphate Et₃N salt (17)

A) Counterion exchange



Resin preparation:

DOWEX 50W X80 H⁺ acidic resin was gently shaken for 2 hours with MeOH, filtered, dried under vacuum over night and regenerated with 5% aqueous solution of HCl for two hours.

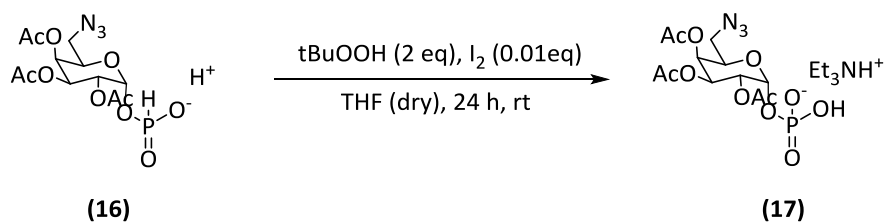
The required volume of HCl solution was determined from this equation, where Y is 4 for a strong resin, and the capacity exchange is equal to 1.7 meq/ml:

$$V(\text{ml})_{\text{regenerant}} = \frac{X(\text{ml})_{\text{resin}} * \text{Capacity Exchange} * \text{MW regenerant} * 100}{1000 * \text{regenerant}(\% \frac{w}{v})} * Y$$

Ion exchange column:

The regenerated resin was washed with distilled H₂O to remove the HCl excess, and the water was removed with several washing cycles with THF. A column (2 cm of diameter) was then prepared (10 ml of resin in THF) and the H-phosphonate (15) (72 mg, 182 μ mol) was dissolved in the smallest volume of THF and passed slowly through the exchange column, monitoring by TLC (DCM:MeOH=7:3). The product (16) was collected and the solvent was removed under reduced pressure and the crude was left under vacuum for several hours.

B) Oxidation:



The crude (16) (70.2 mg, 178 μmol) was dissolved in dry THF (2.83 ml) under nitrogen atmosphere. *t*-BuOOH (5.5 M in Undecane, 65 μl , 356 μmol) and I_2 (1.78 μmol , 0.5mg), in catalytic amount, were subsequently added. The reaction mixture was left stirring in the dark, over night at room temperature. The reaction was controlled with TLC (DCM:MeOH=7:3).

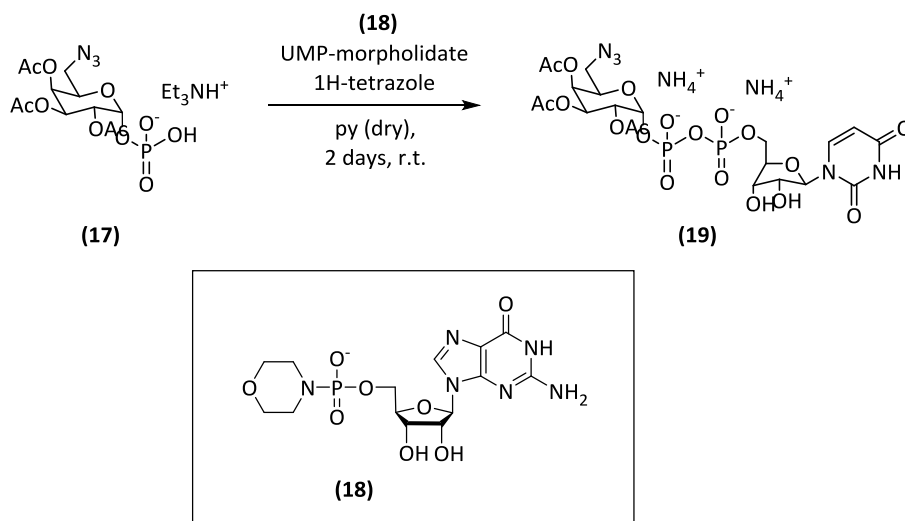
Work up:

Once the starting material (16) was consumed, the reaction mixture was neutralized by triethylamine (356 μmol , 49.6 μl , 2 eq.) and then concentrated under reduced pressure. The crude was purified by automated chromatography on a C18 reverse-phase column (water as eluent in the presence of 1% of TEA) to give the phosphate (17) in a 30% yield.

$^1\text{H-NMR}$ (400MHz, CD_3OD) δ : 5.78 (dd, 1H, $J_{\text{H-P}} = 7.7$ Hz, $J_{1-2} = 3.4$ Hz, H-1 α), 5.50 (d, 1H, $J_{4-3} = 3.3$ Hz, H-4), 5.41 (dd, 1H, $J_{3-4} = 3.3$ Hz, $J_{3-2} = 10.7$ Hz, H-3), 5.31 (dd, 1H, $J_{2-3} = 10.7$ Hz, $J_{2-1} = 3.4$ Hz, H-2), 4.43 (m, 1H, H-5), 3.51 (dd, 1H, $J_{6-6'} = 12.5$ Hz, $J_{6-5} = 6.2$ Hz, H-6), 3.30 (dd, 1H, $J_{6'-6} = 12.5$ Hz, $J_{6'-5} = 5.5$ Hz, H-6'), 3.21 (q, 6H, $J = 7.3$ Hz, $(\text{CH}_3\text{CH}_2)_3\text{NH}^+$), 2.15 (s, 3H, $\text{CH}_3\text{-COO}$), 2.09 (s, 3H, $\text{CH}_3\text{-COO}$), 1.99 (s, 3H, $\text{CH}_3\text{-COO}$), 1.34 (t, 9H, $(\text{CH}_3\text{CH}_2)_3\text{NH}^+$).

$^{31}\text{P-NMR}$ (121.5 MHz, CD_3OD) δ : -0.13 (s, 1P, P-OH).

Uridine 5'-(2,3,4-tri-O-acetyl-6-azido-6-deoxy- α -D-galactopyranosyl) diphosphate bis-triethylammonium salt (**19**)



Using a rotary evaporator flushed with argon, phosphate (**17**) (16.9 mg, 27.54 μ mol, 1 eq.) was dried by repeated co-evaporation with distilled pyridine (3 x 1.3 ml) and dried in vacuum (\approx 3 hours). UMP-morpholidate (**18**) (4'-morpholine-N,N'-dicyclohexylcarboxamidinium) (37.8 mg, 55.08 μ mol, 2 eq.) and tetrazole (122.4 μ l, 0.45 M in CH_3CN , 55.08 μ mol, 2 eq.) were then dried by repeated co-evaporation with distilled pyridine (3 x 1.3 ml) and dried in vacuum (\approx 1 hour).

To the dried phosphate (**17**) was added a solution of the dried UMP-morpholidate (**18**) in freshly distilled pyridine (10 ml). The mixture was dried by co-evaporation with distilled pyridine (2 x 1.5 ml), dried in vacuum (\approx 1 hour) and dry pyridine was added (\approx 500 μ l). From the reaction mixture about 60% of the solvent was removed and was stirred in the dark at room temperature under argon atmosphere. After 2 days, toluene was added and the mixture was concentrated in vacuum. After lyophilization, product (**19**) was purified on a semi-preparative HPLC C18-column using the eluent and conditions described below to obtain the purified protected UDP-6-azido-galactose (**19**) (12.5 mg, 17.46 μ mol) as a white solid, after lyophilization in the presence of NH_4HCO_3 .

Yield= 63.4 %

HPLC semi-preparative column C-18

Eluent A: NH_4HCO_3 , 50 mM (pH 7.6)

Eluent B: CH_3CN 50% in milliQ H_2O

Velocity= 14 ml/min , Rt (product)= 11 min

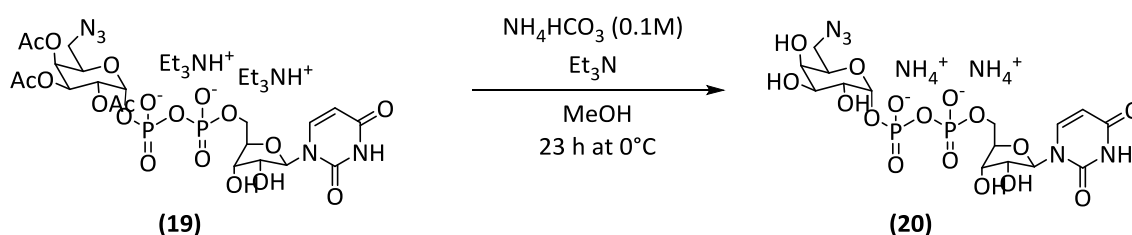
Maximum injectable sample: 30-100 mg.

Using a gradient from pure Eluent A to 50% of EluentB in 40 min.

$^1\text{H-NMR}$ (400MHz, D_2O) δ : 8.02 (d, 1H, $J_{b-a} = 8$ Hz, Hb), 6.04-5.98 (m, 2H, Ha, H-1rib), 5.84 (dd, 1H, $J_{1-2} = 3.5$ Hz, $J_{1-p} = 7.6$ Hz, H-1 α), 5.56 (d, 1H, $J_{4-3} = 3.0$ Hz, H-4), 5.41 (dd, 1H, $J_{3-2} = 10.7$ Hz, $J_{3-4} = 3.2$ Hz, H-3), 5.18 (m, 1H, H-2), 4.54 (m, 1H, H-5), 4.44-4.19 (5H, H-3rib, H4-rib, H5-rib, H5'-rib), 3.60 (dd, 1H, $J_{6-6'} = 12.8$ Hz, $J_{5-6} = 6.4$ Hz, H-6), 3.47 (dd, 1H, $J_{6'-6} = 13$ Hz, H-6'), 2.24 (s, 3H, $\text{CH}_3\text{-COO}$), 2.17 (s, 3H, $\text{CH}_3\text{-COO}$), 2.05 (s, 3H, $\text{CH}_3\text{-COO}$).

MS (ESI-negative mode): calculated for $\text{C}_{21}\text{H}_{28}\text{N}_5\text{O}_{19}\text{P}_2^-$ [M $^-$] 716.08, found 716.2

Uridine 5'-(6-azido-6-deoxy- α -D-galactopyranosyl) diphosphate bis-triethylammonium salt (20)



To a methanol solution (681 μ l) of the triethylammonium salt of the triacetate (19) (8 mg, 9.8 μ mol, 1 eq.) an aqueous solution of NH_4HCO_3 (0.1M, 900 μ l) and Et_3N (34.8 μ l, 26 eq.) was added at 0°C. After 20 h at 0°C, the solution (kept at 0°C) was diluted with water (4 ml) and the pH was adjusted to 7.2 with DOWEX 50W (H^+ form) resin. The resin was removed by filtration through a porous filter and washed with water (2 ml). After lyophilization, product (20) was purified on a semi-preparative HPLC C18-column with the eluent and conditions described below to afford UDP-azidogalactose (20) (4 mg, 6.4 μ mol) as a white solid after lyophilization with NH_4^+ as the counter-ion.

Yield= 65%

HPLC semi-preparative column C-18

Eluent A: NH_4HCO_3 , 50 mM (pH 7.6)

Eluent B: CH_3CN 50% in milliQ H_2O

Velocity= 14 ml/min , R_t (product)= 3 min

Maximum injectable sample: 30-100 mg.

Using a gradient from pure Eluent A to 50% of EluentB in 40 min.

$^1\text{H-NMR}$ (400MHz, D_2O) δ : 7.9 (d, 1H, $J_{b-a} = 8$ Hz, Hb), 5.90 (d, 2H, Ha, H-1rib), 5.55 (dd, 1H, $J_{1-2} = 3.6$ Hz, $J_{1-p} = 7.2$ Hz, H-1), 4.31-4.22 (m, 2H, H-2rib, H-3rib), 4.21-4.14 (m, 4H, H-4rib, H-5, H-5rib, H-5'rib), 3.91 (d, 1H, $J_{3-4} = 2.8$ Hz, H-4), 3.83 (dd, 1H, $J_{3-4} = 3.2$ Hz, $J_{3-2} = 10.4$ Hz, H-3), 3.72 (dt, 1H, H-2), 3.49 (dd, 1H, $J_{6-6'} = 12.8$ Hz, $J_{5-6} = 7.2$ Hz, H-6), 3.38 (dd, 1H, $J_{6'-6} = 12.8$ Hz, $J_{5-6'} = 6.0$ Hz, H-6').

MS (ESI-negative mode): calculated for $\text{C}_{15}\text{H}_{22}\text{N}_5\text{O}_{16}\text{P}_2^-$ [M^-] 590.05, found 590.7.

9.2.3. Microarray surface coating and characterization

Coating of microarray slides with poly(DMA-PMA-MAPS)

The coating solution of poly(DMA-PMA-MAPS) was obtained dissolving the polymer in deionized (DI) water to a final concentration of 2 % w/v. The solution was then diluted 1:1 with an aqueous $(\text{NH}_4)_2\text{SO}_4$ solution at 40% of saturation. The Si/SiO₂ slides were immersed into the polymer solution for 30 minutes, rinsed in DI water, dried with nitrogen flow and then cured at 80°C under vacuum for 15 minutes. Before the immersion, the Si/SiO₂ slide was pre-treated with oxygen plasma in a Plasma Cleaner from Harrick Plasma (Ithaca, NY, USA). The oxygen pressure was set to 1.2 Bar with a power of 29.6 W for 10 min.

Goniometry: Surface coating characterization by Contact Angle measurements

Contact angle measurements were collected via the sessile drop method using a CAM200 instrument (KSV Ltd), which utilizes video capture and subsequent image analysis. Deionized water was used, and its purity was confirmed by correlating the measured surface tension based on the pendant drop shape to the literature values for pure water (72 mN/m at 25°C).

Dual Polarization Interferometry (DPI)

Dual polarization interferometry (DPI) measurements were conducted using an Analight Bio 200 (Farfield Group, Manchester, UK) running Analight Explorer software. A silicon oxynitride AnaChipTM surface treated with oxygen plasma was used in this study. To measure the coating thickness, the chip was inserted into the fluidic compartment of an Analight Bio 200 and a polymer solution (1% w/v in a 20% saturated ammonium sulphate) was slowly introduced into the chip channels at a flow rate of 6 $\mu\text{l}/\text{min}$ for 15 minutes. The flow was then stopped, and the solution was allowed to stay in contact with the surface for 30 minutes before washing the channel with water, which was injected into the channel at a flow rate of 50 $\mu\text{l}/\text{min}$.

Before each experiment, a standard calibration procedure was performed using an 80 % (w/v) ethanol and MQ H₂O solution. The data were analyzed using Analight Explorer software to calculate the mass, density and thickness of the poly(DMA-PMA-MAPS) adsorbed onto the surface.

9.2.4. Microarray experiments

9.2.4.1. *Qualitative fluorescence analysis*

In the study of lectin-glycan interactions, an array was printed of the eight α -mannose derivatives (**Table 3, paragraph 6.1**) carrying an azido linker using a piezoelectric spotter (SciFlexArrayer S5, Scienion, Berlin Germany) on the surface of a polymer coated Si/SiO₂ slide. Four hundred pL of each glycan solution was spotted at 10 μ M or 50 μ M concentration in aqueous solution in the presence of Cu₂SO₄ · 5H₂O (2.5 mM) and ascorbic acid (12.5 mM). An α -mannoside and β -galactoside were used as positive and negative controls and were spotted in the same conditions described above. The immobilization reaction took place during an overnight incubation in a humid chamber at room temperature. The printed slides were sequentially washed with PBS buffer for 10 minutes with stirring, rinsed in DI water and dried by a nitrogen stream.

The arrayed slides were then incubated with biotinylated α -mannose-binding lectin Concanavalin A (ConA, 100 ng/ml) in the lectin binding buffer (LBB, 50 mM HEPES, pH 7.4, 5mM MnCl₂, 5 mM CaCl₂) in the presence of 0.2 mg/ml of bovine serum albumin (BSA). After 2 hours of incubation at room temperature on a lab shaker, the slides were washed 10 minutes in washing buffer on a lab shaker (0.05 M Tris·HCl pH9, 0.25 M NaCl, 0.05% v/v Tween 20), rinsed in DI water and dried with nitrogengas. A final incubation for 1 h with 2 μ g/ml Cy-3-labelled Streptavidin in PBS (Phosphate Saline Buffer) in a humid chamber at room temperature under static conditions enabled the fluorescence detection of the surface bound ConA by means of a scanner (ProScanArray scanner from Perkin Elmer, Boston, MA, USA) used at 70% laser power and 60% photomultiplier (PMT) gain. The fluorescence intensities of 11 spot replicates were confirmed by three experiments that provided the same fluorescence intensities for each glycomimetic, with a standard deviation lower than 5%.

9.2.4.2. Determination of the surface dissociation constant ($K_{D,surf}$)

Fluorescence microarray experiments

The surface equilibrium constant, $K_{D,surf}$ for the interaction of the eight α -mannose derivatives (Table 3, 2-9) with ConA was determined according to a method previously reported by Wong and co-workers¹⁶⁷. Several silicon/silicon oxide slides coated with poly(DMA-PMA-MAPS) were printed with 11 replicates of each glycan at 50 μ M concentration to form an array of eight different α -mannose derivatives (Table 3, paragraph 6.1.). Each slide was incubated for 2 hours with a given concentration of biotinylated ConcanavalinA (ConA) (from 47.2 pM to 9.43 nM) dissolved in LBB (50 mM HEPES, pH 7.4, 5mM $MnCl_2$, 5 mM $CaCl_2$) containing 0.2mg/ml BSA. After 2 hours of incubation at room temperature on a lab shaker, the slides were washed 10 minutes in washing Buffer (0.05 M Tris·HCl pH9, 0.25 M NaCl, 0.05% v/v Tween 20), rinsed in DI water and dried by a nitrogen stream. After 1 hour of incubation with Cy-3 labeled streptavidin (2 μ g/ml) in PBS, the slides were scanned for fluorescence to evaluate the amount of ConA captured by the immobilized glycans. The fluorescence intensities of 11 replicated spots were averaged.

The experimental conditions used during the incubation were optimized to ensure equilibration. The mean fluorescence intensities of the different glycans (spotted in 11 replicates) obtained from each single incubation was plotted against ConA concentration. The fluorescence values were fitted using OriginPro-8 that enables the calculation of $K_{D,surf}$ as EC50 for each glycan, depending on its affinity for ConA.

For the study of $K_{D,surf}$ at lower glycan density (from 0.5 to 5 μ M) the protocol used was the same described above for the spotting step, using the glycan at the desired concentration in an aqueous solution of $Cu_2SO_4 \cdot 5H_2O$ (2.5 mM) and ascorbic acid (12.5 mM). The concentration range of Concanavalin A used during the incubation step was expanded to the micromolar concentration (from 0.45 nM up to 13.4 μ M).

9.2.5. Antibody modification

9.2.5.1. Site-specific enzymatic modification

The site-specific modification consists of two steps: (1) antibody carbohydrates domain modification (i.e. removal of the terminal galactose) and (2) the attachment, on the antibody domain, of a synthetically modified galactose (Figure 48, section 7.1.2.).

Step (1): Removal of terminal galactose using β -(1,4)-galactosidase:

The first step includes the use of the commercial available enzyme β -(1,4)-galactosidase, from *Aspergillus oryzae* (SIGMA Aldrich), that breaks the covalent binding between glucose and galactose presented on the heavy chain of the Fc region of the antibody. The interleukin-6 (IL-6) capturing-antibody, previously concentrated, was diluted in sodium acetate buffer (10 mM, pH 5) at a final 1 mg/ml concentration and β -galactosidase (1U) was added. The reaction mixture was left overnight at 30°C.

Once the required time for the antibody carbohydrates domain modification was completed, using a centrifugal filter (Amicon Ultra 0.5 ml, Ultracel-30K) the buffer was changed to an alkaline Tris·HCl buffer (50 mM, pH 7.4), preparing the condition for the second reaction step.

Step (2): Attachment of a synthetically modified galactose using β -(1,4)-galactosyltransferase:

The second step consists of the attachment of a 6-azidogalactose (GalNAz), through the use of the commercial available β (1,4)-galactosyltransferase (a mammalian glycosyltransferases from bovin milk, from Sigma Aldrich) and the synthetic UDP-6-azidogalactose (synthesis reported in paragraph 9.2.2.).

From the 1 mg/ml solution of the modified antibody, 125 μ l were extracted and put in a 1 ml Eppendorf (1 ml vial). Alkaline phosphatase (2 U) , β -(1,4)-GalT (15 mU), unnatural UDP-GalNAz (220 μ g, 0.37 μ mol), MnCl₂·4H₂O (20 mM) were added to the antibody solution. The reaction mixture was brought up to a final volume of 250 μ l by adding Tris·HCl buffer (50 mM, pH 7.4) and left to react at 37°C for 24 hours. The reaction is complete when a white precipitate forms (due to the hydrolysis of uridine-diphosphate from alkaline phosphatase). Once the reaction was terminated, the antibody was purified through centrifugal filters (Amicon Ultra 0.5 ml, Ultracel-30K) and the Tris·HCl buffer was changed to sodium phosphate buffer (50 mM, pH 7.4) to facilitate the following click-reaction.

A similar procedure was adopted for the site-specific modification using the “Site-Click” Antibody Labelling Kit from Life Technologies.

9.2.5.2. Random modification

Peg-ylation of the interleukin-6 capturing antibody

To randomly modified 1 mg/ml of IL-6 capturing antibody, a peg-ylation chemistry was adopted. In a PBS buffer (50 mM, pH 7.4) antibody solution (5 mg/ml), NHS-PEG₈-N₃ (0,30 µl, 4 eq) from a 5 mg/ml stock in DMF was added, and the reaction mixture was left react at room temperature for 2 hours. Once the reaction time was completed, using a centrifugal filter (Amicon Ultra 0.5 ml, Ultracel-30K), the unreacted PEG was removed and the buffer was changed to sodium phosphate buffer (50 mM, pH 7.4) to facilitate the following click-reaction.

9.2.6. Interleukin-6 sandwich test

In the study of the critical role of antibody orientation during a microarray analysis, the IL-6 test was chosen. An array of IL-6 capture antibody, carrying an azido β-galactose on the Fc region (Ab-N₃ (C-6), paragraph 7.1.4.), was printed using a piezoelectric spotter (SciFlexArrayer S5, Scienion, Berlin Germany) on the surface of a poly(DMA-PMA-MAPS) coated silicon/silicon oxide IRIS slide. Four hundred pL of the capture antibody was spotted at 0.35 mg/ml concentration in buffered solution (sodium phosphate 50 mM, pH 7.4) mixed with Cu₂SO₄ · 5H₂O (100 µM), THPTA (400 µM) and ascorbic acid (6.25 mM). To validate this alternative protocol for the site-specific antibody modification, the same antibody modified through the use of “Site-Click” Antibody Labelling Kit from Life Technologies (Ab-N₃ (C-2), paragraph 7.1.4.) was printed in the same condition.

Furthermore, to demonstrate both the advantage of using a bio-orthogonal and regiospecific surface chemistry (CuAAC) and the use of an oriented antibody on a 3D-matrix environment, 0.35 mg/ml of PEG-ylated IL-6 capture antibody (Ab-PEG₈-N₃, paragraph 7.1.4.) was also spotted on the same slide in the same conditions: in sodium phosphate buffer (50 mM, pH 7.4) with Cu₂SO₄ · 5H₂O (100 µM), THPTA (400 µM) and ascorbic acid (6.25 mM).

A slide coated with poly(DMA-NAS-MAPS) was spotted with 0.35 mg/ml of the unmodified IL-6 capturing antibody (Ab, paragraph 7.1.4.) in the usual spotting buffer (50 mM sodium acetate buffer, pH 4), to compare oriented and random antibody immobilization via active ester/amine reactivity.

The immobilization reaction took place in at least in 30 minutes in a humid chamber at room temperature. The printed slides were washed with PBS buffer for 10 minutes, rinsed with DI water and dried by with nitrogen gas.

Before the first incubation step, IRIS images were acquired and fitted with Zoiray Acquire software to obtain a mass quantification for each modified printed antibody. For each antibody, signals from 48 replicate spots were averaged.

The arrayed slides were then incubated with the antibody IL-6 in incubation buffer (50 mM Tris/HCl, 0.15 M NaCl, 0.02% Tween20, pH 7.6) at 2 ng/ml in the presence of BSA (1%). After 2 hours of incubation at room temperature on a lab shaker, the slides were washed for 10 minutes in washing Buffer (0.05 M Tris/HCl pH9, 0.25 M NaCl, 0.05% v/v Tween 20), rinsed in DI water and dried with nitrogen gas. Subsequently the chip was incubated, under static conditions for 1 hour at room temperature in a humid chamber, with the biotinylated antibody (or detection antibody), diluted 1:200 in incubation buffer (50 mM Tris/HCl, 0.15 M NaCl, 0.02% Tween20, pH 7.6) in the presence of 1% (w/v) BSA (bovine serum albumin). Once the incubation time was finished, the chip was washed in PBS buffer for 10 minutes on a lab shaker, rinsed in DI water and dried with nitrogen gas.

The final step was the incubation with 2 µg/ml Cy-3-labelled Streptavidin in PBS (Phosphate Saline Buffer) in a humid chamber at room temperature for 1 hour under static conditions.

This incubation step enables the fluorescence detection of the surface bound IL-6 by means of a confocal scanner laser (ProScanArray scanner from Perkin Elmer, Boston, MA, USA) used at 70% laser power and 70% photomultiplier (PMT) gain.

Bibliography

- ¹ S.Y. Seong, C.Y. Choi, *Proteomics*, 2003, 3, 2176.
- ² M. Bosco, S. Le Gall, C. Rihouey, S. Couve-Bonnaire, M. Bardol, P. Lerouge, X. Pannecoucke, *Tetrahedron Lett.*, 2008, 49, 2294.
- ³ R.P. Huang, B. Burkholder, V.S. Jones, W.D. Jiang, Y.Q. Mao, Q.L. Chen, Z. Shi, *Current Proteomics*, 2012, 9, 55.
- ⁴ L.F. Thompson, C. G. Willson, M. J. Bowden, *Introduction to Microlithography*, 2nd Ed., 1994, American Chemical Society, Washington DC.
- ⁵ J. R uhe, V. Novotny, T. Clarke, G.B. Street, *Journal of Tribology Transactions of the ASME*, 1996, 118, 663.
- ⁶ M. Tirrell, E. Kokkoli, M. Biesalski, *Surf. Sci.*, 2002, 500, 61.
- ⁷ J. Klein, E. Kumacheva, D. Mahalu, D. Perahia, L.J. Fetters, *Nature*, 1994, 370, 634.
- ⁸ G.S. Grest, *Curr. Opin. Colloid Interface Sci.*, 1997, 2, 271.
- ⁹ B.D. Ratner, A.S. Hoffmann, F.J. Schoen, J.E. Lemons *Biomaterials Science, An Introduction to Materials in Medicine*, 1996, Academic Press, San Diego.
- ¹⁰ G. Pirri, F. Damin, M. Chiari, E. Bontempi, L. E. Depero, *Anal. Chem.*, 2004, 76, 1352.
- ¹¹ M. Chiari, M. Cretich, F. Damin, G. Di Carlo, C. Oldani, *J. Chromatogr. B*, 2008, 866, 89.
- ¹² R. A. L. Jones, R. W. Richards, *Polymers at Surfaces and Interfaces*, 1999, Cambridge University Press, Cambridge.
- ¹³ K. Mathauer, F. Embs, G. Wegner, *Comprehensive Polymer Science*, Vol. 1. Suppl., 1992, Ed. G. Allen, Pergamon Press, Oxford.
- ¹⁴ A. Halperin, M. Tirrell, T. P. Lodge, *Adv. Polym. Sci.*, 1992, 100, 31.
- ¹⁵ G. Decher, *Multilayer Thin Films. Sequential Assembly of Nanocomposite Materials*, 2002, Wiley-VCH, Weinheim.
- ¹⁶ A. Ulman, *An Introduction to Ultrathin Organic Films*, 1991, Academic Press, New York.
- ¹⁷ Y. N. Xia, G. M. Whitesides, *Angew. Chem. Int. Ed.*, 1998, 37, 551.
- ¹⁸ D. Kambhampati, P. E. Nielsen, W. Knoll, *Biosens. Bioelectron.*, 2001, 16, 1109.
- ¹⁹ W. Knoll, M. Zizlsperger, T. Liebermann, S. Arnold, A. Badia, M. Liley, D. Piscevic, F. J. Schmitt, J. Spinke, *Colloids and Surfaces: Physicochemical and Engineering Aspects*, 2000, 161, 115.
- ²⁰ N. Tsubokawa, M. Hosoya, K. Yanadori, Y. Sone, *J. Macromol. Sci., Pure Appl. Chem.*, 1990, A27, 445.
- ²¹ N. Tsubokawa, A. Kuroda, Y. Sone, *J. Polym. Sci., Part A: Polym. Chem.*, 1989, A27, 1701.
- ²² A. V. Dimitrenko, N. E. Shadrina, S. S. Ivanchev, N. N. Ulinskaya, A. M. Volkov, *J. Chromatogr.*, 1990, 520, 21.
- ²³ K. Hashimoto, T. Fujisawa, M. Kobayashi, R. Yosomiya, *J. Macromol. Sci., Pure Appl. Chem.*, 1982, A18, 173.
- ²⁴ M. Swann, L. Peel, S. Carrington, N. Freeman, *Anal. Biochem.*, 2004, 329, 190.
- ²⁵ S.A. Thube, B.S. Budhwani, M.P. Atif, *JPR*, 2009, 2, 1823.
- ²⁶ D. Gresham, M. J. Dunham and D. Botstein, *Nature Rev. Genet.*, 2008, 9, 291.
- ²⁷ Y. Li, Y. Wang, C. Jia, Y. Ma, Y. Lan, S. Wang, *Cancer Genet. Cytogenet.*, 182, 12.

-
- ²⁸ M. Cretich, V. Sedini, F. Damin, M. Pelliccia, L. Sola, M. Chiari, *Anal. Biochem.*, 2009, 397, 84.
- ²⁹ R.M. Kumar, *Am. J. Infect. Dis.*, 2009, 5, 214.
- ³⁰ S.P. Gygi, Y. Rochon, B.R. Franza, R. Aebersold, *Mol. Cell. Biol.*, 1999, 19, 1720.
- ³¹ H. Kaufmann, J.E. Bailey, M. Fussenegger, *Proteomics*, 2001, 1, 194.
- ³² N. Taniguchi, A. Ekuni, J.H. Ko, E. Miyoshi, Y. Ikeda, Y. Ihara, A. Nishikawa, K. Honke, M. Takahashi, *Proteomics*, 2001, 1, 239.
- ³³ H. Sarioglu, F. Lottspeich, T. Walk, G. Jung, C. Eckerskorn, *Electrophoresis*, 2000, 21, 2209.
- ³⁴ V. Santoni, S. Kieffer, D. Desclaux, F. Masson, T. Rabilloud, *Electrophoresis*, 2000, 21, 3329.
- ³⁵ M.P. Molloy, N.D. Phadke, H. Chen, R. Tyldesley, D.E. Garfin, J.R. Maddock, P.C. Andrews, *Proteomics*, 2002, 2, 899.
- ³⁶ W.F. Patton, *J. Chromatogr. B*, 1999, 722, 203..
- ³⁷ D. Kambhampati, *Protein Microarray Technology*, 2003, Wiley-VCH, Weinheim.
- ³⁸ E.T. Fung, *Methods in Molecular Biology*, Vol. 264: *Protein Arrays: Methods and Protocols*, 2004, Humana Press, Totowa.
- ³⁹ D. S. Wilson and S. Nock, *Angew. Chem. Int. Ed.*, 2003, 42, 494.
- ⁴⁰ S. Fukui, T. Feizi, C. Galustian, A. M. Lawson, W. Chai, *Nat. Biotechnol.*, 2002, 20, 1011.
- ⁴¹ B. T. Houseman and M. Mrksich, *Chem. Biol.*, 2002, 9, 443.
- ⁴² W. G. Willats, S. E. Rasmussen, T. Kristensen, J. D. Mikkelsen, J. P. Knox, *Proteomics*, 2002, 2, 1666.
- ⁴³ M. Chiari, M. Cretich, A. Corti, F. Damin, G. Pirri, R. Longhi, *Proteomics*, 2005, 5, 3600.
- ⁴⁴ H.J. Lee, Y. Yan, G. Marriott and R.M. Corn, *Journal of Physiology*, 2005, 563, 61-71.
- ⁴⁵ M. Cretich, G. Di Carlo, R. Longhi, C. Gotti, N. Spinella, S. Coffa, C. Galati, L. Renna and M. Chiari, *Anal. Chem.*, 2009, 81, 5197.
- ⁴⁶ A.J. Holloway, R.K. van Laar, R.W. Tothill and D.D. Bowtell, *Nature Genet.*, 2002, 32, 481.
- ⁴⁷ P. Bergese, M. Cretich, C. Oldani, G. Oliviero, G. Di Carlo, L.E. Depero and M. Chiari, *Curr. Med. Chem.*, 2008, 15, 1706.
- ⁴⁸ M.C. Pirrung, *Angew. Chem. Int. Ed.*, 2002, 41, 1276.
- ⁴⁹ G. MacBeath, A.N. Koehler and S.L. Schreiber, *J. Am. Chem. Soc.*, 1999, 121, 7967.
- ⁵⁰ J. Sagiv, *J. Am. Chem. Soc.*, 1980, 102, 92.
- ⁵¹ R. Benters, C.M. Niemeyer and D. Wöhrle, *ChemBioChem*, 2001, 2, 686.
- ⁵² M. Beier, J. D. Hoheisel, *Nucleic Acids Research*, 1999, 27, 1970-1977.
- ⁵³ P.K. Ajikumar, J.K. Ng, Y.C. Tang, J.Y. Lee, G. Stephanopoulos and H.P. Too, *Langmuir*, 2007, 23, 5670-5677.
- ⁵⁴ V. Le Berre, E. Trevisiol, A. Dagkessamanskaia, A.M. Caminade, J.P. Majoral, B. Meunier, J. François, *Nucleic Acids Research*, 2003, 31, 88e.
- ⁵⁵ S. Pathak, A.K. Singh, J.R. McElhanon, P.M. Dentinger, *Langmuir*, 2004, 20, 6075-6079.
- ⁵⁶ M. Cretich, M. R. Monroe, A. Reddington, X. Zhang, G. G. Daaboul, F. Damin, L. Sola, M. S. Unlu and M. Chiari, *Proteomics*, 2012, 12, 2963.
- ⁵⁷ E. H. Helle, D. Axelrod, *J. Opt. Soc. Am. B*, 1987, 4, 337.
- ⁵⁸ L. Moiseev, C.R. Cantor, M.I. Aksun, M. Dogan, et al., *J. Appl. Phys.*, 2004, 96, 5311.

-
- ⁵⁹ M. R. Monroe, A. P. Reddington, A. D. Collin, C. LaBoda, M. Cretich, M. Chiari, F. F. Little and M. S. Unlu, *Anal. Chem.*, 2011, 83, 9485.
- ⁶⁰ E. Ozkumur, J.W. Needham, D.A. Bergstein, R. Gonzalez, M. Cabodi, J. M. Gershoni, B. B. Goldberg, M. S. Ünlü, *PNAS*, 2008, 105, 7988.
- ⁶¹ A. Del Campo, I.J. Bruce, *Top. Curr. Chem.*, 2005, 260, 77.
- ⁶² S. Lemeer, R. Ruijtenbeek, M.W.H. Pinkse, C. Jopling, A.J.R. Heck, J. den Hertog, M. Slijper, *Mol. Cell. Proteom.*, 2007, 6, 2088.
- ⁶³ E.N. Timofeev, A.D. Kochetkova, A. D. Mirzabekov, V.L. Florentiev, *Nucleic Acids Re.*, 1996, 24, 3142.
- ⁶⁴ D. Guschin, G. Yershov, A. Zaslavsky, A. Gemmel, V. Shick, D. Proudnikov, P. Arenkov, A.D. Mirzabekov, *Anal. Biochem.*, 1997, 250, 203.
- ⁶⁵ S. Piletsky, E. Piletska, A. Bossi, N. Turner, A. Turner, *Biotechnol. Bioeng.*, 2003, 82, 86.
- ⁶⁶ S. Kiyonaka, K. Sada, I. Yoshimura, S. Shinkai, N. Kato, I. Hamachi, *Nature Materials*, 2004, 3, 58- 64.
- ⁶⁷ J.J. Yoon, Y.S. Nam, J.H. Kim, T.G. Park, *Biotechnol. Bioeng.*, 2002, 78, 1.
- ⁶⁸ V. Hlady, J. Buijs, *Curr. Op. Biotechnol.*, 1996, 7, 72.
- ⁶⁹ N. Nath, J. Hyun, H. Ma, A. Chilkoti, *Surf. Sci.*, 2004, 570, 98.
- ⁷⁰ E. Ostuni, R.G. Chapman, R. E. Holmlin, S. Takayama, G.M. Whitesides, *Langmuir*, 2001, 17, 5605.
- ⁷¹ J. Ponten, L. Stolt, *Exp. Cell Res.*, 1980, 129, 367.
- ⁷² S.B. Carter, *Nature*, 1965, 208, 1183.
- ⁷³ Y.Y. Luk, M. Kato, M. Mrksich, *Langmuir*, 2000, 16, 9604.
- ⁷⁴ K.S. Ko, F.A. Jaipuri, N.L. Pohl, *J. Am. Chem. Soc.*, 2005, 127, 13162.
- ⁷⁵ R. Michel, S. Pasche, M. Textor, D.G. Castner, *Langmuir*, 2005, 21, 12327.
- ⁷⁶ D. Batra, S. Vogt, P.D. Laible, M.A. Firestone, *Langmuir*, 2005, 21, 10301.
- ⁷⁷ C.M. Yam, M. Deluge, D. Tang, A. Kumar, C. Cai, *J. Colloid Interface Sci.*, 2006, 296, 118.
- ⁷⁸ M. Mrksich, G.B. Sigal, G.M. Whitesides, *Langmuir*, 1995, 11, 4383.
- ⁷⁹ S.J. Dilly, M.P. Beecham, S. P. Brown, J.M. Griffin, A.J. Clark, C.D. Griffin, J. Marshall, R.M. Napier, P.C. Taylor, A. Marsh, *Langmuir*, 2006, 22, 8144.
- ⁸⁰ K.L. Prime, G.M. Whitesides, *J. Am. Chem. Soc.*, 1993, 115, 10714.
- ⁸¹ S. Chen, J. Zheng, L. Li, S. Jiang, *J. Am. Chem. Soc.*, 2005, 127, 14473.
- ⁸² R.S. Kane, P. Deschatelets, G.M. Whitesides, *Langmuir*, 2003, 19, 2388.
- ⁸³ J.R. Crowther, *ELISA: Theory and Practice*, 1995, Humana, New Jersey.
- ⁸⁴ M. Cretich, G. Pirri, F. Damin, I. Solinas and M. Chiari, *Analytical Biochemistry*, 2004, 332, 67-74.
- ⁸⁵ M. Cretich, V. Sadini, F. Damin, G. Di Carlo, C. Oldani and M. Chiari, *Sens. Actuators, B*, 2008, 132, 258..
- ⁸⁶ Wong, E. L. S.; Chow, E. and Gooding, J. J., *Langmuir*, 2005, 21, 6957.
- ⁸⁷ C. D. Hein, X-M. Liu and D. Wang, *Pharm. Res.*, 2008, 25, 2216.
- ⁸⁸ D. Wang, S. Liu, B. J. Trummer, C. Deng and A. Wang, *Nat. Biotechnol.*, 2002, 20, 275.
- ⁸⁹ E. W. Adams, D. M. Ratner, H. R. Bokesch, J. B. MacMahon, B. R. O'Keefe and P. H. Seeberger, *Chem. Biol.*, 2004, 11, 875.

-
- ⁹⁰ O. Blixt, S. Head, T. Mondala, C. Scanlan, M. E. Hufiejt, R. Alvarez, M. C. Bryan, F. Fazio, D. Calarese, J. Stevens, N. Razi, D. J. Stevens, J. J. Skehel, I. van Die, D. R. Burton, I. A. Wilson, R. Cummings, N. Bovin, C. H. Wong and J. C. Paulson, *PNAS*, 2004, 101, 17033.
- ⁹¹ S. Park, M. R. Lee and I. Shin, *Nat. Protoc.*, 2007, 2, 2747.
- ⁹² S. Park and I. Shin, *Angew. Chem. Int. Ed.*, 2002, 41, 3180.
- ⁹³ Z. Pei et al., *ChemBioChem*, 2007, 8, 166.
- ⁹⁴ R. Huisgen, *Pure Appl. Chem.*, 1989, 61, 613.
- ⁹⁵ H. C. Kolb, M. G. Finn and K. B. Sharpless, *Angew. Chem. Int. Ed.*, 2001, 40, 2004.
- ⁹⁶ C. W. Tornøe, C. Christensen and M. Meldal, *J. Org. Chem.*, 2002, 67, 3057.
- ⁹⁷ A. E. Speers, G. C. Adam and B. F. Cravatt, *J. Am. Chem. Soc.*, 2003, 125, 4686.
- ⁹⁸ K. E. Beatty, F. Xie, Q. Wang, D. A. Tirrel, *J. Am. Chem. Soc.*, 2005, 127, 14150.
- ⁹⁹ M. Meldal and C. W. Tornøe, *Chem. Rev.*, 2008, 108, 2952.
- ¹⁰⁰ X.-L. Sun, C. L. Stabler, C. S. Cazalis and E. L. Chaikof, *Bioconjugate Chem.*, 2006, 17, 52.
- ¹⁰¹ Q. Wang, T. R. Chan, R. Hilgraf, V. V. Fokin, K. B. Sharpless, M. G. Finn, *J. Am. Chem. Soc.*, 2003, 125, 3192.
- ¹⁰² J. Gierlich, G. A. Burley, P. M. E. Gramlich, D. M. Hammond, T. Carrell, *Org. Lett.*, 2006, 8, 3639.
- ¹⁰³ J. M. Baskin, J. A. Prescher, S. T. Laughlin, N. J. Agard, P. V. Chang, I. A. Miller, A. Lo, J. A. Codelli, and C. R. Bertozzi, *PNAS*, 2007, 104, 16793.
- ¹⁰⁴ C. Uttamapinant, A. Tangpeerachaikul, S. Grecian, S. Clarke, U. Singh, P. Slade, K. R. Gee and A. Y. Ting, *Angew. Chem. Int. Ed.*, 2012, 51, 5852.
- ¹⁰⁵ C. Besanceney-Webler, H. Jiang, T. Zheng, L. Feng, D. Soriano del Amo, W. Wang, L. M. Klivansky, F. L. Marlow, Y. Liu and P. Wu, *Angew. Chem. Int. Ed.*, 2011, 50, 8051.
- ¹⁰⁶ V. Hong, S. I. Presolski, C. Ma and M. G. Finn, *Angew. Chem. Int. Ed.*, 2009, 48, 9879.
- ¹⁰⁷ M. Cretich, F. Damin, G. Pirri, M. Chiari, *Biomol. Eng.*, 2006, 23, 77.
- ¹⁰⁸ J.M. Blackburn, D.J. Hart, *Methods Mol. .*, 2005, 310, 197.
- ¹⁰⁹ Q. Zhu, M. Uttamchandani, D. Li, M.L. Lesaichere, S.Q. Yao, *Org. Lett.*, 2003, 5, 1257.
- ¹¹⁰ S.H. Kim, A. Tamrazi, K.E. Carlson, J.A. Katzenellenbogen, *Mol. Cell. Proteomics*, 2005, 4, 267.
- ¹¹¹ H. Zhu, M. Snyder, *Curr. Op. Chem. Biol.*, 2003, 7, 55.
- ¹¹² M. Cretich, G. Di Carlo, C. Giudici, S. Pokoj, I. Lauer, S. Scheurer, M. Chiari, *Proteomics*, 2009, 9, 2098.
- ¹¹³ http://www.phadia.it/dia_templates/Page44203.aspx
- ¹¹⁴ C. Hultschig, J. Kreutzberger, H. Seitz, Z. Konthur, K. Büssov and H. Lehrach, *Curr. Op. Chem. Biol.*, 2006, 10, 4.
- ¹¹⁵ L. Yang, S. Guo, Y. Li, S. Zhou and S. Tao, *Acta Biochim. Biophys. Sin.*, 2011, 1.
- ¹¹⁶ T. Cha, A. Guo and X-Y. Zhu, *Proteomics*, 2005, 5, 416.
- ¹¹⁷ G. Elia, M. Silacci, S. Scheurer, J. Scheuermann, D. Neri, *Trends Biotechnol.*, 2002, 20, S19.
- ¹¹⁸ J. Kim, H. Park, D. Jung, S. Kim, *Anal. Biochem.*, 2003, 313, 41.
- ¹¹⁹ C. D. Hodneland, Y-S. Lee, D.-H. Min, M. Mrksich, *PNAS*, 2002, 99, 5048.
- ¹²⁰ M. B. Soellner, K. A. Dickson, B. L. Nilsson and R. T. Raines, *J. Am. Chem. Soc.*, 2003, 125, 11790.

-
- ¹²¹ A. K. Trilling, M. M. Harmsen, V. J. B. Ruigrok, H. Zuilhof and J. Beekwilder, *Biosens. Bioelectron.*, 2013, 40, 219.
- ¹²² A. K. Trilling, J. Beekwilder and H. Zuilhof, *Analyst*, 2013, 138, 1619.
- ¹²³ T. Q. Huy, N. T. H. Hanh, P. V. Chung, D. D. Anh, P. T. Nga and M. A. Tuan, *Appl. Surf. Sci.*, 2011, 257, 7090.
- ¹²⁴ H. Chen, J. Huang, J. Lee, S. Hwang and K. Koh, *Sens. Actuators B*, 2010, 147, 548.
- ¹²⁵ K.-T. C. Shade and R. M. Anthony, *Antibodies*, 2013, 2, 392.
- ¹²⁶ A. M. Scott, J. D. Wolchok, L. J. Old, *Nat. Rev. Cancer*, 2012, 12, 278.
- ¹²⁷ J.N.J. Arnold, M.R.M. Wormald, R.B.R. Sim, P.M.P. Rudd, R.A.R. Dwek, *Immunology*, 2007, 25, 21.
- ¹²⁸ P. Peluso, *Anal. Biochem.*, 2003, 312, 113.
- ¹²⁹ J. Turkova, S. Vohnik, S. Helusova, M.J. Benes, et al., *J. Chromatogr.*, 1992, 597, 19.
- ¹³⁰ L.V. Pyrohova, M.F. Starodub, *Ukr. Biokhim. Zh.*, 2002, 74, 45.
- ¹³¹ Adak et al., *Appl. Mater. Interfaces*, 2014, 6, 10452.
- ¹³² B. M. Zeglis, C. B. Davis, R. Aggeler, H. C. Kang, A. Chen, B. J. Anew and J. S. Lewis, *Bioconjugate Chem.*, 2013, 24, 1057.
- ¹³³ B. Ramakrishnan and P. K. Qasba, *J. Biol. Chem.*, 2002, 7, 20833.
- ¹³⁴ T. Horlacher, P. H. Seeberger, *Chem. Rev.*, 2008, 37, 1414.
- ¹³⁵ S. Roseman, *J. Biol. Chem.*, 2001, 276, 41527.
- ¹³⁶ A. Varki, R. Cummings, J. D. Esko, H. Freeze, G. Hart and J. Marth, *Essential Glycobiology*, 2002, Cold Spring Harbor Laboratory Press, Plainview, NY.
- ¹³⁷ P. H. Seeberger and D. B. Werz, *Nat. Rev. Drug Discovery*, 2005, 4, 751.
- ¹³⁸ D. H. Dube and C. R. Bertozzi, *Nat. Rev. Drug Discovery*, 2005, 4, 477.
- ¹³⁹ P. H. Seeberger and D. B. Werz, *Nature*, 2007, 446, 1046.
- ¹⁴⁰ J. Stevens, O. Blixt, J. C. Paulson and I. A. Wilson, *Nat. Rev. Microbiol.* 2006, 4, 857.
- ¹⁴¹ T.M. Gloster, G.J. Davies, *Org. Biomol. Chem.*, 2010, 8, 305.
- ¹⁴² D. B. Werz, R. Ranzinger, S. Herget, A. Adibekian, C. W. von der Lieth and P. H. Seeberger, *ACS Chem. Biol.*, 2007, 2, 685.
- ¹⁴³ P. Stanley and E. Iofie, *FASEB J.*, 1995, 9, 1436.
- ¹⁴⁴ L. L. Kiessling, J. E. Gestwicki and L. E. Strong, *Angew. Chem. Int. Ed.*, 2006, 45, 2348.
- ¹⁴⁵ D. M. Ratner, E. W. Adams, M. D. Disney and P. H. Seeberger, *ChemBioChem*, 2004, 5, 1375.
- ¹⁴⁶ M. Schena, D. Shalon, R. W. Davis, P. O. Brown, *Science*, 1995, 270, 467.
- ¹⁴⁷ G. MacBeath, S. L. Schreiber, *Science*, 2000, 289, 1760.
- ¹⁴⁸ O. Oyelaran and J. C. Gildersleeve, *Curr. Opin. Chem. Biol.*, 2009, 13, 406.
- ¹⁴⁹ C. D. Rillahan and J. C. Paulson, *Annu. Rev. Biochem.*, 2011, 80, 797.
- ¹⁵⁰ O. J. Plant, E. R. Palmacci and P. H. Seeberger, *Science*, 2001, 291, 1523.
- ¹⁵¹ Z. Zhang, I. R. Ollman, X-S. Ye, R. Wischnat, T. Baasov and C. H. Wong, *J. Am. Chem. Soc.*, 1999, 121, 734.
- ¹⁵² H. C. Kolb, B. Ernst, *Chem. Eur. J.*, 1997, 3, 10, 1571.
- ¹⁵³ N. Kaila, B. E. Thomas, *IV Medicinal Research Reviews*, 2002, 22, 566.
- ¹⁵⁴ B. Ernst and J. L. Magnani *Nat. Rev. Drug Discovery*, 2009, 8, 661.

-
- ¹⁵⁵ L. R. Prost, J. C. Grim, M. Tonelli, and L. L. Kiessling, *ACS Chem. Biol.*, 2012, 7, 1603.
- ¹⁵⁶ A. Bernardi, P. Cheshev, *Chem. Eur. J.*, 2008, 14, 7434.
- ¹⁵⁷ N. Horan, L. Yan, H. Isobe, G. M. Whitesides and D. Kahne, *PNAS*, 1999, 96, 11782.
- ¹⁵⁸ C. Fasting, C. A. Schalley, M. Weber, O. Seitz, S. Hecht, B. Koksich, J. Dervede, C. Graf, E.-W. Knapp and R. Haag, *Angew. Chem. Int. Ed.*, 2012, 51, 10472.
- ¹⁵⁹ V. Wittmann and R. J. Pieters, *Chem. Soc. Rev.*, 2013, 42, 4492.
- ¹⁶⁰ Y. Zhang, Q. Li and J. C. Gildersleeve *J. Am. Chem. Soc.*, 2010, 132, 28, 9653.
- ¹⁶¹ O. Oyelaran, Q. Li and J. C. Gildersleeve *J. Proteom Res.*, 2009, 3529.
- ¹⁶² O.C. Grant, H.M.K. Smith, D. Firsova, E. Fadda and R.J. Woods, *Glycobiology*, 2014, 24, 17.
- ¹⁶³ D.M. Lewallen, D. Siler, S.S. Iyer, *ChemBioChem*, 2009, 10, 1486.
- ¹⁶⁴ M.B. Tessier, O.C. Grant, J. Heimburg-Molinaro, D. Smith, S. Jadey, A.M. Gulick, J. Glushka, S.L. Deutscher, K. Rittenhouse-Olson, R.J. Woods, *PLoS One*, 8, e54874.
- ¹⁶⁵ W. Peng, C. M. Nycholat, N. Razi, *Methods Mol. Biol.*, 2013, 1022, 1.
- ¹⁶⁶ D. W. Grainger, C. H. Greef, P. Gong, M. J. Lochhead *Microarrays Methods in molecular Biology*, 2007, 381, 37.
- ¹⁶⁷ P. H. Liang, S. K. Wang and C. H. Wong, *J. Am. Chem. Soc.*, 2007, 129, 11177.
- ¹⁶⁸ M. D. Disney and P. H. Seeberger, *Chem. Biol.*, 2004, 11, 1701.
- ¹⁶⁹ <http://functionalglycomics.org/static/index.shtml>
- ¹⁷⁰ W. C. Boyd and E. Shapleigh, *Science*, 1954, 119, 419.
- ¹⁷¹ G. Ashwell and J. Harford, *Annu. Rev. Biochem.*, 1982, 51, 531.
- ¹⁷² J. Melrose, N. Tsurushita, G. Liu and E. L. Berg, *J. Immunol.*, 1998, 161, 2457.
- ¹⁷³ N. Watanabe, H. Kawashima, Y.-F. Li and M. Miyasaka, *J. Biochem.*, 1999, 125, 826.
- ¹⁷⁴ J. B. Sumner, *J. Biol. Chem.*, 1919, 37, 137.
- ¹⁷⁵ J. B. Sumner and S. F. Howell, *J. Bacteriol.*, 1936, 32, 227.
- ¹⁷⁶ N. Sharon and H. Lis, *Lectins*, 1989, Chapman and Hall, London.
- ¹⁷⁷ S. H. Barondes, *Trends Biochem. Sci.*, 1988, 13, 480.
- ¹⁷⁸ H. Lis and N. Sharon, *Chem. Rev.*, 1998, 98, 637.
- ¹⁷⁹ A. Pusztai, *Plant Lectins*, 1991, Cambridge University Press, Cambridge.
- ¹⁸⁰ Y. D. Lobsanov, M. A. Gitt, H. Leffler, S. H. Barondes and J. M. Rini, *J. Biol. Chem.*, 1993, 268, 27034.
- ¹⁸¹ N. K. Sauter, J.E. Hanson, G.D. Glick, J. H. Brown, R. L. Crowther, S.-J. Park, J. J. Skehel and D. C. Wiley, *Biochem.*, 1992, 31, 9609.
- ¹⁸² K. Drickamer, *J. Biol. Chem.*, 1988, 263, 9557.
- ¹⁸³ I. Ofek and R. J. Doyle, 1994, *Bacterial Adhesion to Cells and Tissues*, Chapman and Hall, London.
- ¹⁸⁴ M. Inbar and L. Sachs, *Nature*, 1969, 223, 710.
- ¹⁸⁵ N. Srinivasan, S.D. Rufino, M.B. Pepys, S. Wood and T.L. Blundell, *Chemtracts: Biochem. Mol. Biol.*, 1996, 6, 149.
- ¹⁸⁶ V. R. Srinivas, G. B. Reddy, N. Ahmad, C. P. Swaminathan, N. Mitra and A. Surolia, *Biochim. Biophys. Acta*, 2001, 1527, 102.
- ¹⁸⁷ W.W. Fish, L.M. Hamlin and R.L. Miller, *Arch. Biochem. Biophys.*, 1978, 190, 693.

-
- ¹⁸⁸ M. Decastel, H. De Boeck, Y. Goussault, C. K. De Bruyne, F. G. Loontjens and J.-P. Frénoy, *Arch. Biochem. Biophys.*, 1985, 240, 811.
- ¹⁸⁹ W. I. Weis and K. Drickamer, *Annu. Rev. Biochem.*, 1996, 65, 441.
- ¹⁹⁰ R. Banerjee, K. Das, R. Ravishankar, K. Suguna, A. Surolia and M. Vijayan, *J. Mol. Biol.*, 1996, 259, 281.
- ¹⁹¹ V. Sharma and A. Surolia, *J. Mol. Biol.*, 1997, 267, 433.
- ¹⁹² B. G. Davis, *J. Chem. Soc., Perkin Trans. 1*, 1999, 3125.
- ¹⁹³ J. M. Rini, *Annu. Rev. Biophys. Biomol. Struct.*, 1995, 24, 551.
- ¹⁹⁴ M. E. Etzler, in *Glycoconjugates. Composition, Structure and Functions*, ed. H. J. Allen and E. C. Kisailus, Marcel Dekker Inc., New York, 1992, 21.
- ¹⁹⁵ J. W. Kijne, *Chemtracts Biochem. Mol. Biol.*, 1996, 6, 180.
- ¹⁹⁶ N. Sharon and H. Lis, *Science*, 1989, 246, 227.
- ¹⁹⁷ P. Mylona, D. Pawlowski and T. Bisseling, *Plant Cell*, 1995, 7, 869.
- ¹⁹⁸ M. Ambrosi, N. R. Cameron and B. G. Davis, *Org. Biomol. Chem.* 2005, 3, 1593.
- ¹⁹⁹ P. N. Kanellopoulos, K. Pavlou, A. Perrakis, B. Agianian, C. E. Vorgias, C. M. Soufi, M. Soufi, P. Tucker and S. J. Hamodrakas, *J. Struct. Biol.*, 1996, 116, 345.
- ²⁰⁰ S. Sinha, G. Gupta, M. Vijayan, A. Surolia, *Curr. Opin. Struct. Biol.*, 2007, 17, 498.
- ²⁰¹ W-W. Li, J-Y. Yu, H-L. Xu, J-K. Bao, *Biochem. Biophys. Res. Comm.*, 2011, 414, 282.
- ²⁰² B. B. L. Agrawal, I. J. Goldstein, *Biochem. J.*, 1965, 96, 23c.
- ²⁰³ R.A. Decreau, J.P. Ollman, Y. Yang, Y. Yan, N.K. Devaraj, *J. Org. Chem.*, 2007, 72, 2794.
- ²⁰⁴ S. Prakash, T.M. Long, J.C. Selby, J.S. Moore, M.A. Shannon, *Anal. Chem.*, 2007, 79, 1661.
- ²⁰⁵ Y. Zhang, S. Luo, Y. Tang, L. Lu, K.-Y. Hou, J.-P. Cheng, X. Zeng, P.G. Wang, *Anal. Chem.*, 2006, 78, 2001.
- ²⁰⁶ Y. Miura, T. Yamauchi, H. Sato, T. Fukuda, *Thin Solid Films*, 2008, 516, 2443.
- ²⁰⁷ J.-F. Lutz and Z. Zarafshani, *Adv. Drug Delivery Rev.*, 2008, 60, 958.
- ²⁰⁸ J.-F. Lutz, *Angew. Chem. Int. Ed.*, 2007, 46, 1018.
- ²⁰⁹ H. Nandivada, X. Jiang and J. Lahann, *Adv. Mater.*, 2007, 19, 2197.
- ²¹⁰ B. P. Duckworth, J. H. Xu, T. A. Taton, A. Guo, M. D. Distefano, *Bioconjugate Chem.*, 2006, 17, 967.
- ²¹¹ H. Nandivada, H. Y. Chen, L. Bondarenko, J. Lahann, *Angew. Chem. Int. Ed.*, 2006, 45, 3360.
- ²¹² F. Fazio, M. C. Bryan, O. Blixt, J. C. Paulson, C.-H. Wong, *J. Am. Chem. Soc.*, 2002, 124, 14397.
- ²¹³ X. Wei, W. Gu, L. Li, X. Shen, J.-K. Kim, T. P. Russell, *J. Polym. Sci., Part B: Polym. Phys.*, 2013, 51, 78.
- ²¹⁴ V. Ladmiraal, G. Mantovani, G. J. Clarkson, S. Cauet, J. L. Irwin, D. M. Haddleton *J. Am. Chem. Soc.*, 2006, 128, 4823.
- ²¹⁵ R. Loris, T. Hamelryck, J. Bouckaert, L. Wyns, *Biochim. Biophys. Act.*, 1998, 1383, 9.
- ²¹⁶ E. J. M. Van Damme, W. J. Peumans, A. Barre, P. Rougé, *Crit. Rev. Plant Sci.*, 1998, 17, 575.
- ²¹⁷ R. Liang, L. Yan, J. Loebach et al., *Science*, 1996, 274, 1520.
- ²¹⁸ R. Liang, J. Loebach, N. Horan et al., *PNAS*, 1997, 94, 10554.
- ²¹⁹ Y. C. Lee, R. T. Lee, *Acc. Chem. Res.*, 1995, 28, 321.
- ²²⁰ E. A. Smith, W. D. Thomas, L. L. Kiessling and R. M. Corn, *J. Am. Chem. Soc.*, 2003, 125, 6140.
- ²²¹ R. Gutiérrez Gallego, S. R. Haseley, V. F. Van Miegem, J. F. Vliegthart, J. P. Kamerling, *Glycobiology*, 2004, 14, 373.

-
- ²²² E. Engvall and P. Perlmann, *Immunochemistry*, 1971, 8, 871.
- ²²³ P. Jonkheijm, D. Weinrich, H. Schröder, C. M. Niemeyer and H. Waldmann, *Angew. Chem., Int. Ed.*, 2008, 47, 9618.
- ²²⁴ P.C. Lin, S.H. Ueng, M.C. Tseng, J.L. Ko, K.T. Huang, S.C. Yu, A. Kumar Adak, Y.J. Chen, and C.C. Lin, *Angew. Chem. Int. Ed.*, 2006, 45, 4286.
- ²²⁵ S.M. Hsu and L. Raine, *J. Hystochem. Cytochem.*, 1981, 29, 1349.
- ²²⁶ M. Arlt, O. Hindsgaul, *J. Org. Chem.*, 1995, 60, 14.
- ²²⁷ J. G. Moffatt, H. G. Khorana, *J. Am. Chem. Soc.*, 1961, 83, 649.
- ²²⁸ V. Wittmann and C. H. Wong, *J. Org. Chem.*, 1997, 62, 2144.
- ²²⁹ C. Ahn, R. Correia and P. DeShong, *J. Org. Biomol. Chem.*, 2010, 10, 9090.
- ²³⁰ L. Morelli, PhD thesis, University of Milan, a.a. 2010-11, "Synthesis and conjugation of *Neisseria Meningitidis* X. Capsular Polysaccharide Fragments".
- ²³¹ K. Takaya, N. Nagahori, M. Kuroguchi, T. Furuyke, N. Miura, K. Monde, Y. C. Lee, S.-H. Nishimura, *J. Med. Chem.*, 2005, 48, 6054.
- ²³² S. Oscarson, F. W. Sehgelmeble, *Tetrahedron: Asim.*, 2005, 16, 121.
- ²³³ M.M. Sim, H. Kondo, C.-H. Wong, *J. Am. Chem. Soc.*, 1993, 115, 2260.
- ²³⁴ V.F. Zarytova, D.G. Knorre, *Nucleic Acids Res.*, 1984, 4, 2091 and cited references.
- ²³⁵ S. Berner, K. Mühlegger, H. Seliger, *Nucl. Acids Res.*, 1989, 17, 853.
- ²³⁶ V. Hong, N. F. Steinmetz, M. Manchester, M. G. Finn, *Bioconjugate Chem.*, 2010, 21, 1912.
- ²³⁷ R.P. Huang, B. Burkholder, V.S. Jones, W.D. Jiang, Y.Q. Mao, Q.L. Chen, Z. Shi, *Curr. Prot.*, 2012, 9, 55.